Using near-term forecasts and uncertainty partitioning to improve predictions of low- frequency cyanobacterial events

Mary E. Lofton[1], Jennifer A. Brentrup[2], Whitney S. Beck[3], Jacob A. Zwart[4], Ruchi Bhattacharya[5], Ludmila S. Brighenti[6], Sarah H. Burnet[7], Ian M. McCullough[8], Bethel G. Steele[9], Cayelan C. Carey[1], Kathryn L. Cottingham[10], Michael C. Dietze[11], Holly A. Ewing[12], Kathleen C. Weathers[9], and Shannon L. LaDeau[9]

[1]Virginia Tech
[2]University of Vermont
[3]Colorado State
[4]United States Geological Survey
[5]University of Waterloo
[6]Universidade do Estado de Minas Gerais
[7]University of Idaho
[8]Michigan State University
[9]Cary Institute of Ecosystem Studies
[10]Dartmouth College
[11]Boston University
[12]Bates College

November 22, 2022

Abstract

Near-term ecological forecasts provide resource managers advance notice of changes in ecosystem services, such as fisheries stocks, timber yields, or water and air quality. Importantly, ecological forecasts can identify where uncertainty enters the forecasting system, which is necessary to refine and improve forecast skill and guide interpretation of forecast results. Uncertainty partitioning identifies the relative contributions to total forecast variance (uncertainty) introduced by different sources, including specification of the model structure, errors in driver data, and estimation of initial state conditions. Uncertainty partitioning could be particularly useful in improving forecasts of high-density cyanobacterial events, which are difficult to predict and present a persistent challenge for lake managers. Cyanobacteria can produce toxic or unsightly surface scums and advance warning of these events could help managers mitigate water quality issues. Here, we calibrate fourteen Bayesian state-space models to evaluate different hypotheses about cyanobacterial growth using data from eight summers of weekly cyanobacteria density samples in an oligotrophic (low nutrient) lake that experiences sporadic surface scums of the toxin-producing cyanobacterium, Gloeotrichia echinulata. We identify dominant sources of uncertainty for near-term (one-week to four-week) forecasts of G. echinulata densities over two years. Water temperature was an important predictor in calibration and at the four-week forecast horizon. However, no environmental covariates improved over a simple autoregressive (AR) model at the one-week horizon. Even the best fit models exhibited large variance in forecasted cyanobacterial densities and often did not capture rare peak density occurrences, indicating that significant explanatory variables in calibration are not always effective for near-term forecasting of low-frequency events. Uncertainty partitioning revealed that model process specification and initial conditions uncertainty dominated forecasts at both time horizons. These findings suggest that observed densities result from both growth and movement of G. echinulata, and that imperfect observations as well as spatial misalignment of environmental data and cyanobacteria observations affect forecast skill. Future research efforts should prioritize long-term studies to refine process understanding

and increased sampling frequency and replication to better define initial conditions. Our results emphasize the importance of ecological forecasting principles and uncertainty partitioning to refine and understand predictive capacity across ecosystems.

Running head: Uncertainty partitioning of forecasts

Title: Using near-term forecasts and uncertainty partitioning to improve predictions of low-frequency cyanobacterial events

Mary E. Lofton[1*], Jennifer A. Brentrup[2], Whitney S. Beck[3], Jacob A. Zwart[4], Ruchi Bhattacharya[5], Ludmila S. Brighenti[6], Sarah H. Burnet[7], Ian M. McCullough[8], Bethel G. Steele[9], Cayelan C. Carey[10], Kathryn L. Cottingham[11], Michael C. Dietze[12], Holly A. Ewing[13], Kathleen C. Weathers[14], Shannon L. LaDeau[15]

[1]Department of Biological Sciences, Virginia Tech, Blacksburg, VA, USA; melofton@vt.edu

[2a]Department of Biological Sciences, Dartmouth College, Hanover, NH, USA; Jennifer.A.Brentrup@dartmouth.edu

[3b]Department of Biology and Graduate Degree Program in Ecology, Colorado State University, Fort Collins, CO, USA; whitney.beck@colostate.edu

[4]Integrated Information Dissemination Division, US Geological Survey, Middleton, WI, USA; jzwart@usgs.gov

[5]Legacies of Agricultural Pollutants (LEAP), University of Waterloo, Waterloo, Ontario, Canada; ruchi.bhattacharya@gmail.com

[6]Universidade do Estado de Minas Gerais, Divinópolis, Brazil; ludmilasb@gmail.com

[a] Current affiliation: Rubenstein School of Environment and Natural Resources, University of Vermont, Burlington, VT, USA; jennifer.brentrup@uvm.edu

[b] Current affiliation: U.S. Environmental Protection Agency, Washington, DC, USA; wbeck1990@gmail.com

[7]Department of Fish and Wildlife Resources, University of Idaho, Moscow, Idaho, USA; shburnet@uidaho.edu

[8]Department of Fisheries and Wildlife, Michigan State University, East Lansing, MI, USA; immccull@gmail.com

[9]Cary Institute of Ecosystem Studies, Millbrook, NY, USA; steeleb@caryinstitute.org

[10]Department of Biological Sciences, Virginia Tech, Blacksburg, VA, USA; cayelan@vt.edu

[11]Department of Biological Sciences, Dartmouth College, Hanover, NH, USA; kathycottingham@esa.org

[12]Department of Earth and Environment, Boston University, Boston, MA, USA; dietze@bu.edu

[13]Environmental Studies, Bates College, Lewiston, ME, USA; hewing@bates.edu

[14]Cary Institute of Ecosystem Studies, Millbrook, NY, USA; weathersk@caryinstitute.org

[15]Cary Institute of Ecosystem Studies, Millbrook, NY, USA; ladeaus@caryinstitute.org

*Corresponding author. Address: Department of Biological Sciences, Derring Hall Room 2125, 926 West Campus Drive, Mail Code 0406, Blacksburg, VA 24061, USA. Phone: +1-540-231-0788. Fax: +1-540-231-9307. Email: melofton@vt.edu

This manuscript version is the initial submission for consideration as a research article to *Ecological Applications.* Accepted following peer review on 16 September 2021. Currently in production.

Declarations of interest: none

Abstract

Near-term ecological forecasts provide resource managers advance notice of changes in ecosystem services, such as fisheries stocks, timber yields, or water and air quality. Importantly, ecological forecasts can identify where uncertainty enters the forecasting system, which is necessary to refine and improve forecast skill and guide interpretation of forecast results. Uncertainty partitioning identifies the relative contributions to total forecast variance (uncertainty) introduced by different sources, including specification of the model structure, errors in driver data, and estimation of initial state conditions. Uncertainty partitioning could be particularly useful in improving forecasts of high-density cyanobacterial events, which are difficult to predict and present a persistent challenge for lake managers. Cyanobacteria can produce toxic or unsightly surface scums and advance warning of these events could help managers mitigate water quality issues. Here, we calibrate fourteen Bayesian state-space models to evaluate different hypotheses about cyanobacterial growth using data from eight summers of weekly cyanobacteria density samples in an oligotrophic (low nutrient) lake that experiences sporadic surface scums of the toxin-producing cyanobacterium, *Gloeotrichia echinulata*. We identify dominant sources of uncertainty for near-term (one-week to four-week) forecasts of *G. echinulata* densities over two years. Water temperature was an important predictor in calibration and at the four-week forecast horizon. However, no environmental covariates improved over a simple autoregressive (AR) model at the one-week horizon. Even the best fit models exhibited large variance in forecasted cyanobacterial densities and often did not capture rare peak density occurrences, indicating that significant explanatory variables in calibration are not always effective for near-term forecasting of low-frequency events. Uncertainty partitioning revealed that model process specification and initial conditions uncertainty dominated forecasts at both

time horizons. These findings suggest that observed densities result from both growth and movement of *G. echinulata*, and that imperfect observations as well as spatial misalignment of environmental data and cyanobacteria observations affect forecast skill. Future research efforts should prioritize long-term studies to refine process understanding and increased sampling frequency and replication to better define initial conditions. Our results emphasize the importance of ecological forecasting principles and uncertainty partitioning to refine and understand predictive capacity across ecosystems.

Keywords: Bayesian model, blooms, dynamic linear model, ecological forecasting, hindcast, lake, oligotrophic, phytoplankton, scums, state-space model, uncertainty partitioning, variance partitioning

I. Introduction

Near-term ecological forecasts, defined as daily to decadal predictions of the state of ecosystems (Clark et al. 2001, Dietze et al. 2018), can be helpful to resource managers in systems ranging from fisheries stocks to disease outbreaks in protected species populations (Kuikka et al. 2014, Hobbs et al. 2015). For example, near-term forecasts have been used to provide projections for alternate management decisions (Kuikka et al. 2014, Thomas et al. 2018, 2020), help managers allot fisheries take quotas (or used to avoid bycatch; Hobday et al. 2019 and references therein), and provide advance notice of public safety hazards such as red tides (Stumpf et al. 2009, McGowan et al. 2017). Effective near-term forecasts include fully-specified uncertainty by quantifying the total variance around a prediction and identifying the relative

contributions of different sources of uncertainty (Dietze et al. 2018; Box 1).

Uncertainty in ecological forecasts may arise from several different sources, including: initial conditions uncertainty, parameter uncertainty, process uncertainty, observation uncertainty, driver or covariate data uncertainty, and random effects uncertainty (Dietze 2017a; Table 1). Partitioning the variance associated with a forecast into these components allows for more targeted efforts to understand and improve forecasts. For example, the dominant contributor to uncertainty in weather forecasts is from initial conditions because the atmosphere's internal instability amplifies even small errors in initial condition estimates and the physical processes controlling weather given a set of current conditions are relatively well-defined (Dietze 2017b). This has directed weather forecasters to prioritize efforts to better measure starting atmospheric conditions (Shuman 1989, Bauer et al. 2015). In contrast, the dominance of process uncertainty in a forecast indicates that researchers need to consider alternative model structures and additional or different explanatory variables to describe the biological or ecological process of interest (Page et al. 2017, Thomas et al. 2018). Formal, standardized uncertainty partitioning can guide improvements to ecological forecasts and ultimately lead to more informed management of natural resources (Bauer et al. 2015, Page et al. 2018).

Estimating uncertainty has become more common in ecological analyses that generate forecasts (see studies in Table S1 for examples). However, formal uncertainty partitioning that includes all the potential sources of forecast uncertainty is less common and methods are not standardized, making it difficult to compare how different components of uncertainty contribute across ecological systems or among focal state variables. For example, while studies by Gertner et al. 1996, Valle et al. 2009, Wang et al. 2009, and Thomas et al. 2018 (Table S1) all forecast

different metrics of forest biomass and productivity, differences in how they estimate and partition uncertainty limit synthetic understanding of the predominance of process structure or estimation of drivers or parameters to uncertainty in forecasts about forest productivity.

Forecasting freshwater cyanobacterial dynamics has been a persistent challenge for researchers and water quality managers (Janssen et al. 2019, Rousso et al. 2020), and uncertainty partitioning analysis could help refine and advance forecasting capacity in this system. Cyanobacteria are increasing in many lakes and reservoirs worldwide due to climate and land-use change, posing substantial problems for drinking water managers and other stakeholders (Schindler and Vallentyne 2008, Paerl et al. 2011, Carey et al. 2012b, O'Neil et al. 2012). Many cyanobacterial taxa create toxic or unsightly scums that cause taste and odor problems and clog filters at drinking water treatment plants; consequently, knowing when cyanobacterial density is likely to increase could allow managers to take pre-emptive action to mitigate deleterious water quality effects (van Dolah et al. 2015, Ibelings et al. 2016, Stroom and Kardinaal 2016). However, despite substantial research on drivers of cyanobacterial dominance (e.g., Carey et al. 2012b, Paerl and Otten 2013) and recent technological developments permitting high-frequency observations of cyanobacterial density (e.g., Le Vu et al. 2011, Catherine et al. 2012), near-term cyanobacterial abundance model predictions often deviate substantially from observations (Hamilton et al. 2009, Rigosi et al. 2010, Reynolds et al. 2014, Janssen et al. 2019) and few studies have examined forecast uncertainty (Rousso et al. 2020; but see Huang et al. 2013, Page et al. 2017, Massoud et al. 2018). The challenges in forecasting cyanobacteria may be attributable to the rate of cyanobacterial growth relative to the frequency of most sampling campaigns. Cyanobacterial densities can change rapidly on timescales of days to weeks (Dokulil and Teubner 2000, Huisman and Hulot 2005, Rolland et al. 2013, Carpenter et al. 2020), with

densities in many lakes remaining relatively low for much of the year and then rapidly increasing from one sample period to the next (e.g., Bormans et al. 2005, Rolland et al. 2013, Carey et al. 2014a).

Cyanobacterial blooms are often associated with high nutrient levels (Dokulil and Teubner 2000), and so much of the effort to predict cyanobacterial densities has been focused on nutrient-rich lakes (Rousso et al. 2020). As a result, prediction efforts for high-density cyanobacterial events in oligotrophic lakes have lagged behind, and understanding why cyanobacterial densities change over the short term in low-nutrient lakes is especially challenging. However, teasing apart the different sources of uncertainty and their relative importance to cyanobacterial forecast precision may help prioritize research efforts in economically important oligotrophic waterbodies. Increases in the occurrence of high-density cyanobacterial events have been documented in north temperate oligotrophic lakes throughout the United States (Carey et al. 2012a), Canada (Winter et al. 2011), and Europe (Freeman et al. 2020), and these increases are often associated with significant economic losses and public health concerns (Dodds et al. 2009, Mueller et al. 2016, Stoddard et al. 2016). High water quality in oligotrophic lakes provides substantial economic benefit through recreational use and high lakeside property values (Wilson and Carpenter 1999, Dodds et al. 2009, Mueller et al. 2016, Stoddard et al. 2016). Moreover, some oligotrophic systems are permitted as drinking water sources with reduced filtration requirements when their water quality meets United States Environmental Protection Agency (U.S. EPA) standards, thereby reducing water treatment costs (U.S. EPA 1991, Kauffman 2016, Ravindranath et al. 2016).

Prior studies provide several hypotheses for what environmental drivers likely trigger cyanobacterial growth or accumulation of cyanobacterial surface scums, including: increased

159 growth at higher temperatures (Paerl and Huisman 2008, Hamilton et al. 2009); light-induced
160 triggering of cell germination and growth (Roelofs and Oglesby 1970, Karlsson-Elfgren et al.
161 2004); more recruitment of dormant cells from the sediment and/or dilution of surface water
162 cyanobacterial density due to water column mixing, which can occur due to temperature
163 changes, precipitation events, or wind (Jennings et al. 2012, Carey et al. 2014, de Eyto et al.
164 2016, Kuha et al. 2016); greater incidence of surface scums during periods of stronger thermal
165 stratification (Carey et al. 2012b); and aggregation of cells or colonies in nearshore zones by
166 wind (Roelofs and Oglesby 1970, Cyr 2017). The development of forecast models with
167 uncertainty partitioning is needed to compare and evaluate these hypotheses in a predictive
168 framework.

169 While there are a variety of techniques that can be used to develop forecast models with
170 partitioned uncertainty, Bayesian state-space models are particularly suitable (Clark 2007, Hobbs
171 and Hooten 2015, Dietze 2017a). State-space models focus on estimating the true, latent state of
172 the system by explicitly accounting for observation and process uncertainty. These dynamic
173 models are structured so that each modeled latent state is a function of the previous latent state,
174 independent of observations at other time points (Hobbs and Hooten 2015, Dietze 2017a; Fig. 1).
175 Bayesian state-space models use distributions rather than fixed values to represent all unknown
176 values, including parameters, initial conditions, and as-yet-unobserved future values for driver
177 variables, allowing for quantification of uncertainty associated with each of these components
178 and missing data.

179 We developed and evaluated a suite of Bayesian state-space models with different
180 structures and tested different environmental variables hypothesized to be important in driving
181 cyanobacterial density, including water temperature, thermal stability, wind, and light. We

calibrated each model to weekly cyanobacterial densities measured from 2009-2014 in Lake Sunapee, NH, USA, an oligotrophic lake that exhibits variable densities of the toxin-producing cyanobacterium *Gloeotrichia echinulata*. We then generated hindcasts (defined in Table 1) of cyanobacterial density for 2015-2016. We assessed and conducted uncertainty partitioning of our hindcasts to address the following questions: A) Which model structures and environmental covariates best predict oligotrophic lake cyanobacterial density over one to four week forecast horizons? B) What are the dominant sources of uncertainty in oligotrophic lake cyanobacterial forecasts? and C) How do the relative contributions of different sources of uncertainty vary among models with differing complexity and environmental covariates? We discuss how our results inform future efforts to forecast oligotrophic lake cyanobacterial density and relate to patterns of predictive uncertainty observed in other ecosystems.

II. Methods

Focal cyanobacterium

Gloeotrichia echinulata is a colonial, filamentous cyanobacterium commonly found in oligotrophic north temperate lakes in the United States, Canada, and Europe (Karlsson-Elfgren et al. 2005, Winter et al. 2011, Carey et al. 2012a, Freeman et al. 2020). *G. echinulata* is capable of forming surface scums and producing toxins (Karlsson-Elfgren et al. 2005, Carey et al. 2012a). Occurrence of *G. echinulata* surface scums in oligotrophic north temperate lakes has been increasing in recent decades (Carey et al. 2008, 2012a, Winter et al. 2011), motivating researchers to improve understanding and prediction of *G. echinulata* density in these ecosystems. While nutrients are often a driver of cyanobacterial growth in eutrophic lakes

(Dokulil and Teubner 2000), current understanding of dynamics in oligotrophic systems suggests that other environmental drivers may be important for determining *G. echinulata* densities (Roelofs and Oglesby 1970, Karlsson-Elfgren et al. 2004, Carey et al. 2014, Cyr 2017).

Study site

We sampled *G. echinulata* surface abundance and collected environmental data weekly in May-October from 2009-2016 at two nearshore sites in Lake Sunapee, NH, USA, a recreational lake with high property values that also serves as a public drinking water supply (Fig. 2). Lake Sunapee is a large, oligotrophic lake (lat 43°24′N, long 72°2′W, max. depth = 33.7 m, surface area = 16.69 km^2, volume = 1.94 × 10 m^3, mean depth = 11.6 m, Lake Sunapee Protective Association (LSPA), unpublished data). High-nutrient (eutrophic) lakes can have total phosphorus (TP) concentrations ≥ 24 μg L^{-1} and total nitrogen (TN) concentrations ranging from ~400-1600 μg L^{-1} (Carlson 1977, Carlson and Simpson 1996, Gibson et al. 2000). Mean TP concentration in the surface waters of Lake Sunapee between 2009-2016 was 6.3 ± 1.7 μg L^{-1} (mean ± 1 S.D.), and mean Secchi depth was 6.6 ± 0.6 m (LSPA, unpub. data). Mean TN concentration from 2009-2012 at our study site was 172 ± 25 μg L^{-1} (Cottingham 2020). Lake Sunapee typically thermally stratifies from June-September with a mean thermocline depth of 7-9 m from 2009-2016. The watershed (~107 km^2 not including lake surface area) is 80% forested but shoreline development has been increasing in recent decades (Cobourn et al. 2018).

Our research team began a weekly *G. echinulata* monitoring program at two sampling sites in collaboration with the Lake Sunapee Protective Association (LSPA) in 2005 (Carey et al. 2008, 2014b). Our focal sampling site for this study (Site 1; Fig. 2) was chosen because it frequently exhibits high densities of *G. echinulata*. We used data from the second nearshore site

(Site 2) only to generate informed priors for *G. echinulata* observation error and nearshore water temperature and these data were not included in any hindcasting analyses. We focused our analyses on 2009-2016 for this study because those years had at least 20 weeks of sampling data (Cottingham et al. 2020a); however, during our eight-year study period there were six missing weekly *G. echinulata* observations, four of which occurred during the 2015-2016 hindcasting period.

G. echinulata data collection and sample processing

G. echinulata surface abundance at both nearshore sites was sampled each week in the top 1 m of the water column by combining two vertical tows from 1 m to the surface using a 30 cm diameter, 80 μm mesh plankton net (Wildlife Supply Co., Yulee, Florida). *G. echinulata* were transferred from the net and preserved in opaque plastic bottles using Lugol's iodine (Carey et al. 2014). Total *G. echinulata* samples were counted using a Leica MZ12 dissecting microscope (Leica, Buffalo Grove, Illinois). Density was quantified according to the number of colonies and filament bundles (immature, developing colonies) per liter rather than biovolume following protocols used in previous studies of *G. echinulata* (Roelofs and Oglesby 1970, Barbiero and Welch 1992, Karlsson-Elfgren et al. 2005). We then converted abundance to density by dividing the total number of colonies and filament bundles in each sample by the volume of water sampled by the plankton net (Carey et al. 2014b). All data are publicly available through the Environmental Data Initiative repository (Cottingham et al. 2020a, 2020b, LSPA et al. 2020a, 2020b; Lofton et al. 2020).

Environmental driver data

To capture the effect of temperature on *G. echinulata* growth, water temperature was monitored hourly using Onset loggers at our nearshore sampling sites (Sites 1 and 2; Fig. 2; Cottingham et al. 2020b). Growing degree days (GDD), a measure of heat accumulation during the growing season, were calculated using these water temperatures for each day when *G. echinulata* was sampled. To investigate effects of thermal stratification on *G. echinulata* surface density, water temperature profiles from the Global Lake Ecological Observatory Network (GLEON) buoy, deployed in the lake by the LSPA since 2007 (Site 3), were used to calculate Schmidt stability, a measure of thermal stratification strength that indicates the amount of energy required to homogenize temperature across the water column (Idso 1973, LSPA et al. 2020b). To examine whether wind could drive nearshore aggregation of *G. echinulata* colonies, wind data from the LSPA/GLEON buoy (Site 3) were aggregated from minute and hourly scales, respectively, to calculate daily summary statistics (LSPA et al. 2020a). Solar radiation data from the North American Land Data Assimilation System Phase 2 (NLDAS-2) forcing dataset (https://ldas.gsfc.nasa.gov/nldas; Lofton et al. 2020) and photosynthetically active radiation (PAR) data from the LSPA/GLEON buoy (LSPA et al. 2020a) were similarly aggregated to determine whether light was an important predictor of *G. echinulata* density. Finally, we calculated summary statistics of daily precipitation data from the Parameter-elevation Relationships on Independent Slopes Model (PRISM) model (http://www.prism.oregonstate.edu; Lofton et al. 2020) to examine the effect of storm events and subsequent water column mixing on *G. echinulata* pelagic populations (see Text S1 for further information on environmental data processing).

Selection of environmental covariates for Bayesian models

We performed a standardized selection process to determine which potential environmental drivers of *G. echinulata* density to include in Bayesian state-space models (Text S2). We examined associations between natural log-transformed *G. echinulata* density from 2009-2014 (calibration period) and 82 summary statistics of candidate environmental covariates identified as potential drivers in previous studies (Roelofs and Oglesby 1970, Karlsson-Elfgren et al. 2004, Paerl and Huisman 2008, Hamilton et al. 2009, Carey et al. 2012b, 2014, Jennings et al. 2012, de Eyto et al. 2016, Kuha et al. 2016, Cyr 2017). We used Spearman correlations to prioritize inclusion in our Bayesian models (Text S2). The full list of covariate summary statistics is in Table S2. This approach identified eight drivers for further evaluation (Table 2): daily minimum water temperature on the sampling day (MinWaterTemp), daily minimum water temperature with a one-week lag (MinWaterTempLag), seven-day moving average of water temperature (WaterTempMA), weekly difference in median Schmidt stability (ΔSchmidt), daily maximum Schmidt stability with a one-week lag (SchmidtLag), daily mean of a wind direction indicator variable with a two-day lag (WindDir; see Text S1 for details on wind indicator variable calculation), growing degree days (GDD), and daily sum of precipitation (Precip).

Development of Bayesian state-space models

A suite of Bayesian state space models were fit to data collected from Site 1 and increased in complexity from a random walk with no covariates (intercept model) to models containing one or two of the eight prioritized driver variables (Fig. 3; Table 2). We calibrated each model over a 6-year period from 2009-2014, assessed model performance during a two-year hindcasting period of 2015-2016, and then conducted uncertainty partitioning. We investigated

297 whether sequential increases in model complexity translated to changes in the relative
298 contributions of different uncertainty sources to total hindcast uncertainty, increases in skill of *G.*
299 *echinulata* density hindcasts, or both (Fig. 3; Table 2).
300 We assessed hindcast skill of the twelve models including environmental covariates
301 compared to two baseline models: first, a model with a random walk process and an informed
302 prior for observation error developed using data from Site 2 (RW model; Fig. 3; Text S3), and
303 second, a linear autoregressive process model with a single lag (AR model; Fig. 3; Table 2). We
304 also assessed a random walk model with a random year effect as a possible baseline model but
305 determined during model calibration that the estimated year effect was not substantially different
306 from 0 in any year (Table S3); as a result, we did not include a random year effect in subsequent
307 models. We next incorporated a single environmental covariate into the linear AR(1) process
308 model based on our environmental covariate selection process (MinWaterTemp,
309 MinWaterTempLag, WaterTempMA, ΔSchmidt, SchmidtLag, WindDir, Precip, and GDD). The
310 influence of GDD was visibly non-linear in our preliminary analyses (Fig. S1) and thus, a
311 quadratic term was included in the model to evaluate GDD influence on *G. echinulata* growth.
312 We subsequently developed two-covariate models based on the performance of the
313 single-covariate models during the hindcasting validation period (Schmidt+Temp,
314 Schmidt+Precip, Temp+Precip, Precip+GDD). Finally, following observations that model
315 ensembles can provide more skilled predictions than a single model even when some ensemble
316 members are low-performing (Johansson et al. 2019), we generated a simple, unweighted model
317 ensemble to determine if it could out-perform our individual models (see Text S4 for model
318 ensemble details).
319

320 *Calibration using 2009-2014 data*

321 We calibrated each Bayesian state-space model to observed weekly data collected in
322 2009-2014 using the R packages *rjags* and *runjags* (*rjags* v.4-8, *runjags* v. 2.0.4-2, Denwood
323 and Plummer 2019, Plummer et al. 2019) in the R statistical environment (R version 4.0, R Core
324 Development Team, 2020). Models were structured as an annual loop for 20 weeks per year,
325 with each season extending from the last week in May to the first week in October. We natural
326 log-transformed *G. echinulata* densities and standardized all covariates using Z-scores to
327 facilitate model convergence. We ran three Markov chain Monte Carlo (MCMC) chains for each
328 model, with an adaptation period of 5,000 iterations, a burn-in of 10,000 iterations, and a sample
329 size of 50,000 iterations, which we thinned to 7,500 samples for hindcasting and model
330 assessment. We evaluated convergence using the potential scale reduction factor of the Gelman-
331 Rubin statistic, sometimes referred to as $\hat{R}$, where a value approaching 1 indicates that the model
332 has converged well on a parameter estimate both within and among MCMC chains (Table S4;
333 Table S5). Missing data occurred for several of our candidate environmental drivers, so NA
334 values were imputed using a missing data model with a Gaussian prior with mean and variance
335 of observations from the same week across the calibration period (2009-2014).

336

337 *Hindcasting validation using 2015-2016 data*

338 To validate our Bayesian state-space models, we conducted one-week-ahead and four-
339 week-ahead hindcasts of *G. echinulata* density in 2015-2016 using each of the fourteen models.
340 We assimilated data by iteratively adding one week of data to our model input dataset and re-
341 running our Bayesian models in *runjags* to update parameter calibrations and initial conditions.
342 The posterior output of each re-calibrated model was then used to produce hindcasts at one and

four weeks into the future. We hindcasted "future" driver data for each environmental covariate using data observations from 2009-2014 for the 2015 hindcasts and from 2009-2015 for the 2016 hindcasts. These historical driver timeseries were resampled with replacement for each of the 7,500 hindcast model iterations to account for week-to-week autocorrelation in driver data. As hindcasts were running, driver data from 2015-2016 were assimilated along with *G. echinulata* observations and thereby used to update posteriors throughout the hindcasting period.

Our primary criterion for hindcast model selection was based on predictive loss, calculated using the root mean square error (RMSE) of predictions and the variance of the predictive interval (defined in Table 1) via the following equation:

$$\text{Predictive loss} = \sqrt{RMSE^2 + predictive\ interval\ variance} \quad \text{eqn. 1}$$

The model with the smallest predictive loss at a particular forecast horizon indicates the best-performing model at that horizon (Gelfand and Ghosh 1998). We further compared models by subtracting the predictive loss of the best-performing model from the predictive loss of all other models to calculate change in predictive loss (ΔPL), with smaller ΔPL indicating better-performing models. We also calculated the standard deviation of the predictive interval (predictive S.D.), the percent of observations falling within the 95% predictive interval (coverage), the mean difference between median predicted and observed values (bias), and the difference in weeks between when maximum *G. echinulata* density was observed during the hindcasting period and when each model predicted maximum *G. echinulata* density (peak timing; Table 3).

Uncertainty partitioning of 2015-2016 hindcasts

We conducted uncertainty partitioning of our 2015-2016 cyanobacterial density hindcasts using a one-at-a-time ahead approach, where all sources of uncertainty were initially held at fixed values and then sequentially added back into the hindcasts. For example, all model parameter values were initially set to the mean of the posterior distribution of the calibrated model for all 7,500 hindcasting iterations; then, when we wanted to add parameter uncertainty to our hindcasts, we allowed parameter values to be drawn from the full posterior distribution, resulting in a variety of possible parameter values and subsequent estimation of uncertainty in those parameters. We added sources of uncertainty to our hindcasts in the following order: initial condition uncertainty, parameter uncertainty, driver data uncertainty, and process uncertainty. The order of uncertainties is important to specify as different sources of uncertainty can interact with each other. We were then able to calculate the relative contribution of each uncertainty source to total hindcast variance based on the incremental increase in variance as each source of uncertainty was added. Not all models included all the potential sources of uncertainty (e.g., the random walk model does not have driver data uncertainty because it does not include any environmental covariates).

Observation uncertainty is not included in our partitioning results because it does not propagate and therefore does not affect our uncertainty about the latent state of the system (Dietze 2017). However, to examine the relative importance of observation error in our study system, we assessed the estimated value of τ_{obs}, which is the precision ($\frac{1}{S.D.^2}$) of the normal distribution used to fit *G. echinulata* latent states to *G. echinulata* observations in the data model component of our Bayesian state-space models (Fig. 1). We also examined the increase in variance between our 95% credible interval (CI) and our 95% predictive interval (PI; CI and PI

are defined in Table 1).

All code used for data processing, model calibration and validation, uncertainty partitioning, and assessment of hindcast output are publicly available on the GLEON Github repository (https://github.com/GLEON/Bayes_forecast_WG/tree/eco_apps_release; DOI:10.5281/zenodo.3878781).

III. Results

Variability in G. echinulata abundance

Median *G. echinulata* density during the entire study period from 2009-2016 was 0.25 ± 8.2 colonies L^{-1} (median ± 1 S.D.; Fig. 4). During the model calibration period (2009-2014), *G. echinulata* density ranged from an annual maximum density of 1.2 colonies L^{-1} in 2012 to 81.6 colonies L^{-1} in 2013. Notably, while the calibration years included two periods of high *G. echinulata* density with visible surface scums (42.1 colonies L^{-1} in August 2010 and 81.4 colonies L^{-1} in September 2013), maximum density during the 2015-2016 hindcasting validation period was 14.1 colonies L^{-1} (Fig. 4). Temporal variability in environmental drivers of *G. echinulata* density included in state-space models is reported in Text S5 and Figures S2 – S9.

Models of G. echinulata growth

G. echinulata growth was dependent on *G. echinulata* density at the previous timestep, as indicated by a converged coefficient value ranging from 0.63 to 0.76 ± 0.06 to 0.10 for the AR(1) term across models (Table S4). Parameter estimates from calibrated models indicated that *G. echinulata* growth was positively associated with increases in water temperature, high

Schmidt stability, and a higher daily proportion of wind blowing towards the focal nearshore site (see Table S4; Table S5 for model coefficient values). The coefficient on the quadratic term for growing degree days based on water temperature (GDD) converged at -0.59 ± 0.17 (Table S5), indicating that increases in GDD at high values (i.e., late in the sampling season) were associated with decreasing *G. echinulata* growth.

Some variables that seemed promising based on our covariate selection protocol had estimated model coefficients close to 0 in calibrated state-space models (Precip, ΔSchmidt), indicating a limited effect on *G. echinulata* growth. The daily sum of precipitation (Precip) and weekly difference in median Schmidt stability (ΔSchmidt) model coefficients did not differ from zero (Table S5). Model coefficient values did not substantially change when environmental covariates were combined in two-covariate models (Schmidt+Temp, Schmidt+Precip, Temp+Precip, Precip+GDD, Table S5).

Environmental drivers no better than AR model at one-week-ahead hindcasts

All single and two-covariate models and the AR model had improved performance over the null RW model for one-week-ahead hindcasts based on predictive loss. Three models (AR, ΔSchmidt, and Precip) had a predictive loss of 2.25 ln(colonies L^{-1}) and were also comparable in terms of RMSE, coverage, and bias (Table 3; Fig. 5; models not shown in Fig. 5 can be found in Fig. S10, S11). Other environmental covariates that had non-zero model coefficients ($\widehat{\boldsymbol{\beta}}$ parameters; Table S5), such as the water temperature covariates, SchmidtLag, and WindDir, were not good predictors of *G. echinulata* densities at the one-week horizon (Table 3).

No model correctly predicted the week or magnitude of peak *G. echinulata* density for the 2015-2016 hindcasting period (10 September 2015) at the one-week horizon; however, the

best-performing AR model was able to predict when peak density occurred with only a one week lag after the observed peak (Table 3).

Water temperature models more skilled than AR at four-week forecast horizon

Models containing water temperature covariates out-performed the AR model at the four-week horizon (Table 3; Fig. 6; models not shown in Fig. 6 may be found in Fig. S12, S13). The three best-performing models at the four-week horizon were MinWaterTempLag, WaterTempMA, and Schmidt+Temp, all with a predictive loss of 2.42 ln(colonies L^{-1}). Other models containing water temperature covariates (MinWaterTemp, GDD, Temp+Precip, Precip+GDD) also performed relatively well at the four-week horizon, all with $\Delta PL = 0.01$ ln(colonies L^{-1}). Models containing water temperature covariates tended to have lower bias and lower predictive S.D. than other models at the four-week horizon; however, the reduction in predictive S.D. corresponded to a loss in coverage (Table 3).

Despite the improvement of water temperature models over the AR model, no examined model successfully predicted the timing of peak *G. echinulata* density at the four-week horizon, and all models missed the peak by 12 or 14 weeks. Given the structure of our models (seasonal for-loop), this means that models missed the 10 September 2015 peak altogether (Fig. 6).

The unweighted model ensemble was not among the top-performing models at either the one-week or four-week forecast horizon, with a ΔPL of 0.05 ln(colonies L^{-1}) at the one-week horizon and 0.09 ln(colonies L^{-1}) at the four-week horizon (Table 3; Text S4).

Process uncertainty dominates hindcast credible intervals

Process uncertainty represented the largest proportion of uncertainty in the credible interval for all models. The proportion of the variance attributed to process uncertainty increased with hindcast horizon, largely due to a reduction in initial conditions uncertainty (Fig. 7; models not shown in Fig. 7 can be found in Fig. S14). Neither increases in model structural complexity or differences in model covariates substantially decreased the proportional contribution of process uncertainty (Fig. 8). The mean contribution of process uncertainty across the hindcasting period ranged from 73% of hindcast uncertainty in the RW model to 81% in the MinWaterTempLag model for one-week-ahead hindcasts, and from 83% in the SchmidtLag model to 93% in the AR model for four-week-ahead hindcasts. However, the relative contribution of process uncertainty to total hindcast uncertainty did vary across the hindcasting period for individual models (mean, minimum, and maximum contributions of all uncertainty sources during 2015-2016 can be found in Tables S6-S7). Excluding the RW and AR models, whose credible intervals became almost completely comprised of process error as the forecast horizon progressed, process error was sometimes as low as 54% (ΔSchmidt, SchmidtLag, WindDir) or as high as 96% (ΔSchmidt, Precip) for one-week-ahead hindcasts, and as low as 73% (SchmidtMaxLag) or as high as 95% (Precip) for four-week-ahead hindcasts.

The second largest component of uncertainty in hindcasts was due to initial conditions estimation, although this source of uncertainty quickly declined to negligible levels by the four-week-ahead forecast horizon for all models (Fig. 7; Fig. 8). Averaged across the hindcasting period, initial conditions uncertainty contributed from 13% (MinWaterTempLag; Schmidt+Temp) to 27% (RW) of the uncertainty for one-week-ahead hindcasts but comprised only from 1 % to 9% of total uncertainty for four-week ahead hindcasts. Initial conditions

uncertainty was largest (30-43% of total uncertainty) for one-week-ahead hindcasts following a week with a missing *G. echinulata* observation (Fig. S15a).

Parameter and driver error had negligible contributions to total hindcast uncertainty for both one-week-ahead and four-week-ahead hindcasts (Fig. 7; Fig. 8; Fig. S14 and Tables in Supplemental Material).

Observation uncertainty in 95% PI

Observation uncertainty was a substantial component of uncertainty for all models and τ_{obs} ranged from 1.72 to 1.89 ± 0.35 to 0.38 ln(colonies L^{-1})$^{-2}$ across models. This corresponds to a standard deviation of ~0.75 ln(colonies L^{-1}) or ~2.1 colonies L^{-1}, which is large considering that median *G. echinulata* density during the hindcasting period was 0.56 ± 2.9 colonies L^{-1}. These relatively large estimates of observation uncertainty contributed to an average increase of 0.94 ln(colonies L^{-1}) in the 95% predictive interval (PI) over the 95% credible interval (CI; mean range 4.88 ± 0.40 ln(colonies L^{-1})) across all models for one-week-ahead hindcasts (Fig. 5). The difference in PI was higher for the four-week-ahead hindcasts, with a 1.16 ln(colonies L^{-1}) increase over the 95% CI (mean CI range 5.61 ± 1.11 ln(colonies L^{-1})) across all models (Fig. 6). Again considering the relatively low density of *G. echinulata* during our hindcasting period, these 95% PI – 95% CI range differences translate to a large contribution of observation uncertainty to predicted *G. echinulata* densities (95% PI – 95% CI range differences of 2.56 colonies L^{-1} at the one-week horizon and 3.12 colonies L^{-1} at the four-week horizon).

IV. Discussion

Understanding ecological systems to better forecast future events is a critical challenge for managing resources and public health. Use of standardized ecological forecasting approaches provides a much-needed framework for prioritizing research efforts to meet this challenge. While there are numerous hypotheses and studies linking environmental drivers to the *G. echinulata* surface scums that challenge water quality management in oligotrophic lakes (e.g., Roelofs and Oglesby 1970, Istvánovics et al. 1993, Hyenstrand et al. 2000, Karlsson-Elfgren et al. 2005, Carey et al. 2014, Napiórkowska-Krzebietke and Hutorowicz 2015), few have fully evaluated the predictive influence of these environmental variables. We calibrated models to evaluate how well environmental variables that had previously been associated with cyanobacterial density explain changes in density over near-term timescales and evaluated each model for forecast skill. We demonstrate that significant explanatory variables in calibration or best-fit models are not necessarily effective driver variables in near-term ecological forecasts, and that driver variables that may adequately capture low densities may not successfully predict rare high-density events. The dominance of process and initial conditions uncertainty in our forecasts emphasizes that *G. echinulata* densities are likely a product of both growth and movement of colonies, that spatial and temporal misalignment of driver data and density observations are ongoing challenges in this forecasting system, and that imperfect observation of both *G. echinulata* density and environmental covariates substantially affect forecast skill.

Of all the environmental covariates we examined, water temperature metrics were important in both calibration and hindcast models and may be a promising suite of drivers for predicting *G. echinulata* density. Both lagged and moving average measures of water temperature (MinWaterTempLag, WaterTempMA) were positively associated with changes in

G. echinulata density and more skilled than the baseline AR model in hindcasting *G. echinulata* density at the four-week horizon. This is consistent with studies demonstrating that cyanobacteria benefit from warmer temperatures (e.g., Paerl and Huisman 2008, Carey et al. 2012b), that water temperature is a good predictor of cyanobacterial density (Rousso et al. 2020), and that antecedent conditions can affect cyanobacterial growth and phytoplankton community structure (Bormans et al. 2005, Madgwick et al. 2006). Our results further suggest that a minimum water temperature predictor (MinWaterTempLag) may be useful for forecasting *G. echinulata* density, which agrees with findings from a previous study examining predictors of *Lyngbya majuscula* blooms in an Australian bay (Hamilton et al. 2009). However, we were unable to identify any environmental covariates that improved *G. echinulata* density predictions over the AR model at the one-week horizon, suggesting that water temperature is likely not adequate to forecast cyanobacterial densities at this time scale.

Process uncertainty dominated hindcast uncertainty across all models. Neither increases in model structural complexity nor differences in model covariates substantially decreased the proportional contribution of process uncertainty to forecast uncertainty. The predominance of process uncertainty, coupled with low parameter uncertainty (Fig. 8), indicates a substantial need for research to better understand how and why *G. echinulata* densities change. Some of the environmental covariates we explored may sufficiently explain weekly differences in frequently-observed low densities but none of the models we calibrated had skill at forecasting peak abundances, which appeared and declined suddenly. In theory, it is possible that *G. echinulata* dynamics are dominated by stochasticity (e.g., Carpenter et al. 2020), in which case improvement to model structure would not effectively reduce process uncertainty. However, our results suggest that a process model more aligned with the biology of the focal cyanobacterium,

as well as more frequent sampling events, could be promising avenues for model development to reduce process uncertainty and improve forecast skill.

The low-frequency surface scum events in Lake Sunapee likely result from the compound effects of cyanobacterial population growth in the water column, recruitment of dormant cells from the sediments, movement of colonies within the lake, and accumulation on the lake surface (Roelofs and Oglesby 1970, Karlsson-Elfgren et al. 2005, Carey et al. 2014, Cyr 2017). Each of these may be best predicted by different drivers at different temporal or spatial scales, and many more years of data are likely needed to identify significant predictors of these low-frequency, high-density cyanobacterial growth events. Absent the possibility of data-driven models to predict low-frequency events, more mechanistic process structure in the forecasting model is needed. Changes in the relative importance of driver and process uncertainty in our hindcasts may elucidate when during the season currently unaccounted-for ecological processes are important and how we could better align environmental driver and *G. echinulata* density sampling in future studies. For example, one of the best-performing models at the four-week horizon (MinWaterTempLag) exhibited low driver uncertainty but high process uncertainty during the last five weeks of the 2015 sampling season (Fig. S16). This suggests that *G. echinulata* were responding to variables other than water temperature and a careful examination of other environmental conditions during this period could illuminate additional ecological processes that should be included in forecasting models. Further, incorporating more mechanistic representations of explanatory variables that were significant during model calibration but not skilled at forecasting, such as wind direction and thermal stratification (SchmidtLag), might help constrain process uncertainty. Models including both temperature-dependent growth rate equations and a process representation of the effect of thermal stratification on surface scum

formation or of colony transport via wind-driven mixing (e.g., Wallace et al. 2000, Ndong et al. 2017, Cyr 2017) might generate better forecasts. A more complex mechanistic model could also include additional life history stages of *G. echinulata* beyond vegetative growth in the water column. For example, it is well-documented that recruitment from the sediments to the pelagic zone is an important life stage for *G. echinulata*, potentially contributing 4-40% of the water column population each week (e.g., Barbiero and Welch 1992, Carey et al. 2014b).

While the contribution of driver data uncertainty (accuracy of driver measurements and forecasts) to our hindcasts was small, spatial mismatches between driver data and response variable data may also contribute to process uncertainty. Thus, the inclusion of more nearshore site variables, rather than variables collected in the deep-water pelagic zone, might reduce process uncertainty by better characterizing the effect of environmental drivers on localized nearshore processes. For example, we did not consider nearshore nutrient concentrations. *G. echinulata* can both fix nitrogen and sequester excess phosphorus in the sediments before recruiting to the water column, thereby providing its own nutrients for pelagic growth (Barbiero and Welch 1992, Cottingham et al. 2015); moreover, our study lake has very low nitrogen and phosphorus concentrations. However, it is possible that nearshore nutrient concentrations could have an effect on *G. echinulata* growth. In addition, local site variables have been found important in driving benthic recruitment (Carey et al. 2014), so inclusion of more nearshore drivers could be a complementary approach to including benthic recruitment in models.

Forecast skill in this system could also be improved by refining our estimates of initial conditions. In particular, both total hindcast variance and the proportional contribution of initial condition uncertainty exhibited large increases immediately after missing *G. echinulata* density observations, and this increase perpetuated through the four-week horizon (Fig. S11). This

suggests that increasing the spatial or temporal frequency of observations could improve forecast skill (e.g., Fox et al. 2018), as cyanobacterial densities can be spatially heterogeneous (Franks 1997, Serizawa et al. 2008, Wynne and Stumpf 2015) and change quickly on short timescales (Dokulil and Teubner 2000, Huisman and Hulot 2005, Rolland et al. 2013). Because sampling and counting *G. echinulata* is labor-intensive, increasing observational frequency might necessitate assimilating other measures of cyanobacterial abundance into forecasts, such as fluorescence-based biomass measurements (e.g., Catherine et al. 2012) and spectrophotometric pigment analysis (e.g., Küpper et al. 2007, Thrane et al. 2015). Furthermore, as phytoplankton counts are notoriously variable (Rott et al. 2007, Vuorio et al. 2007), increased spatio-temporal sampling frequency and incorporation of measures of cyanobacterial abundance besides counts might constrain the high observation uncertainty in *G. echinulata* density data, thereby improving comparisons of models to data. However, before investing in costly increased *in-situ* monitoring, the potential benefit of increased sampling effort could be determined through simulated data experiments exploring how different sampling techniques and frequencies affect forecast precision (following Dietze 2017a).

Our uncertainty partitioning results from oligotrophic lake cyanobacterial density hindcasts have some commonalities with other uncertainty partitioning efforts, contributing insight into the dominant sources of uncertainty across near-term forecasts in ecological systems. Our hindcasts were dominated by process uncertainty and emphasize the need for research to better understand the ecology of phytoplankton density changes in nutrient-poor systems. Similar results have been reported for ecological forecasts at decadal and multi-decadal timescales predicting variables ranging from forest biomass and productivity (Thomas et al. 2018) to vertebrate species distributions (Diniz-Filho et al. 2009, Watling et al. 2015). In addition, our

finding that initial conditions uncertainty is an important contributor to forecast uncertainty is consistent with terrestrial carbon forecasts at the annual scale (Fox et al. 2018) and lake chlorophyll-*a* forecasts at the weekly scale (Huang et al. 2013). However, several other aquatic and terrestrial forecasts that could leverage good process understanding found that driver data uncertainty dominated ecological forecasts (e.g., Mbogga et al. 2010, Dietze 2017b, Ouellet-Proulx et al. 2017, Jiang et al. 2018, Thomas et al. 2020). Across ecosystems, a skillful process model and correspondingly low process uncertainty are likely prerequisites for other forms of uncertainty, such as driver data uncertainty, to dominate.

Developing forecasts for low-frequency events, like cyanobacterial growth events, is especially challenging and uncertainty partitioning in these highly dynamic systems can help prioritize research to improve process understanding or increase sampling frequency in space or time. Standardized and formal uncertainty partitioning across studies and ecosystems could identify consistent or contrasting patterns in forecast skill at different horizons in ecosystems where low-frequency or rare events have significant consequences, such as cyanobacterial blooms (Kim et al. 2014) and insect (Hobbs et al. 2015) and disease outbreaks (Grünwald et al. 2000). Overall, despite considering dozens of possible environmental covariates, our hindcasts were not skilled enough to predict the sudden, infrequent increases in cyanobacterial density that cause concern for water resource managers and other stakeholders in both oligotrophic and eutrophic lakes. However, formal uncertainty partitioning provided insight on how to target data collection and modeling efforts, following Dietze et al. (2018). Even if our initial forecasting efforts are not very skilled, the process of iteratively confronting our models with data and quantitatively examining forecast uncertainty teaches us how to improve (Bauer et al. 2015). Access to data and standardized expectations for uncertainty partitioning are critical to the

iterative improvement of forecast skill. Our study was enabled both by collaborative sharing of long-term data through the Global Lake Ecological Observatory Network, which facilitated calibration and validation of hindcasting models over many years (Cottingham et al. 2020a, 2020b, LSPA et al. 2020a, 2020b), and access to publicly available R code examples of how to conduct uncertainty partitioning (https://github.com/EcoForecast/EF_Activities). As such, our study illustrates the importance of open science and findable, accessible, interoperable, and reusable (FAIR) scientific practices with respect to data and code (Wilkinson et al. 2016, Powers and Hampton 2019) to reduce barriers to adoption of techniques such as uncertainty partitioning and advance the field of ecological forecasting.

Acknowledgments

The study was initiated as part of a Global Lake Ecological Observatory Network Fellowship Program Bayesian statistics workshop. MEL led development of Bayesian state-space models with SLL and conducted hindcasts and variance partitioning, with substantial contributions from JAB, WSB, JAZ, and MCD. KLC, HAE, KCW, and CCC contributed data. BGS led publication of datasets. All authors provided feedback on the design and scope of the modeling effort, the interpretation of results, and edited and approved the final version of the manuscript. The long-term Sunapee data collection was funded by NSF (DBI-0434684, DEB-0749022, EF-0842267, EF-0842112, EF-0842125, DEB-1010862, CNS-1737424, ICER-1517823), Lake Sunapee Protective Association, Dartmouth College, Auburn Water District/Lewiston Water Division, and Bates College. The forecasting project was funded by NSF MSB DEB-1638575, DEB-1137327, DEB-1702991, and DEB-1638577. MEL and CCC were supported by NSF CNS-

1737424, DEB-1753639, DBI-1933016, and MSB DEB-1926050. MEL was supported by a Virginia Water Resources Research Center William R. Walker Graduate Research Fellow Award and a Virginia Tech College of Science Make-A-Difference Roundtable Scholarship. JAB was supported by funding from the Ecology, Evolution, Environment, and Society program at Dartmouth College and a Midge Eliassen Fellowship. The Eliassen and Fichter families provided generous access to study sites. Special thanks to all of the participants in the December 2017 Global Lake Ecological Observatory Network (GLEON) Bayesian statistics workshop for idea development, to John Foster and other participants in the January 2019 Near-term Ecological Forecasting Initiative workshop for assistance with model development, and to the Spring 2020 Ecological Forecasting seminar class at Virginia Tech for help with literature review, as well as to Hilary Dugan and Nicole Ward for help downloading and processing NLDAS data. GLEON and Ecological Forecasting Initiative (EFI) colleagues provided helpful comments.

Literature Cited

Barbiero, R. P., and E. B. Welch. 1992. Contribution of benthic blue-green algal recruitment to lake populations and phosphorus translocation. Freshwater Biology 27:249–260.

Bauer, P., A. Thorpe, and G. Brunet. 2015. The quiet revolution of numerical weather prediction. Nature 525:47–55.

Bormans, M., P. W. Ford, and L. Fabbro. 2005. Spatial and temporal variability in cyanobacterial populations controlled by physical processes. Journal of Plankton Research 27:61–70.

688 Carey, C. C., H. A. Ewing, K. L. Cottingham, K. C. Weathers, R. Q. Thomas, and J. F. Haney.
689 2012a. Occurrence and toxicity of the cyanobacterium Gloeotrichia echinulata in low-
690 nutrient lakes in the northeastern United States. Aquatic Ecology 46:395–409.
691 Carey, C. C., B. W. Ibelings, E. P. Hoffmann, D. P. Hamilton, and J. D. Brookes. 2012b. Eco-
692 physiological adaptations that favour freshwater cyanobacteria in a changing climate. Water
693 Research 46:1394–1407.
694 Carey, C. C., K. C. Weathers, and K. L. Cottingham. 2008. Gloeotrichia echinulata blooms in an
695 oligotrophic lake: Helpful insights from eutrophic lakes. Journal of Plankton Research
696 30:893–904.
697 Carey, C. C., K. C. Weathers, H. A. Ewing, M. L. Greer, and K. L. Cottingham. 2014. Spatial
698 and temporal variability in recruitment of the cyanobacterium Gloeotrichia echinulata in an
699 oligotrophic lake. Freshwater Science 33:577–592.
700 Carlson, R. E. 1977. A trophic state index for lakes. Limnology and Oceanography 22:361–369.
701 Carlson, R., and J. Simpson. 1996. A Coordinator's Guide to Volunteer Lake Monitoring
702 Methods. North American Lake Management Society.
703 Carpenter, S. R., B. M. S. Arani, P. C. Hanson, M. Scheffer, E. H. Stanley, and E. Van Nes.
704 2020. Stochastic dynamics of Cyanobacteria in long-term high-frequency observations of a
705 eutrophic lake. Limnology and Oceanography Letters.
706 Catherine, A., N. Escoffier, A. Belhocine, A. B. Nasri, S. Hamlaoui, C. Yéprémian, C. Bernard,
707 and M. Troussellier. 2012. On the use of the FluoroProbe®, a phytoplankton quantification
708 method based on fluorescence excitation spectra for large-scale surveys of lakes and
709 reservoirs. Water Research 46:1771–1784.
710 Clark, J. 2007. Models for ecological data. Princeton University Press, Princeton, NJ, USA.

711 Clark, J. S., S. R. Carpenter, M. Barber, S. Collins, A. Dobson, J. A. Foley, D. M. Lodge, M.
712 Pascual, J. Pielke R., W. Pizer, C. Pringle, W. V. Reid, K. A. Rose, O. Sala, W. H.
713 Schlesinger, D. H. Wall, and D. Wear. 2001. Ecological forecasts: An emerging imperative.
714 Science 293:657–660.
715 Cobourn, K. M., C. C. Carey, K. J. Boyle, C. Duffy, H. A. Dugan, K. J. Farrell, L. Fitchett, P. C.
716 Hanson, J. A. Hart, V. R. Henson, A. L. Hetherington, A. R. Kemanian, L. G. Rudstam, L.
717 Shu, P. A. Soranno, M. G. Sorice, J. Stachelek, N. K. Ward, K. C. Weathers, W. Weng, and
718 Y. Zhang. 2018. From concept to practice to policy: modeling coupled natural and human
719 systems in lake catchments. Ecosphere 9:1–15.
720 Cottingham, K. L. 2020. Surface pelagic total nitrogen concentrations in Lake Sunapee, USA
721 2009 to 2012. Environmental Data Initiative.
722 Cottingham, K. L., C. C. Carey, and K. C. Weathers. 2020a. Gloeotrichia echinulata density at
723 four nearshore sites in Lake Sunapee, NH, USA from 2005-2016 ver. 2. Environmental
724 Data Initiative.
725 Cottingham, K. L., C. C. Carey, and K. C. Weathers. 2020b. High-frequency temperature data
726 from four near-shore sites, Lake Sunapee, NH, USA, 2006-2018. Environmental Data
727 Initiative.
728 Cottingham, K. L., H. A. Ewing, M. L. Greer, C. C. Carey, and K. C. Weathers. 2015.
729 Cyanobacteria as biological drivers of lake nitrogen and phosphorus cycling. Ecosphere
730 6:1–19.
731 Cyr, H. 2017. Winds and the distribution of nearshore phytoplankton in a stratified lake. Water
732 Research 122:114–127.
733

Denwood, M., and M. Plummer. 2019. Interface Utilities, Model Templates, Parallel Computing Methods and Additional Distributions for MCMC Models in JAGS v. 2.0.4-2.

Dietze, M. C. 2017a. Ecological Forecasting. 1st edition. Princeton University Press, Princeton, NJ, USA.

Dietze, M. C. 2017b. Prediction in ecology: A first-principles framework: A. Ecological Applications 27:2048–2060.

Dietze, M. C., A. Fox, L. M. Beck-Johnson, J. L. Betancourt, M. B. Hooten, C. S. Jarnevich, T. H. Keitt, M. A. Kenney, C. M. Laney, L. G. Larsen, H. W. Loescher, C. K. Lunch, B. C. Pijanowski, J. T. Randerson, E. K. Read, A. T. Tredennick, R. Vargas, K. C. Weathers, and E. P. White. 2018. Iterative near-term ecological forecasting: Needs, opportunities, and challenges. Proceedings of the National Academy of Sciences of the United States of America 115:1424–1432.

Diniz-Filho, A. F., L. M. Bini, T. F. Rangel, R. D. Loyola, C. Hof, D. Nogue, and M. B. Arau. 2009. Partitioning and mapping uncertainties in ensembles of forecasts of species turnover under climate change. Ecography 32:897–906.

Dodds, W., W. W. Bouska, J. L. Eitzmann, T. J. Pilger, K. L. Pitts, A. J. Riley, J. T. Schloesser, and D. J. Thornbrugh. 2009. Eutrophication of U.S. Freshwaters: Analysis of Potential Economic Damages. Environmental Science & Technology 43:12–19.

Dokulil, M. T., and K. Teubner. 2000. Cyanobacterial Dominance in Lakes. Hydrobiologia 438:1–12.

van Dolah, E. R., M. Paolisso, K. Sellner, and A. Place. 2015. Employing a socio-ecological systems approach to engage harmful algal bloom stakeholders. Aquatic Ecology 50:1–18.

de Eyto, E., E. Jennings, E. Ryder, K. Sparber, M. Dillane, C. Dalton, and R. Poole. 2016. Response of a humic lake ecosystem to an extreme precipitation event: physical, chemical, and biological implications. Inland Waters:483–498.

Fox, A. M., T. J. Hoar, J. L. Anderson, A. F. Arellano, W. K. Smith, M. E. Litvak, N. MacBean, D. S. Schimel, and D. J. P. Moore. 2018. Evaluation of a Data Assimilation System for Land Surface Models Using CLM4.5. Journal of Advances in Modeling Earth Systems 10:2471–2494.

Franks, P. J. S. 1997. Spatial patterns in dense algal blooms. Limnology and Oceanography 42:1297–1305.

Freeman, E. C., I. F. Creed, B. Jones, and A.-K. Bergstrom. 2020. Global changes may be promoting a rise in select cyanobacteria in nutrient-poor northern lakes. Global Change Biology.

Gelfand, A. E., and S. K. Ghosh. 1998. Model Choice : A Minimum Posterior Predictive Loss Approach. Biometrika Trust 85:1–11.

Gertner, G., P. Parysow, and B. Guan. 1996. Projection Variance Partitioning of a Conceptual Forest Growth Model with Orthogonal Polynomials. Forest Science 42:474–486.

Gibson, G., R. Carlson, J. Simpson, E. Smeltzer, J. Gerritson, S. Chapra, S. Heiskary, J. Jones, and R. Kennedy. 2000. USEPA Nutrient Criteria Technical Guidance Manual Lakes and Reservoirs. United States Environmental Protection Agency.

Grünwald, N. J., O. A. Rubio-Covarrubias, and W. E. Fry. 2000. Potato late-blight management in the Toluca Valley: Forecasts and resistant cultivars. Plant Disease 84:410–416.

Hamilton, G., R. McVinish, and K. Mengersen. 2009. Bayesian model averaging for harmful algal bloom prediction. Ecological Applications 19:1805–1814.

780 Hobbs, N. T., C. Geremia, J. Treanor, R. Wallen, P. J. White, M. B. Hooten, and J. C. Rhyan.
781 2015. State-space modeling to support management of brucellosis in the Yellowstone bison
782 population. Ecological Monographs 85:525–556.
783 Hobbs, N. T., and M. B. Hooten. 2015. Bayesian Models: A Statistical Primer for Ecologists. 1st
784 edition. Princeton University Press, Princeton, NJ, USA.
785 Hobday, A. J., J. R. Hartog, J. P. Manderson, K. E. Mills, M. J. Oliver, A. J. Pershing, and S.
786 Siedlecki. 2019. Ethical considerations and unanticipated consequences associated with
787 ecological forecasting for marine resources. ICES Journal of Marine Science 76:1244–1256.
788 Huang, J., J. Gao, J. Liu, and Y. Zhang. 2013. State and parameter update of a hydrodynamic-
789 phytoplankton model using ensemble Kalman filter. Ecological Modelling 263:81–91.
790 Huisman, J., and F. D. Hulot. 2005. Population Dynamics of Harmful Cyanobacteria. Pages 143–
791 176 *in* J. Huisman, H. C. P. Matthijs, and P. M. Visser, editors. Harmful Cyanobacteria.
792 Aquatic Ecology Series, vol. 3 Springer, Dordrecht.
793 Hyenstrand, P., E. Rydin, and M. Gunnerhed. 2000. Response of pelagic cyanobacteria to iron
794 additions--enclosure experiments from Lake Erken. Journal of Plankton Research 22:1113–
795 1126.
796 Ibelings, B. W., M. Bormans, J. Fastner, and P. M. Visser. 2016. CYANOCOST special issue on
797 cyanobacterial blooms: synopsis-a critical review of the management options for their
798 prevention, control and mitigation. Aquatic Ecology 50:1–11.
799 Idso, S. B. 1973. On the concept of lake stability. Limnol. Oceanogr. 18:681–683.
800 Istvánovics, V., K. Pettersson, M. A. Rodrigo, D. Pierson, J. Padišk, and W. Colom. 1993.
801 Gloeotrichia echinulata, a colonial cyanobacterium with a unique phosphorus uptake and
802 life strategy. Journal of Plankton Research 15:531–552.

803 Janssen, A. B., J. H. Janse, A. H. Beusen, M. Chang, J. A. Harrison, I. Huttunen, X. Kong, J.
804 Rost, S. Teurlincx, T. A. Troost, D. van Wijk, and W. M. Mooij. 2019. How to model algal
805 blooms in any lake on earth. Current Opinion in Environmental Sustainability 36:1–10.
806 Jennings, E., S. Jones, L. Arvola, P. A. Staehr, E. Gaiser, I. D. Jones, K. C. Weathers, G. A.
807 Weyhenmeyer, C. Y. Chiu, and E. De Eyto. 2012. Effects of weather-related episodic
808 events in lakes: an analysis based on high-frequency data. Freshwater Biology 57:589–601.
809 Jiang, J., Y. Huang, S. Ma, M. Stacy, Z. Shi, D. M. Ricciuto, P. J. Hanson, and Y. Luo. 2018.
810 Forecasting Responses of a Northern Peatland Carbon Cycle to Elevated CO2 and a
811 Gradient of Experimental Warming. Journal of Geophysical Research: Biogeosciences
812 123:1057–1071.
813 Johansson, M. A., K. M. Apfeldorf, S. Dobson, J. Devita, A. L. Buczak, B. Baugher, L. J. Moniz,
814 T. Bagley, S. M. Babin, E. Guven, T. K. Yamana, J. Shaman, T. Moschou, N. Lothian, A.
815 Lane, G. Osborne, G. Jiang, L. C. Brooks, D. C. Farrow, S. Hyun, R. J. Tibshirani, R.
816 Rosenfeld, J. Lessler, N. G. Reich, D. A. T. Cummings, S. A. Lauer, S. M. Moore, H. E.
817 Clapham, R. Lowe, T. C. Bailey, M. García-Díez, M. S. Carvalho, X. Rodó, T. Sardar, R.
818 Paul, E. L. Ray, K. Sakrejda, A. C. Brown, X. Meng, O. Osoba, R. Vardavas, D. Manheim,
819 M. Moore, D. M. Rao, T. C. Porco, S. Ackley, F. Liu, L. Worden, M. Convertino, Y. Liu,
820 A. Reddy, E. Ortiz, J. Rivero, H. Brito, A. Juarrero, L. R. Johnson, R. B. Gramacy, J. M.
821 Cohen, E. A. Mordecai, C. C. Murdock, J. R. Rohr, S. J. Ryan, A. M. Stewart-Ibarra, D. P.
822 Weikel, A. Jutla, R. Khan, M. Poultney, R. R. Colwell, B. Rivera-García, C. M. Barker, J.
823 E. Bell, M. Biggerstaff, D. Swerdlow, L. Mier-Y-Teran-Romero, B. M. Forshey, J. Trtanj,
824 J. Asher, M. Clay, H. S. Margolis, A. M. Hebbeler, D. George, and J. P. Chretien. 2019. An
825 open challenge to advance probabilistic forecasting for dengue epidemics. Proceedings of

the National Academy of Sciences of the United States of America 116:24268–24274.

Jolliffe, I., and D. Stephenson. 2003. Forecast Verification : A Practitioner's Guide in Atmospheric Science. 2nd edition. Wiley, Chichester, West Sussex, England.

Karlsson-Elfgren, I., P. Hyenstrand, and E. Riydin. 2005. Pelagic growth and colony division of Gloeotrichia echinulata in Lake Erken. Journal of Plankton Research 27:145–151.

Karlsson-Elfgren, I., K. Rengefors, and S. Gustafsson. 2004. Factors regulating recruitment from the sediment to the water column in the bloom-forming cyanobacterium Gloeotrichia echinulata. Freshwater Biology 49:265–273.

Kauffman, G. J. 2016. Economic Value of Nature and Ecosystems in the Delaware River Basin. Journal of Contemporary Water Research & Education 158:98–119.

Kim, K., M. Park, J. H. Min, I. Ryu, M. R. Kang, and L. J. Park. 2014. Simulation of algal bloom dynamics in a river with the ensemble Kalman filter. Journal of Hydrology 519:2810–2821.

Kuha, J., L. Arvola, P. Hanson, J. Huotari, T. Huttula, J. Juntunen, M. Jarvinen, K. Kallio, M. Ketola, K. Kuoppamaki, A. Lepisto, A. Lohila, R. Paavola, J. Vuorenmaa, L. Winslow, and J. Karjalainen. 2016. Response of boreal lakes to episodic weather-induced events. Inland Waters 6:523–534.

Kuikka, S., J. Vanhatalo, H. Pulkkinen, S. Mäntyniemi, and J. Corander. 2014. Experience in Bayesian Inference in Baltic Salmon Management. Statistical Science 29:42–49.

Küpper, H., S. Seibert, and A. Parameswaran. 2007. Fast, sensitive, and inexpensive alternative to analytical pigment HPLC: Quantification of chlorophylls and carotenoids in crude extracts by fitting with Gauss peak spectra. Analytical Chemistry 79:7611–7627.

Lofton, M. E., J. A. Brentrup, W. S. Beck, J. A. Zwart, R. Bhattacharya, L. S. Brighenti, S. H. Burnet, I. M. McCullough, B. G. Steele, C. C. Carey, K. L. Cottingham, M. C. Dietze, H. A. Ewing, K. C. Weathers, and S. L. LaDeau. 2020. Lake Sunapee Gloeotrichia echinulata density near-term hindcasts from 2015-2016 and meteorological model driver data, including shortwave radiation and precipitation from 2009-2016 ver 4. Environmental Data Initiative staging environment.

LSPA; Lake Sunapee Protective Association, K. C. Weathers, and B. G. Steele. 2020. Lake Sunapee Instrumented Buoy: High Frequency Water Temperature and Dissolved Oxygen Data – 2007-2019. Environmental Data Initiative.

LSPA; Lake Sunapee Protective Association, B. Steele, and K. C. Weathers. 2020. Lake Sunapee High Frequency Weather Data measured on buoy - 2007-2017 ver. 3. Environmental Data Initiative.

Madgwick, G., I. D. Jones, S. J. Thackeray, J. A. Elliott, and H. J. Miller. 2006. Phytoplankton communities and antecedent conditions: high resolution sampling in Esthwaite Water. Freshwater Biology 51:1798–1810.

Massoud, E. C., J. Huisman, E. Beninca, M. C. Dietze, W. Bouten, and J. A. Vrugt. 2018. Probing the limits of predictability: data assimilation of chaotic dynamics in complex food webs. Ecology Letters 21:93–103.

Mbogga, M. S., X. Wang, and A. Hamann. 2010. Bioclimate envelope model predictions for natural resource management: dealing with uncertainty. Journal of Applied Ecology 47:731–740.

McGowan, J. A., E. R. Deyle, H. Ye, M. L. Carter, C. T. Perretti, M. Hilbern, K. Seger, A. de Verniel, and G. Sugihara. 2017. Predicting coastal algal blooms in Southern California 98:1419–1433.

Mueller, H., D. P. Hamilton, and G. J. Doole. 2016. Evaluating services and damage costs of degradation of a major lake ecosystem. Ecosystem Services 22:370–380.

Napiórkowska-Krzebietke, A., and A. Hutorowicz. 2015. The physicochemical background for the development of potentially harmful cyanobacterium Gloeotrichia echinulata J. S. Smith ex Richt. Journal of Elementology 20:363–376.

Ndong, M., D. Bird, T. Nguyen Quang, R. Kahawita, D. Hamilton, M. L. de Boutray, M. Prévost, and S. Dorner. 2017. A novel Eulerian approach for modelling cyanobacteria movement: Thin layer formation and recurrent risk to drinking water intakes. Water Research 127:191–203.

O'Neil, J. M., T. W. Davis, M. A. Burford, and C. J. Gobler. 2012. The rise of harmful cyanobacteria blooms: The potential roles of eutrophication and climate change. Harmful Algae 14:313–334.

Ouellet-Proulx, S., O. Chimi Chiadjeu, M. A. Boucher, and A. St-Hilaire. 2017. Assimilation of water temperature and discharge data for ensemble water temperature forecasting. Journal of Hydrology 554:342–359.

Paerl, H. W., N. S. Hall, and E. S. Calandrino. 2011. Controlling harmful cyanobacterial blooms in a world experiencing anthropogenic and climatic-induced change. Science of the Total Environment 409:1739–1745.

Paerl, H. W., and J. Huisman. 2008. Blooms Like It Hot. Science 320:57–58.

Paerl, H. W., and T. G. Otten. 2013. Harmful Cyanobacterial Blooms: Causes, Consequences, and Controls. Microbial Ecology 65:995–1010.

Page, T., P. J. Smith, K. J. Beven, I. D. Jones, J. A. Elliott, S. C. Maberly, E. B. Mackay, M. De Ville, and H. Feuchtmayr. 2017. Constraining uncertainty and process-representation in an algal community lake model using high frequency in-lake observations. Ecological Modelling 357:1–13.

Page, T., P. J. Smith, K. J. Beven, I. D. Jones, J. A. Elliott, S. C. Maberly, E. B. Mackay, M. De Ville, and H. Feuchtmayr. 2018. Adaptive forecasting of phytoplankton communities. Water Research 134:74–85.

Plummer, M., A. Stukalov, and M. Denwood. 2019. Bayesian Graphical Models using MCMC.

Powers, S. M., and S. E. Hampton. 2019. Open science, reproducibility, and transparency in ecology. Ecological Applications 29:1–8.

Ravindranath, A., N. Devineni, and P. Kolesar. 2016. An environmental perspective on the water management policies of the Upper Delaware River Basin. Water Policy 18:1399–1419.

Reynolds, C. S., J. Alex Elliott, and M. A. Frassl. 2014. Predictive utility of trait-separated phytoplankton groups: A robust approach to modeling population dynamics. Journal of Great Lakes Research 40:143–150.

Rigosi, A., W. Fleenor, and F. Rueda. 2010. State-of-the-art and recent progress in phytoplankton succession modelling. Environmental Reviews 18:423–440.

Roelofs, T. D., and R. T. Oglesby. 1970. Ecological Observations on the Planktonic Cyanophyte Gleotrichia Echinulata. Limnol. Oceanogr. 15:224–229.

Rolland, D. C., S. Bourget, A. Warren, I. Laurion, and W. F. Vincent. 2013. Extreme variability of cyanobacterial blooms in an urban drinking water supply. Journal of Plankton Research 35:744–758.

Rott, E., N. Salmaso, and E. Hoehn. 2007. Quality control of Utermöhl-based phytoplankton counting and biovolume estimates - An easy task or a Gordian knot? Hydrobiologia 578:141–146.

Rousso, B. Z., E. Bertone, R. Stewart, and D. P. Hamilton. 2020. A systematic literature review of forecasting and predictive models for cyanobacteria blooms in freshwater lakes. Water Research.

Schindler, D. W., and J. R. Vallentyne. 2008. The algal bowl: overfertilization of the world's freshwaters and estuaries. 1st edition. University of Alberta Press, Edmonton.

Serizawa, H., T. Amemiya, and K. Itoh. 2008. Patchiness in a minimal nutrient - phytoplankton model. Journal of Biosciences 33:391–403.

Shuman, F. G. 1989. History of Numerical Weather Prediction at the National Meteorological Center. Weather and Forecasting 4:286–296.

Stoddard, J. L., J. Van Sickle, A. T. Herlihy, J. Brahney, S. Paulsen, D. V. Peck, R. Mitchell, and A. I. Pollard. 2016. Continental-Scale Increase in Lake and Stream Phosphorus: Are Oligotrophic Systems Disappearing in the United States? Environmental Science and Technology 50:3409–3415.

Stroom, J. M., and W. E. A. Kardinaal. 2016. How to combat cyanobacterial blooms: strategy toward preventive lake restoration and reactive control measures. Aquatic Ecology 50:1–36.

941 Stumpf, R. P., Mi. C. Tomlinson, J. A. Calkins, B. Kirkpatrick, K. Fisher, K. Nierenberg, R.
942 Currier, and T. T. Wynne. 2009. Skill assessment for an operational algal bloom forecast
943 system. Journal of Marine Systems 76:151–161.
944 Thomas, R. Q., R. J. Figueiredo, V. Daneshmand, B. J. Bookout, L. K. Puckett, and C. C. Carey.
945 2020. A near-term iterative forecasting system successfully predicts reservoir
946 hydrodynamics and partitions uncertainty. bioRxiv.
947 Thomas, R. Q., A. L. Jersild, E. B. Brooks, V. A. Thomas, and R. H. Wynne. 2018. A mid-
948 century ecological forecast with partitioned uncertainty predicts increases in loblolly pine
949 forest productivity. Ecological Applications 28:1503–1519.
950 Thrane, J. E., M. Kyle, M. Striebel, S. Haande, M. Grung, T. Rohrlack, and T. Andersen. 2015.
951 Spectrophotometric analysis of pigments: A critical assessment of a high-throughput
952 method for analysis of algal pigment mixtures by spectral deconvolution. PLoS ONE 10:1–
953 24.
954 U.S. EPA. 1991. Guidance manual for compliance with the filtration and disinfection
955 requirements for public water systems using surface water sources. United States
956 Environmental Protection Agency, Washington, D.C.
957 Valle, D., C. L. Staudhammer, W. P. Cropper, and P. R. Van Gardingen. 2009. The importance
958 of multimodel projections to assess uncertainty in projections from simulation models.
959 Ecological Applications 19:1680–1692.
960 Le Vu, B., B. Vinçon-Leite, B. J. Lemaire, N. Bensoussan, M. Calzas, C. Drezen, J. F.
961 Deroubaix, N. Escoffier, Y. Dégrés, C. Freissinet, A. Groleau, J. F. Humbert, G. Paolini, F.
962 Prévot, C. Quiblier, E. Rioust, and B. Tassin. 2011. High-frequency monitoring of
963 phytoplankton dynamics within the European water framework directive: Application to

964 metalimnetic cyanobacteria. Biogeochemistry 106:229–242.
965 Vuorio, K., L. Lepistö, and A. L. Holopainen. 2007. Intercalibrations of freshwater
966 phytoplankton analyses. Boreal Environment Research 12:561–569.
967 Wallace, B. B., M. C. Bailey, and D. P. Hamilton. 2000. Simulation of vertical position of
968 buoyancy regulating microcystis aeruginosa in a shallow eutrophic lake. Aquatic Sciences
969 62:320–333.
970 Wang, G., T. Oyana, M. Zhang, S. Adu-prah, S. Zeng, H. Lin, and J. Se. 2009. Mapping and
971 spatial uncertainty analysis of forest vegetation carbon by combining national forest
972 inventory data and satellite images. Forest Ecology and Management 258:1275–1283.
973 Watling, J. I., L. A. Brandt, D. N. Bucklin, I. Fujisaki, F. J. Mazzotti, S. S. Roma, and C.
974 Speroterra. 2015. Performance metrics and variance partitioning reveal sources of
975 uncertainty in species distribution models. Ecological Modelling 309–310:48–59.
976 Wilkinson, M. D., M. Dumontier, Ij. J. Aalbersberg, G. Appleton, M. Axton, A. Baak, N.
977 Blomberg, J.-W. Boiten, L. B. da Silva Santos, P. E. Bourne, J. Bouwman, A. J. Brookes, T.
978 Clark, M. Crosas, I. Dillo, O. Dumon, S. Edmunds, C. T. Evelo, R. Finkers, A. Gonzalez-
979 Beltran, A. J. G. Gray, P. Groth, C. Goble, J. S. Grethe, J. Heringa, P. A. . 't Hoen, R.
980 Hooft, T. Kuhn, R. Kok, J. Kok, S. J. Lusher, M. E. Martone, A. Mons, A. L. Packer, B.
981 Persson, P. Rocca-Serra, M. Roos, R. van Schaik, S.-A. Sansone, E. Schultes, T. Sengstag,
982 T. Slater, G. Strawn, M. a. Swertz, M. Thompson, J. van der Lei, E. van Mulligen, J.
983 Velterop, A. Waagmeester, P. Wittenburg, K. Wolstencroft, J. Zhao, and B. Mons. 2016.
984 The FAIR Guiding Principles for scientific data management and stewardship. Scientific
985 Data 3:160018.
986

Wilson, M. A., and S. R. Carpenter. 1999. Economic valuation of freshwater ecosystem services in the United States: 1971-1997. Ecological Applications 9:772–783.

Winter, J. G., A. M. Desellas, R. Fletcher, L. Heintsch, A. Morley, L. Nakamoto, and K. Utsumi. 2011. Algal blooms in Ontario, Canada: Increases in reports since 1994. Lake and Reservoir Management 27:107–114.

Wynne, T. T., and R. P. Stumpf. 2015. Spatial and temporal patterns in the seasonal distribution of toxic cyanobacteria in western Lake Erie from 2002–2014. Toxins 7:1649–1663.

Tables

Table 1: Terms associated with partitioning uncertainty in ecological models and forecasts. Definitions are adapted from Dietze (2017a) unless otherwise specified.

Term	Definition	Example
Credible interval	Interval within which a parameter or model prediction falls with a specified probability; does not include observation uncertainty	95% interval of possible latent values of chorophyll-*a* forecasted for tomorrow, incorporating initial conditions, process, parameter, and driver data uncertainty
Driver data uncertainty	Uncertainty arising from observation uncertainty in the estimate or measurement of driver data (environmental predictors of the forecasted state)	Uncertainty in observations of soil temperature needed to drive a soil respiration model; uncertainty in weather forecasts
Hindcast	Predictions of a past time period with specified uncertainty using data (withheld from model calibration) that are iteratively assimilated into the model (Jolliffe and Stephenson 2003)	Making model predictions for tick abundances observed two years ago using a model calibrated to observations from ten years prior.
Initial conditions uncertainty	Uncertainty associated with the starting conditions of a forecasting model run	Uncertainty in initial focal states, such as fish abundance, chlorophyll-a, or soil carbon stock
Observation uncertainty	Difference between the observed data and the true (latent) state that the model is designed to predict; does not propagate forward, so it does not affect the credible interval.	Calibration uncertainty in a temperature sensor; sampling uncertainty when estimating species abundance
Parameter uncertainty	Variance around the model parameter estimates	Uncertainty in the growth rate parameter in a timber yield model
Predictive interval	Interval within which predicted observations are expected to fall with a specified probability; includes observation uncertainty; should be used when comparing models to observed data	95% interval of possible observations of chorophyll-*a* forecasted for tomorrow
Process uncertainty	Uncertainty due to model specification (ecological processes that are simplified, absent, or incorrectly represented by the model) or inherent stochasticity in the system	Uncertainty arising from not including an important life history stage in a population growth model; uncertainty arising from demographic stochasticity in plankton communities
Random effects uncertainty	Uncertainty associated with estimation of random effects, which are used to describe shared variance across groups in space and time	Uncertainty in the value of a random site effect in a metacommunity model including many different sampling sites

Table 2: List of Bayesian state-space models and covariates. m_t is the latent state of *G. echinulata* density at time *t*, *N()* represents a normal distribution with mean and precision (τ_{proc}). *x*, *x1* and *x2* are environmental covariates in single-covariate and two-covariate models. $\boldsymbol{\beta}$ represents parameters for the process model equations.

Model name	Model description	Process model	Covariates
RW	Random walk	$m_{t+1} = N(m_t, \tau_{proc})$	
AR	Autoregressive with one lag (AR(1))	$m_{t+1} = N\left((\beta_0 + \beta_1 * m_t), \tau_{proc}\right)$	
MinWaterTemp	AR(1) with a single linear covariate	$m_{t+1} = N\left((\beta_0 + \beta_1 * m_t + \beta_2 * x_{t+1}), \tau_{proc}\right)$	minimum water temperature on sampling day
MinWaterTempLag	AR(1) with a single linear covariate	$m_{t+1} = N\left((\beta_0 + \beta_1 * m_t + \beta_2 * x_t), \tau_{proc}\right)$	minimum water temperature 1 week prior to the sampling day
WaterTempMA	AR(1) with a single linear covariate	$m_{t+1} = N\left((\beta_0 + \beta_1 * m_t + \beta_2 * x_t), \tau_{proc}\right)$	seven-day moving average of water temperature including the sampling day
ΔSchmidt	AR(1) with a single linear covariate	$m_{t+1} = N\left((\beta_0 + \beta_1 * m_t + \beta_2 * (x_{t+1} - x_t)), \tau_{proc}\right)$	difference in median Schmidt stability between 1 week prior to the sampling day and the sampling day
SchmidtLag	AR(1) with a single linear covariate	$m_{t+1} = N\left((\beta_0 + \beta_1 * m_t + \beta_2 * x_t), \tau_{proc}\right)$	maximum Schmidt stability 1 week prior to sthe sampling day
WindDir	AR(1) with a single linear covariate	$m_{t+1} = N\left((\beta_0 + \beta_1 * m_t + \beta_2 * x_t), \tau_{proc}\right)$	proportion of daily wind measurements blowing towards Site 1 with a two-day lag
Precip	AR(1) with a single linear covariate	$m_{t+1} = N\left((\beta_0 + \beta_1 * m_t + \beta_2 * x_t), \tau_{proc}\right)$	sum of daily precipitation on the sampling day
GDD	AR(1) with a single quadratic covariate	$m_{t+1} = N\left((\beta_0 + \beta_1 * m_t + \beta_2 * x_t + \beta_3 * x_t^2), \tau_{proc}\right)$	growing degree days
Schmidt+Temp	AR(1) with two linear covariates	$m_{t+1} = N\left((\beta_0 + \beta_1 * m_t + \beta_2 * x1_t + \beta_3 * x2_t), \tau_{proc}\right)$	difference in median Schmidt stability between 1 week prior the sampling day and the sampling day and seven-day moving average of water temperature including the sampling day
Schmidt+Precip	AR(1) with two linear covariates	$m_{t+1} = N\left((\beta_0 + \beta_1 * m_t + \beta_2 * x1_t + \beta_3 * x2_t), \tau_{proc}\right)$	difference in median Schmidt stability between the previous sampling day and the day of sampling and sum of daily precipitation on the sampling day
Temp+Precip	AR(1) with two linear covariates	$m_{t+1} = N\left((\beta_0 + \beta_1 * m_t + \beta_2 * x1_t + \beta_3 * x2_t), \tau_{proc}\right)$	seven-day moving average of water temperature including the sampling day and sum of daily precipitation on the sampling day
Precip+GDD	AR(1) with one linear and one quadratic covariate	$m_{t+1} = N\left((\beta_0 + \beta_1 * m_t + \beta_2 * x1_t + \beta_3 * x2_t + \beta_4 * x2_t^2), \tau_{proc}\right)$	sum of daily precipitation on the sampling day and growing degree days

Table 3: Hindcasting results across models for the 2015-2016 hindcasting period. RMSE = root mean square error; Predictive variance = mean variance of the predictive interval; Predictive loss = $\sqrt{RMSE^2 + predictive\ variance}$; Δ Predictive loss = the difference between predictive loss for each model and the best-performing model for that forecast horizon; Coverage = the percent of observations falling within the 95% predictive interval; Peak timing = the number of weeks between peak *G. echinulata* density during the hindcasting period and when the model predicted peak density; Bias = mean difference between median predicted and observed values. Note that all assessment metrics are conducted on log-transformed data except for mean bias. *best-performing models at either the one-week or four-week forecast horizon based on evaluation of Δ Predictive loss.

	RMSE *natural log colonies L^{-1}*		**Predictive S.D.** *natural log colonies L^{-2}*		**Predictive loss** *natural log colonies L^{-2}*		**Δ Predictive loss (ΔPL)** *natural log colonies L^{-2}*		**Coverage** *%*		**Peak timing** *weeks*		**Bias** *colonies L^{-1}*	
Model name	1 wk	4 wk	1 wk	4 wk	1 wk	4 wk	1 wk	4 wk	1 wk	4 wk	1 wk	4 wk	1 wk	4 wk
RW	1.89	2.23	1.63	2.98	2.5	3.72	0.25	1.3	97.2	100	1	14	-0.41	-0.96
AR*	1.67	1.61	1.51	2.08	2.25	2.63	0	0.21	97.2	100	1	14	-0.92	-1.52
MinWaterTemp	1.82	1.59	1.43	1.83	2.31	2.43	0.06	0.01	94.4	93.5	14	12	-0.93	-1.41
MinWaterTempLag*	1.79	1.62	1.45	1.79	2.3	2.42	0.05	0	91.7	87.1	14	12	-1	-1.45
WaterTempMA*	1.78	1.59	1.45	1.83	2.3	2.42	0.05	0	94.4	93.5	14	12	-0.95	-1.42
ΔSchmidt*	1.66	1.62	1.52	2.08	2.25	2.63	0	0.21	94.4	100	1	14	-0.91	-1.52
SchmidtLag	1.75	1.58	1.46	2.04	2.28	2.58	0.03	0.16	97.2	100	14	14	-0.9	-1.41
WindDir	1.78	1.55	1.5	2	2.33	2.53	0.08	0.11	94.4	100	1	14	-0.96	-1.51
Precip*	1.66	1.62	1.52	2.09	2.25	2.64	0	0.22	94.4	100	1	14	-0.92	-1.51
GDD	1.84	1.59	1.43	1.84	2.33	2.43	0.08	0.01	94.4	96.8	14	12	-1.08	-1.41
Schmidt+Temp*	1.79	1.61	1.46	1.81	2.31	2.42	0.06	0	91.7	87.1	14	14	-0.97	-1.44
Schmidt+Precip	1.66	1.62	1.53	2.08	2.26	2.64	0.01	0.22	97.2	100	1	14	-0.92	-1.52
Temp+Precip	1.78	1.61	1.46	1.83	2.3	2.43	0.05	0.01	94.4	93.5	14	12	-0.96	-1.43
Precip+GDD	1.81	1.59	1.44	1.84	2.31	2.43	0.06	0.01	97.2	96.8	14	14	-0.88	-1.31
Ensemble	1.76	1.55	1.49	1.97	2.3	2.51	0.05	0.09	97.2	100	14	14	-0.96	-1.48

Figure legends

Figure 1: Conceptual figure of a Bayesian state-space model, where y_t is the observed cyanobacterial density at time t, x_t are driver data (environmental covariates) at time t, m_t is the estimated true, or latent, cyanobacterial density at time t, $\boldsymbol{\beta}$ is a vector of parameters in the process model (slope, intercept, etc.), and τ_{proc} and τ_{obs} are the precisions of normal distributions representing process error and observation error, respectively. Parameters (rounded-edge rectangle) are modeled as distributions in the parameter model. Parameters, along with driver data, determine the predicted latent states (ovals; also modeled as a distributions) in the process model, which are fitted to observations using the data model.

Figure 2: Map of Lake Sunapee, New Hampshire, USA with locator map (inset). Data from Site 1 were used for Bayesian state-space models, data from Site 2 were used to inform priors for Site 1 models, and data from Site 3 provided lake-level covariates for Site 1 models.

Figure 3: Model development workflow diagram. Model equations and descriptions of covariates included in each model can be found in Table 2.

Figure 4: Timeseries of *G. echinulata* density at Site 1 in Lake Sunapee from 2009-2016 (a, c); panels b) and d) show a reduced scale to better illustrate variability at low density.

Figure 5: Timeseries of median predicted and observed *G. echinulata* density for one-week-ahead hindcasts in 2015 for the best-performing models (b-g; Table 3), as well as the RW null model (a). Similar figures for 2016 hindcasts and models not shown here may be in found in the supplemental material (Fig. S10, S11).

Figure 6: Timeseries of median predicted and observed *G. echinulata* density for four-week-ahead hindcasts in 2015 for the best-performing models (b-g; Table 3), as well as the RW null model (a). Similar figures for 2016 hindcasts and models not shown here may be in found in the

supplemental material (Fig. S12, S13). Note the y-axis change between Figures 5 and 6 to accommodate larger credible and predictive intervals at the four-week forecast horizon.

Figure 7: Uncertainty partitioning of the one-week-ahead to four-week-ahead credible interval for hindcasts averaged across the 2015-2016 hindcasting period for the best-performing models (b-g; Table 3), as well as the RW null model (a). Similar figures for other models may be found in the supplemental material (Fig. S14).

Figure 8: Uncertainty partitioning for a) one-week-ahead and b) four-week-ahead hindcasts averaged across the 2015-2016 hindcasting period across models. White triangles indicate a best-performing model at the respective forecast horizon as assessed by Δ Predictive loss (Table 3).

Figures

Figure 1

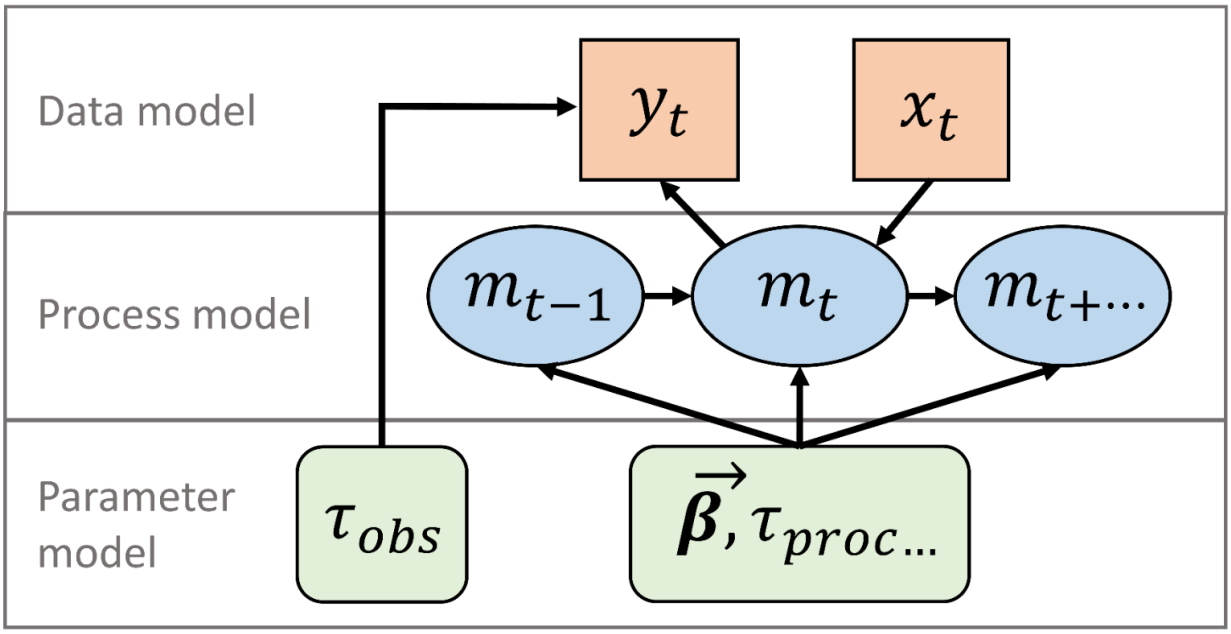

1066 **Figure 2**

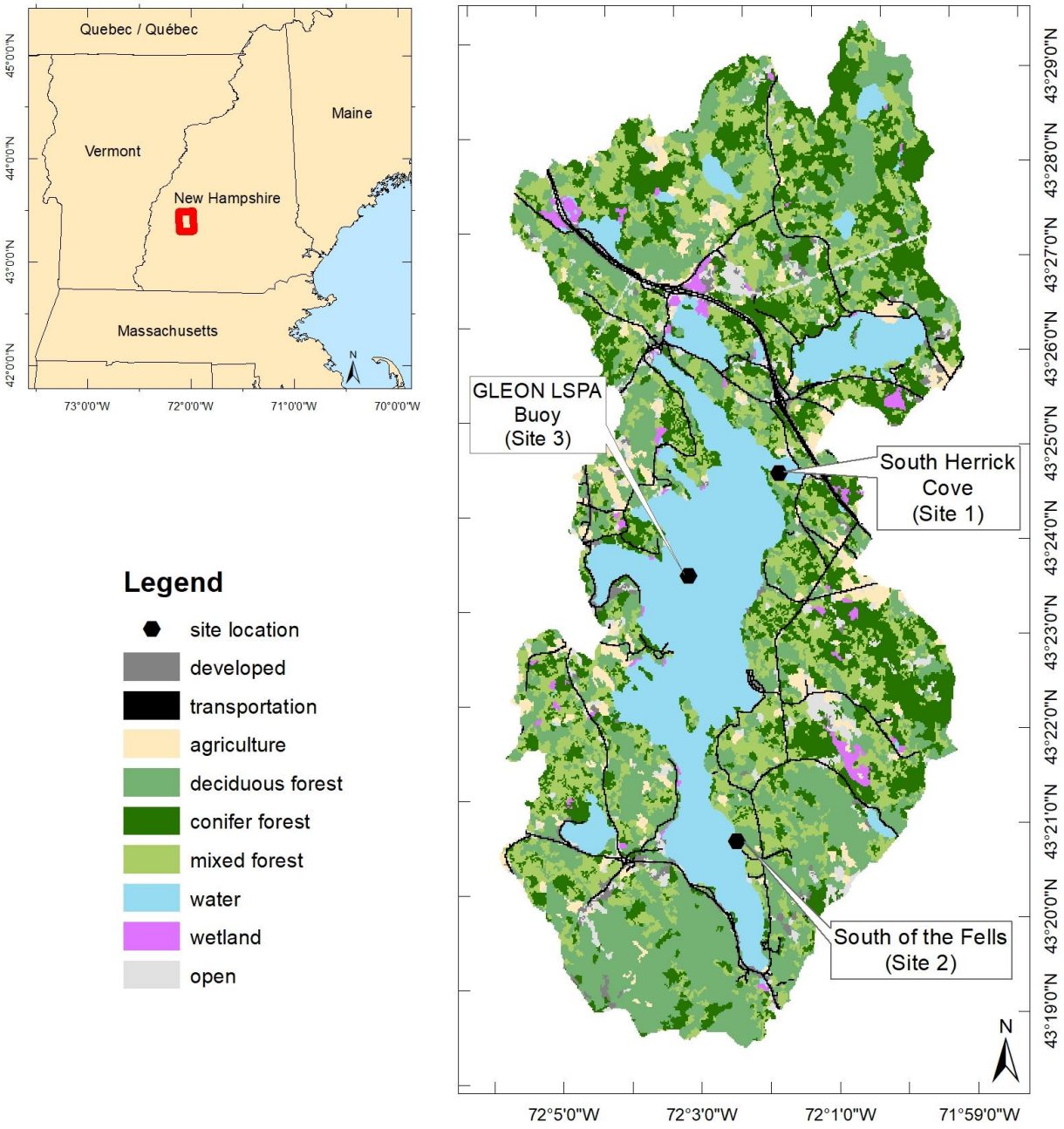

1067

1068

1069

1070

1071

Figure 3

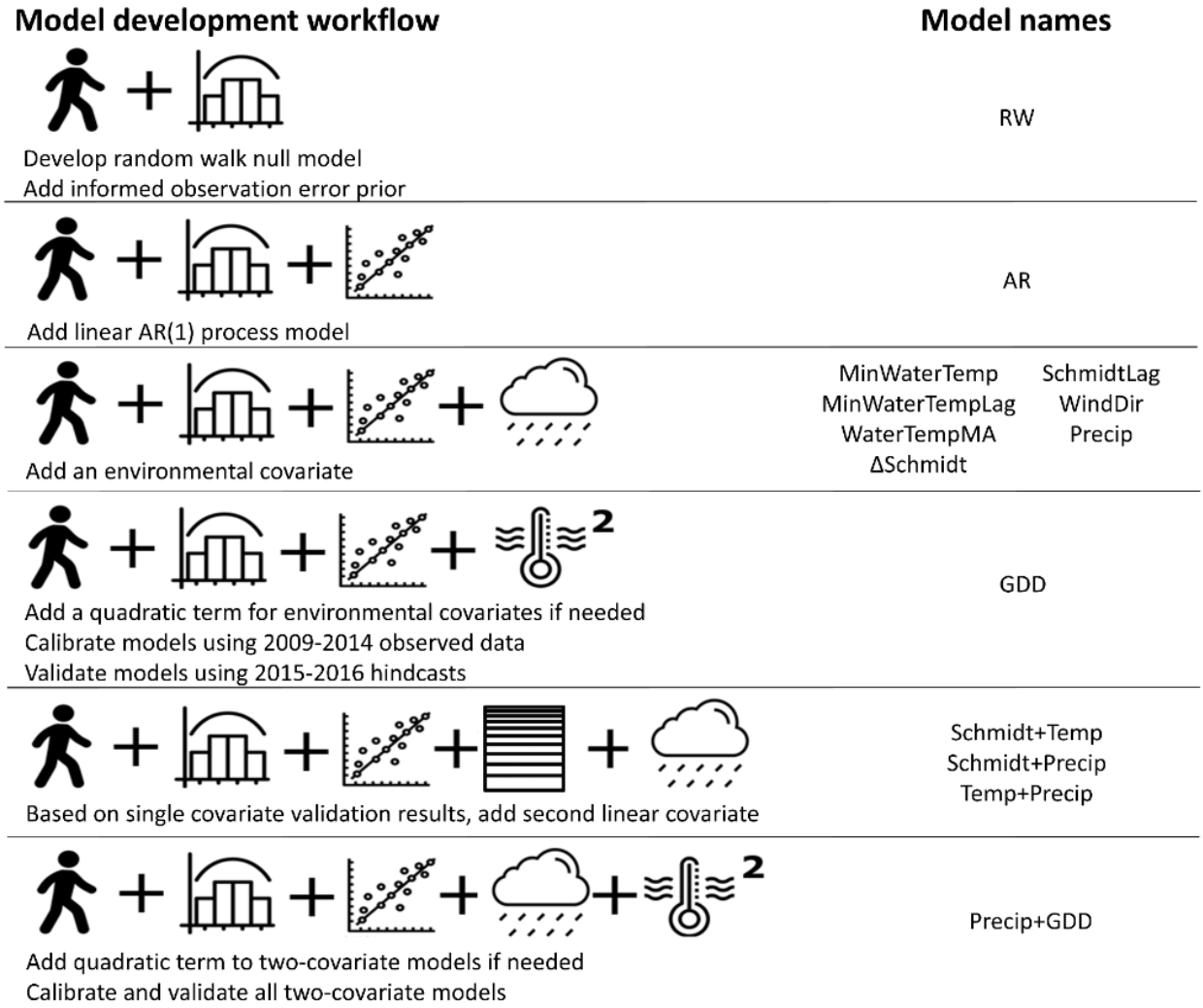
Model development workflow
Model names
Develop random walk null model
Add informed observation error prior
RW
Add linear AR(1) process model
AR
Add an environmental covariate
MinWaterTemp
MinWaterTempLag
WaterTempMA
ΔSchmidt
SchmidtLag
WindDir
Precip
Add a quadratic term for environmental covariates if needed
Calibrate models using 2009-2014 observed data
Validate models using 2015-2016 hindcasts
GDD
Based on single covariate validation results, add second linear covariate
Schmidt+Temp
Schmidt+Precip
Temp+Precip
Add quadratic term to two-covariate models if needed
Calibrate and validate all two-covariate models
Precip+GDD

1082 **Figure 4**

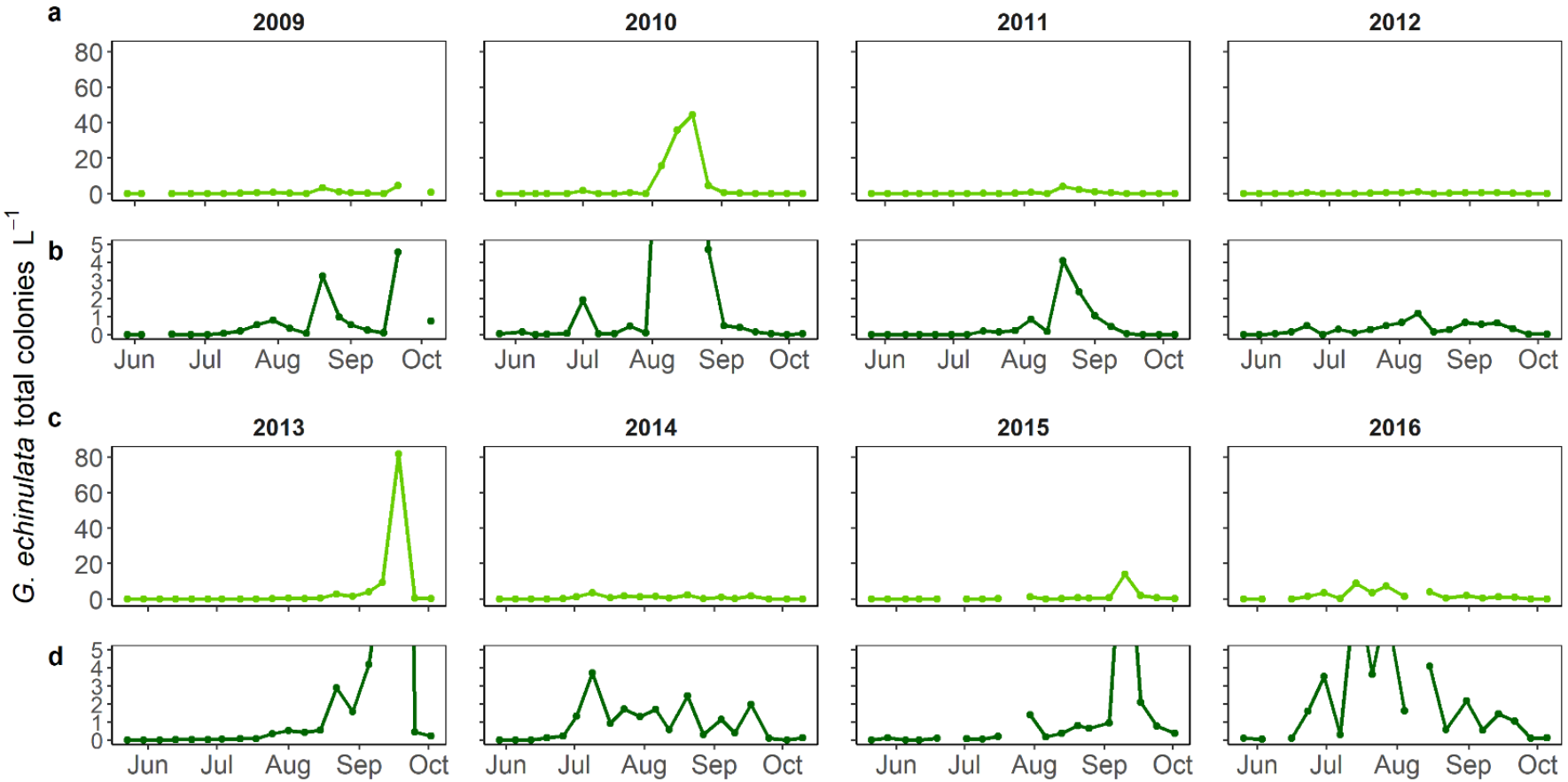

1083

Figure 5

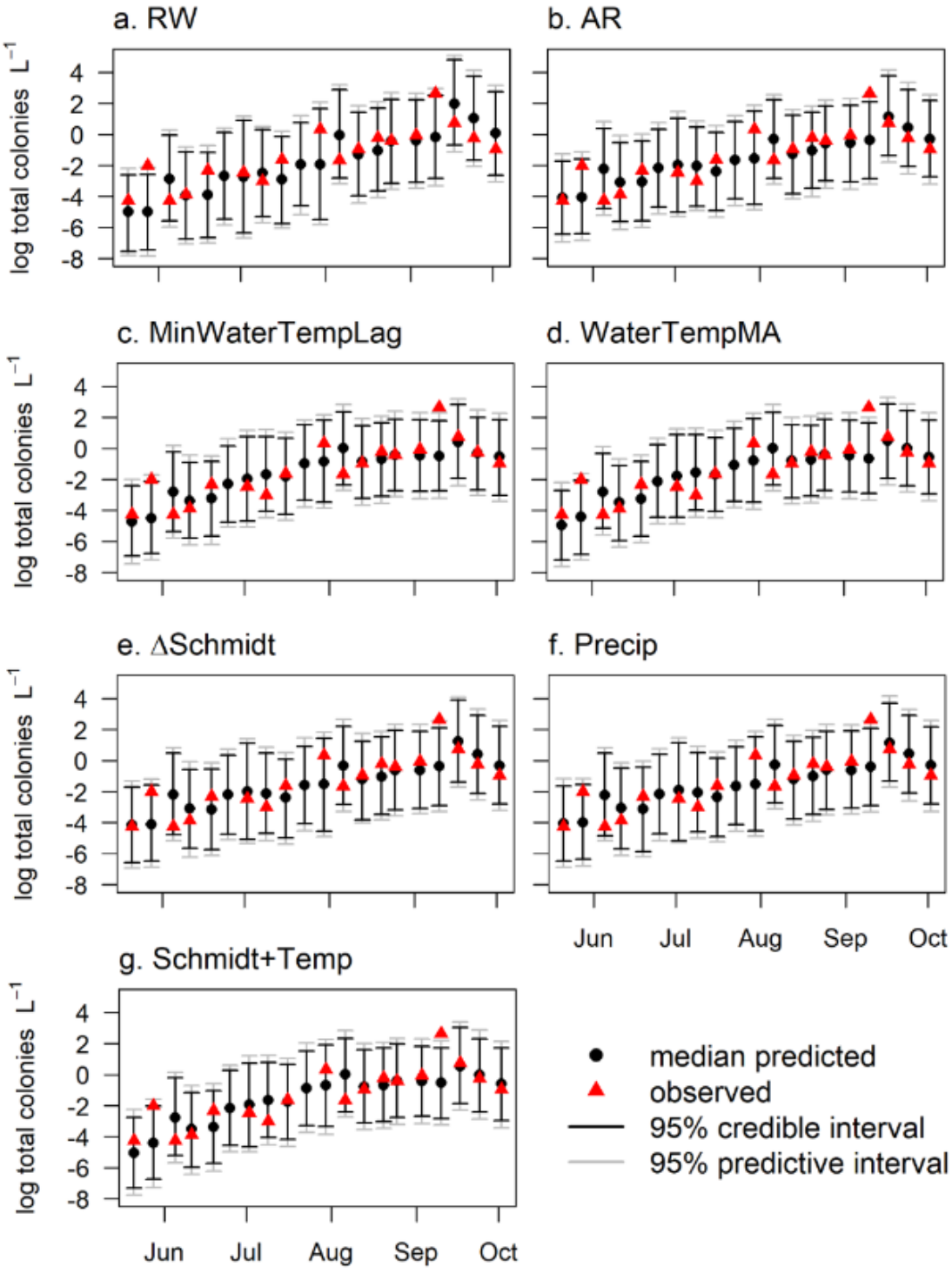
a. RW
b. AR
c. MinWaterTempLag
d. WaterTempMA
e. ΔSchmidt
f. Precip
g. Schmidt+Temp
log total colonies L⁻¹
4
2
0
-2
-4
-6
-8
Jun
Jul
Aug
Sep
Oct
median predicted
observed
95% credible interval
95% predictive interval

Figure 6

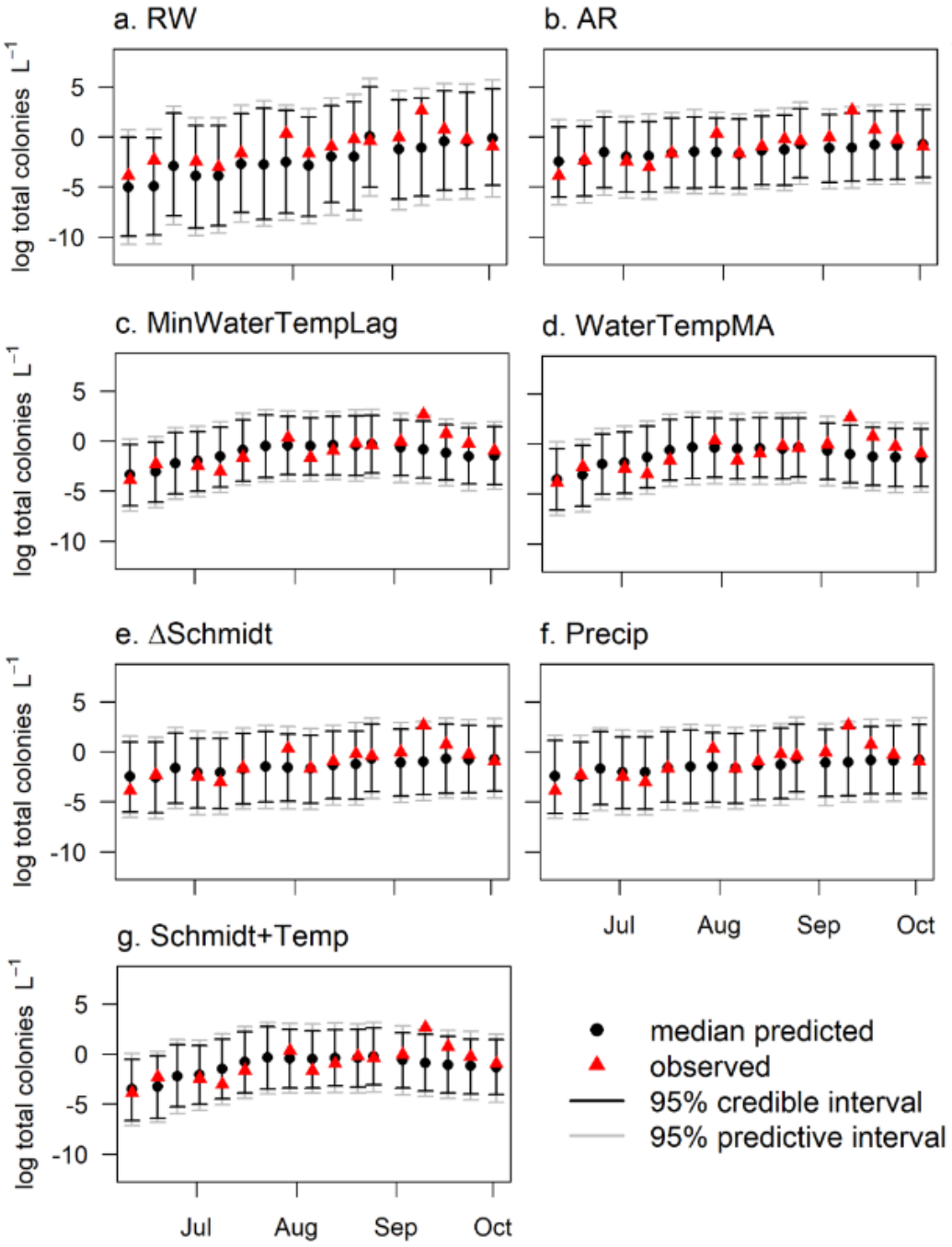
a. RW
b. AR
c. MinWaterTempLag
d. WaterTempMA
e. ΔSchmidt
f. Precip
g. Schmidt+Temp
log total colonies L⁻¹
5
0
-5
-10
Jul
Aug
Sep
Oct
median predicted
observed
95% credible interval
95% predictive interval

Figure 7

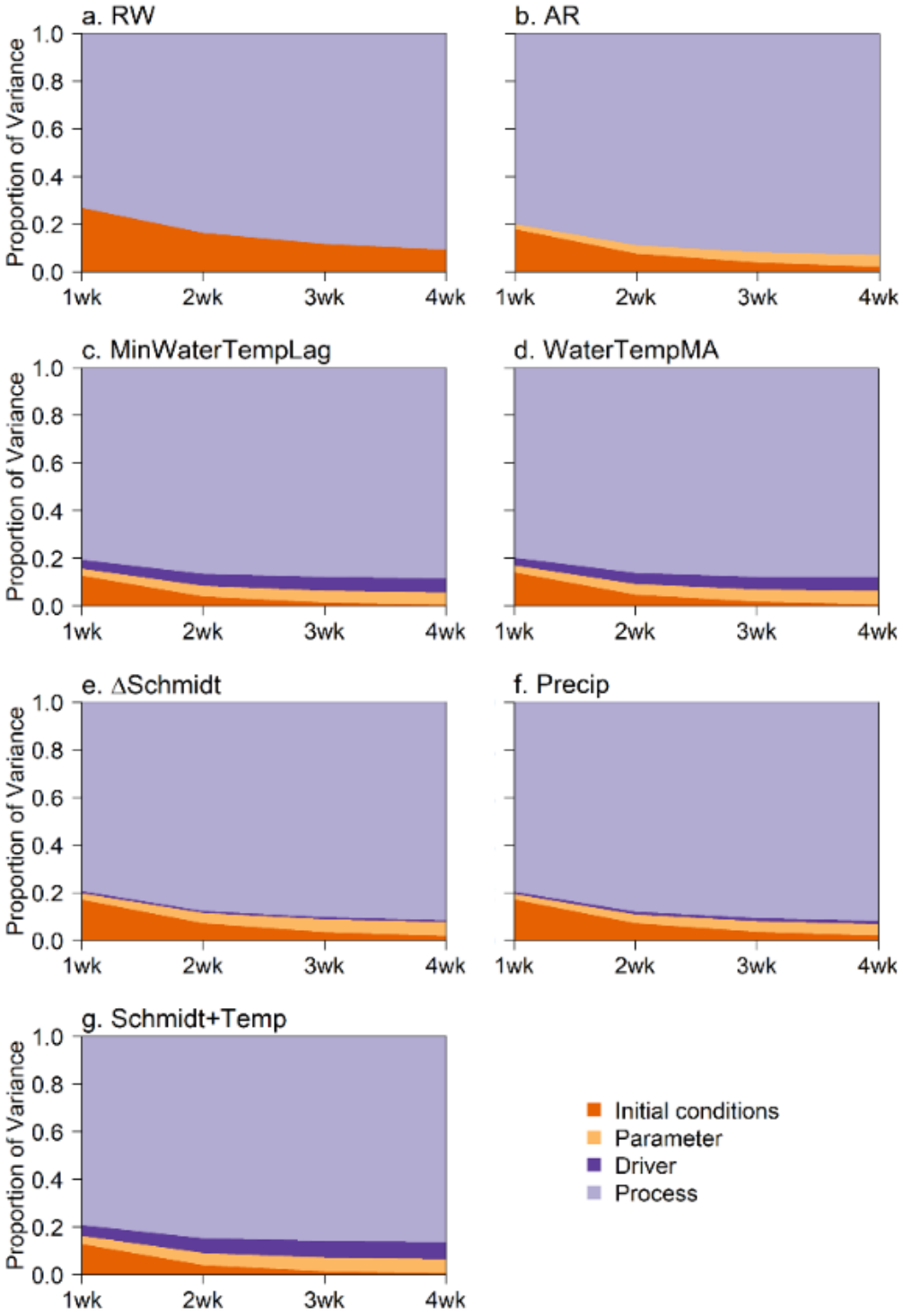
a. RW
b. AR
c. MinWaterTempLag
d. WaterTempMA
e. ΔSchmidt
f. Precip
g. Schmidt+Temp
Proportion of Variance
0.0
0.2
0.4
0.6
0.8
1.0
1wk
2wk
3wk
4wk
Initial conditions
Parameter
Driver
Process

Figure 8

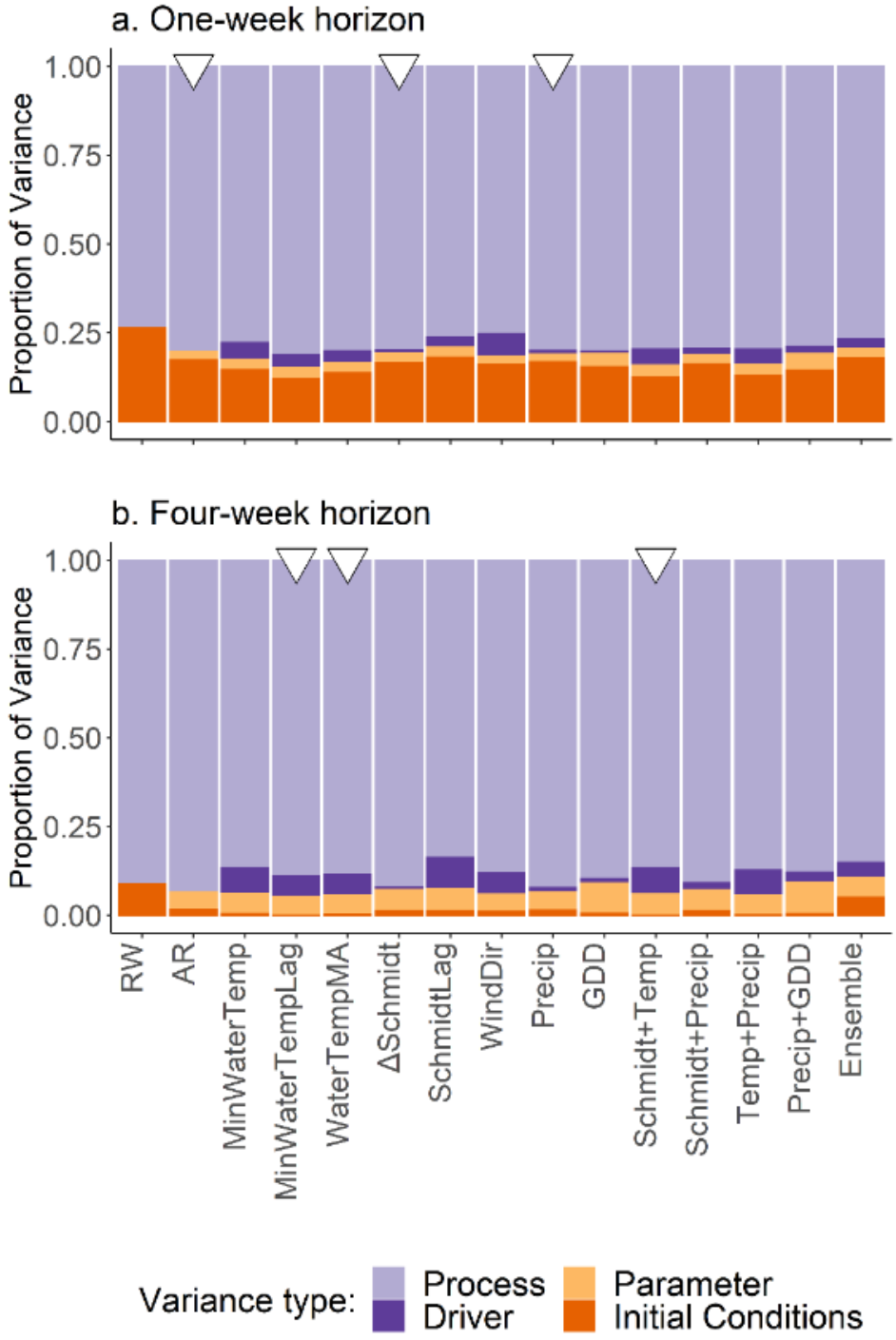
a. One-week horizon
b. Four-week horizon
Proportion of Variance
1.00
0.75
0.50
0.25
0.00
RW
AR
MinWaterTemp
MinWaterTempLag
WaterTempMA
ΔSchmidt
SchmidtLag
WindDir
Precip
GDD
Schmidt+Temp
Schmidt+Precip
Temp+Precip
Precip+GDD
Ensemble
Variance type:
Process
Driver
Parameter
Initial Conditions

Supplemental Information

Using near-term forecasts and uncertainty partitioning to improve predictions of low-frequency cyanobacterial events

Mary E. Lofton, Jennifer A. Brentrup, Whitney S. Beck, Jacob A. Zwart, Ruchi Bhattacharya, Ludmila S. Brighenti, Sarah H. Burnet, Ian M. McCullough, Bethel G. Steele, Cayelan C. Carey, Kathryn L. Cottingham, Michael C. Dietze, Holly A. Ewing, Kathleen C. Weathers, Shannon L. LaDeau

Submitted as an original research article to *Ecological Applications*

Number of pages: 39

Number of text supplements: 5

Number of tables: 7

Number of figures: 16

Number of code repositories: 1[1]

Number of datasets: 5[2]

[1] All code for data collation, model calibration, hindcasting, analysis, and visualization can be found on Github at the following repository URL: https://github.com/GLEON/Bayes_forecast_WG/tree/eco_apps_release; DOI:10.5281/zenodo.3878781

[2] All input datasets used for this study can be found at the Environmental Data Initiative (EDI) Data Portal (https://environmentaldatainitiative.org/) and are listed on page 2 of this supplement as well as cited in the manuscript text with permanent DOIs.

Code repository: Includes all code for data collation, model calibration, hindcasting, analysis, and visualization. Please see:

https://github.com/GLEON/Bayes_forecast_WG/tree/eco_apps_release

DOI:10.5281/zenodo.3878781

Datasets:

LSPA, K.C. Weathers, and B.G. Steele. 2020. High-Frequency Weather Data at Lake Sunapee, New Hampshire, USA, 2007-2019 ver 3. Environmental Data Initiative. https://doi.org/10.6073/pasta/698e9ffb0cdcda81ecf7188bff54445e. Accessed 2020-05-22.

Cottingham, K.L., C.C. Carey, and K.C. Weathers. 2020. Gloeotrichia echinulata density at four nearshore sites in Lake Sunapee, NH, USA from 2005-2016 ver 2. Environmental Data Initiative. https://doi.org/10.6073/pasta/b6f418436088b14666a02467797ff1ad. Accessed 2020-04-25.

LSPA, K.C. Weathers, and B.G. Steele. 2020. Lake Sunapee Instrumented Buoy: High Frequency Water Temperature and Dissolved Oxygen Data – 2007-2019 ver 1. Environmental Data Initiative. https://doi.org/10.6073/pasta/70c41711d6199ac2758764ecfcb9815e. Accessed 2020-05-16.

Cottingham, K.L., C.C. Carey, and K.C. Weathers. 2020. High-frequency temperature data from four near-shore sites, Lake Sunapee, NH, USA, 2006-2018 ver 1. Environmental Data Initiative. https://doi.org/10.6073/pasta/3e325757f0e981d91cd297f257f05f55. Accessed 2020-05-16.

Lofton, M.E., J.A. Brentrup, W.S. Beck, J.A. Zwart, R. Bhattacharya, L.S. Brighenti, S.H. Burnet, I.M. McCullough, B.G. Steele, C.C. Carey, K.L. Cottingham, M.C. Dietze, H.A. Ewing, K.C. Weathers, and S.L. LaDeau. 2020. Lake Sunapee Gloeotrichia echinulata density near-term hindcasts from 2015-2016 and meteorological model driver data, including shortwave radiation and precipitation from 2009-2016 ver 4. Environmental Data Initiative. https://doi.org/DOI_PLACE_HOLDER. Accessed 2020-05-27.[3]

[3] This publication is currently in the staging, or draft, environment of the EDI repository. The current draft may be accessed by navigating to https://portal-s.edirepository.org/nis/home.jsp and searching for the package identifier edi 18.

Text S1: *Data processing for potential environmental drivers of G. echinulata density*

The majority of the environmental covariate data tested as potential drivers of *G. echinulata* density required processing before being used as driver data for Bayesian state-space models.

Growing degree days were calculated for each sampling day using water temperature from Onset loggers at our nearshore sampling site according to the following equation (McMaster and Wilhelm 1997):

$$\frac{(T_{max} + T_{min})}{2} - T_{base} \quad (\text{eqn. } 1)$$

where T_{max} is maximum daily temperature, T_{min} is minimum daily temperature, and T_{base} is the temperature below which *G. echinulata* cannot grow, which we assigned as 4°C for our calculations.

We used water temperature profiles from the GLEON buoy thermistor chain to calculate Schmidt stability, a measure of thermal stratification strength that indicates the amount of energy required to homogenize temperature across the water column (Idso 1973). Schmidt stability calculations were performed using the R package rLakeAnalyzer (Winslow et al. 2019). The 10-min. Schmidt stability data were aggregated to daily summary statistics for days where at least 75% of observations were present for that day.

Following observations that wind can promote nearshore *G. echinulata* scums by facilitating aggregation of colonies in littoral areas (Cyr 2017), wind speed and wind direction data were tested as potential environmental drivers. For 2009-2010 and 2013-2016, 10-minute averages of 1-sec. wind speed and wind direction data were aggregated to hourly means. For 2011-2012, average wind speed and wind direction were not available, so 10-min instantaneous readings were used and also aggregated to an hourly mean. Using the hourly mean wind

direction data, we added an indicator variable coded as 1 for wind directions that could feasibly have blown *G. echinulata* colonies in the direction of our study site our study site (S to NW 180-359°), while wind blowing in the opposite direction was coded as 0 (0-179°). We aggregated the hourly wind speed data to daily mean, median, minimum, maximum, and standard deviation if at least 50% of observations were present for that day. The wind direction indicator variable data were aggregated to a daily mean which ranged from 0-1 depending on the proportion of hourly wind measurements blowing towards Site 1 each day.

Hourly NLDAS-2 solar radiation data were aggregated to daily sum, mean, standard deviation, median, minimum, and maximum values.

Text S2: *Selection of environmental covariates for Bayesian state-space models*

Based on our expectations as to which environmental covariates could be important for driving *Gloeotrichia* density from our knowledge of cyanobacterial dynamics in eutrophic lakes (e.g., Barbiero and Welch 1992, Istvánovics et al. 1993, Karlsson-Elfgren et al. 2005, Carey et al. 2014, Cottingham et al. 2015), we performed a standardized selection process to determine which environmental covariates and summary statistics of those covariates to include in Bayesian state-space models. To select covariates, we conducted Spearman's correlations between summary statistics of candidate environmental covariates and log-transformed *G. echinulata* density between 2009 and 2014 (Table S2). We conducted correlations using multiple summary statistics of the following covariates: water temperature, Schmidt stability, precipitation, wind speed, wind direction, shortwave radiation, photosynthetically active radiation (PAR), and growing degree days. We used the Spearman's *rho* of these correlations to guide which environmental covariates and the specific summary statistic to use in developing Bayesian state-space models.

For each environmental covariate, we conducted correlations for a suite of different summary statistics, including the mean, minimum, and maximum values as well as the standard deviation of the covariate for each sampling day. We also conducted correlations for each of these summary statistics at one-day to one-week lags from the day of sampling when data permitted, as well as for the difference in an environmental covariate from one week to the next to account for antecedent conditions or rapid changes in environmental covariates, according to previous findings that antecedent conditions or changes in conditions such as water temperature and Schmidt stability can affect cyanobacterial growth and phytoplankton community structure (Bormans et al. 2005, Madgwick et al. 2006). For water temperature, we further conducted

correlations using moving averages for 3-14 days prior to each sampling day. Finally, if initial data visualization indicated that environmental covariates exhibited a quadratic relationship with log-transformed *G. echinulata* density and therefore did not meet the assumption of monotonicity for a Spearman's correlation, we used a quadratic R^2 threshold of $|R^2| \geq 0.3$ for covariate selection; this occurred for growing degree days (Fig. S1). The full list of covariate summary statistics can be viewed in Table S2.

After completing all correlations, we assessed which environmental covariate summary statistics to include in our Bayesian state-space models using Spearman's *rho* from 2009-2014. We eliminated any covariate summary statistics for which |Spearman's *rho*| was less than 0.3. We arrived at this threshold because 0.3 was approximately twice the |mean *rho*| across all covariates (|mean *rho*| = 0.14). If multiple summary statistics for a particular environmental covariate had a |Spearman's *rho*| that was greater than or equal to 0.3, we chose the summary statistic with the greatest |Spearman's *rho*| value for Bayesian state-space model development (Table S2). For quadratic variables that did not meet the monotonicity assumption for Spearman's correlations, we used a threshold of |quadratic $R^2| \geq 0.3$ for prioritization.

Using this covariate selection process, we identified eight environmental covariate summary statistics for inclusion in Bayesian state-space models: daily minimum water temperature on the sampling day (MinWaterTemp), daily minimum water temperature with a one-week lag (MinWaterTempLag), seven-day moving average of water temperature (WaterTempMA), weekly difference in median Schmidt stability (ΔSchmidt), daily maximum Schmidt stability with a one-week lag (SchmidtLag), daily mean of the wind direction indicator variable with a two-day lag (WindDir), growing degree days (GDD), and daily sum of precipitation (Precip).

Text S3: *Random walk model and development of informed observation error prior*

Our null Bayesian state-space model was a random walk model, or a linear model with a slope of 0 and a process error term (RW; Table 1), with an informed observation error prior developed using data from Site 2 (Fig. 2). For the informed observation error prior, we used logged *G. echinulata* density data collected weekly at Site 2 in Lake Sunapee from 2009-2014 (Fig. 2) to run a random walk model with vague priors. Observation error was modeled as a normal distribution with precision τ_{obs}, which was assigned a vague gamma distribution prior with shape (a = 0.001) and rate (r = 0.001). After convergence, the model estimated the shape and rate of τ_{obs} to be 15.37 and 7.84, respectively, and these values were used for the prior on τ_{obs} in all models subsequently developed for Site 1 as part of our analysis.

Initial conditions priors for all models were informed using *G. echinulata* densities observed in north temperate lakes in Maine, U.S.A during April and May across multiple years (H. Ewing, unpublished data).

Text S4: *Model ensemble exercise*

Development of model ensemble

Following observations that model ensembles can sometimes provide more skilled predictions than a single model even when some ensemble members are low-performing (Johansson et al. 2019), we conducted a simple, unweighted model ensemble exercise to determine if the model ensemble could out-perform our individual models. We created the ensemble by appending all of the 7,500-member within-model hindcasts for each week for each model (excluding the RW null model) and conducted the same hindcast assessment and uncertainty partitioning on the grouped hindcast output as we did for individual models.

Model ensemble hindcast skill similar to individual models

The model ensemble did not perform better than the best-performing individual models, with a ΔPL of 0.05 ln(colonies L^{-1}) at the one-week forecast horizon and 0.09 ln(colonies L^{-1}) at the four-week horizon (Table 2; Fig. 5; Fig. 6; Fig. S11; Fig. S13). Overall, all models included in the ensemble exhibited a tendency to under-predict *G. echinulata* at both the one-week and four-week forecast horizon (see Bias in Table 2), likely resulting in negligible improvement in hindcast skill using an ensemble approach.

Text S5: *Variability of environmental covariates in Bayesian state-space models*

The environmental covariates selected for Bayesian state-space models were temporally variable from 2009-2016. Minimum daily water temperature at Site 1 (used in MinWaterTemp and MinWaterTempLag models) ranged from 13.4 °C to 26.2 °C and peaked between July 15 – August 20 during the study years (Fig. S2; Fig. S3). Weekly moving averages of water temperature at Site 1 (WaterTempMA model) were similar, ranging from 13.2 °C to 26.2 °C and reaching a maximum between July 11 – August 27 during the study years (Fig. S4). Growing degree days increased throughout the sampling season each year (Fig. S5).

Coinciding with summer increases in surface water temperature, Lake Sunapee was thermally stratified in all study years but did sometimes experience fall turnover (homogenization of water column temperatures) before the end of the sampling season, so daily maximum Schmidt stability (SchmidtMaxLag model) ranged from 0-695 J m^{-2} in June-October (Fig. S6). Thermal stability peaked between July 15 – August 27 in all study years. However, the weekly change in Schmidt stability (SchmidtMedDiff model and two-covariate models) varied substantially both within and among years, with some weeks displaying large increases or decreases in Schmidt stability (± 200 J m^{-2}) while other weeks exhibited no change in stability (Fig. S7).

Precipitation (Precip model and two-covariate models) was also highly variable among years, with 2009, 2011, 2013, and 2014 all including precipitation events of 20 mm day^{-1} or more (Fig. S8). Conditions were drier in other years and 2012 was an especially dry year with a maximum daily sum of precipitation of 4.1 mm. Notably, both of the hindcasting years (2015 and 2016) were drier years.

Finally, the proportion of wind measurements blowing towards Site 1 (WindDir model

and two-covariate models) was also highly variable both within and among years, with values ranging from nearly 0 (no wind blowing towards Site 1) to nearly 1 (all wind blowing towards Site 1) on a week-to-week basis (Fig. S9). In general, wind blew towards Site 1 more often than not, with the proportion of wind measurements blowing towards Site 1 averaging 0.69 throughout the study period. However, actual wind speed was not usually very high, with wind speed in the direction of Site 1 having a median of 2.6 m s^{-1} and maximum of 6.7 m s^{-1} during the study period.

Table S1: Examples of ecological forecasts with partitioned uncertainty. These studies are provided as examples only and do not represent a systematic literature review. IC = initial conditions; SDM = species distribution model; RCP = representative concentration pathway; GCM = global climate model

Paper	Ecosystem or region	Focal forecasting variable	Forecast horizon	Type of model	Types of uncertainty quantified	Dominant source of uncertainty
(Dietze 2017)	Forest	Net ecosystem exchange	Daily	2-covariate Bayesian state-space	Driver, IC, process, parameter	Driver
(Diniz-Filho et al. 2009)	Western hemisphere	Bird population distribution	Multi- decadal	Species distribution model	Driver, process	Process
(Fox et al. 2018)	Arid woodland/ grassland	Carbon stock	Annual	Community land model	Driver, IC	IC
(Gauthier et al. 2016)	Arctic	Snow goose population	Multi- decadal	Time-varying matrix population model	Driver, parameter, process	Parameter
(Gertner et al. 1996)	Forest	Red pine growth	Multi- decadal	Pipe model (process-based)	IC, parameter	Parameter
(Huang et al. 2013)	Lake	Chlorophyll	Biweekly	Complex numerical process-based	IC, parameter	IC
(Jiang et al. 2012)	Global (high latitudes)	Vegetation distribution	Multi-decadal	Dynamic global vegetation model	Driver, parameter	Parameter
(Jiang et al. 2018)	Peatland	Carbon stocks and fluxes	Decadal	Process-based	Driver, parameter	Driver
(Kim et al. 2014)	River	Chlorophyll	Spatial	Process-based	Driver (different sources)	Driver (river flow)
(Massoud et al. 2018)	Plankton mesocosm	Plankton abundance	Daily	Process-based	IC, parameter, process	Process
(Mbogga et al. 2010)	Forest	Aspen habitat	Multi- decadal	Bioclimate envelope model	Driver, process	Driver

Paper	Ecosystem or region	Focal forecasting variable	Forecast horizon	Type of model	Types of uncertainty quantified	Dominant source of uncertainty
(Ouellet-Proulx et al. 2017)	River	Water temperature and discharge	Daily	Process-based	Driver, IC	Driver
(Page et al. 2017)	Lake	Phytoplankton community	Weekly	Complex numerical process-based	Process (different sources)	Process (representation of light, nutrients)
(Raiho et al. in review)	Forest	Tree species biomass	Multi- decadal	Process-based forest gap model	Driver, IC, parameter, process	Process
(Spadavecchia et al. 2011)	Forest	CO_2 flux	Daily	Process-based ecosystem model	Driver, parameter	Parameter
(Thomas et al. 2018)	Forest	Productivity	Decadal	Complex numerical process-based	Driver, parameter, process	Process
(Thomas et al. 2020)	Lake	Water temperature	Daily	Complex numerical process-based	Driver, IC, parameter, process	Driver
(Thuiller et al. 2019)	Global	Vertebrate species distributions	Multi-decadal	Species distribution model	Driver and process (different sources of each)	Driver (RCP scenarios) and process (choice of SDM)
(Wang et al. 2009)	Forest	Forest carbon	Spatial	Kriging algorithm	Driver (different sources)	Driver (satellite data)

Paper	Ecosystem or region	Focal forecasting variable	Forecast horizon	Type of model	Types of uncertainty quantified	Dominant source of uncertainty
(Watling et al. 2015)	Southeastern U.S.	Vertebrate species distribution	Multi-decadal	Species distribution model	Driver, IC, process	Process
(Valle et al. 2009)	Tropical forest	Basal area	Multi-decadal	Complex numerical process-based	IC, parameter, process	Process
(Zhang et al. 2019)	Maize fields	Crop yield	Multi-decadal	Process-based	Driver (different sources) and process	Driver (GCMs)

Table S2: Correlation analysis results to determine which environmental covariates to include in Bayesian state-space models. Variable names are provided to match variables names in the output.csv file generated by the "2A_Covariate_correlation.R" script in the manuscript's Github repository. Quadratic R^2 instead of Spearman's *r* is reported for variables which were determined to have a quadratic relationship with logged *G. echinulata* density during preliminary visualization. Shaded boxes indicate variables that met the prioritization criterion of *r* or $R^2 \geq 0.3$. Asterisks indicate variables chosen for inclusion in Bayesian state-space models. P-values have been adjusted using the Holm-Bonferroni correction to account for multiple comparisons except in the case of growing degree days, where the p-value is for quadratic regression rather than a Spearman's correlation.

Covariate variable name	**Covariate variable description**	**Spearman's *rho***	**Quadratic reg. R^2**	**p-value**
HCS.tempC_mean	mean water temperature on the sampling day	0.49	--	6.9×10^{-6}
HCS.tempC_median	median water temperature on the sampling day	0.49	--	8.5×10^{-6}
HCS.tempC_min	minimum water temperature on the sampling day	0.51	--	2.1×10^{-6}
HCS.tempC_max	maximum water temperature on the sampling day	0.47	--	2.5×10^{-5}
HCS.tempC_sd	standard deviation of water temperature on the sampling day	-0.17	--	1
HCS.tempC_mean_lag	daily mean water temperature one week before the sampling day	0.54	--	2.1×10^{-7}
HCS.tempC_median_lag	daily median water temperature one week before the sampling day	0.54	--	1.6×10^{-7}
HCS.tempC_min_lag	daily minimum water temperature one week before the sampling day	0.56*	--	4.2×10^{-8}
HCS.tempC_max_lag	daily maximum water temperature one week before the sampling day	0.52	--	6.2×10^{-7}
HCS.tempC_sd_lag	daily standard deviation of water temperature one week before the sampling day	-0.19	--	1
wtr_mean_diff	difference in mean water temperature between one week before the sampling day and the day of sampling	-0.2	--	1
wtr_median_diff	difference in median water temperature between one week before the sampling day and the day of sampling	-0.2	--	1

Covariate variable name	Covariate variable description	Spearman's *rho*	Quadratic reg. R^2	p-value
wtr_max_diff	difference in maximum water temperature between one week before the sampling day and the day of sampling	-0.18	--	1
wtr_min_diff	difference in minimum water temperature between one week before the sampling day and the day of sampling	-0.2	--	1
wtr_sd_diff	difference in standard deviation in water temperature between one week before the sampling day and the day of sampling	-0.02	--	1
ma_3	three-day moving average of water temperature prior to the day of sampling	0.44	--	0.00022
ma_5	five-day moving average of water temperature prior to the day of sampling	0.45	--	0.00013
ma_7	seven-day moving average of water temperature prior to the day of sampling	0.49*	--	1.7×10^{-5}
ma_10	ten-day moving average of water temperature prior to the day of sampling	0.44	--	0.00052
ma_14	fourteen-day moving average of water temperature prior to the day of sampling	0.48	--	5.0×10^{-5}
gdd_sum	growing degree days	--	0.52*	1.2×10^{-17}
schmidt.stability_mean	mean Schmidt stability on the day of sampling	0.19	--	1
schmidt.stability_median	median Schmidt stability on the day of sampling	0.19	--	1
schmidt.stability_min	minimum Schmidt stability on the day of sampling	0.18	--	1
schmidt.stability_max	maximum Schmidt stability on the day of sampling	0.2	--	1
schmidt.stability_sd	standard deviation of Schmidt stability on the day of sampling	0.19	--	1
schmidt.stability_mean_lag	daily mean Schmidt stability one week before the sampling day	0.35	--	0.025
schmidt.stability_median_lag	daily median Schmidt stability one week before the sampling day	0.35	--	0.022
schmidt.stability_min_lag	daily minimum Schmidt stability one week before the sampling day	0.34	--	0.047

Covariate variable name	Covariate variable description	Spearman's *rho*	Quadratic reg. R^2	p-value
schmidt.stability_max_lag	daily maximum Schmidt stability one week before the sampling day	0.36*	--	0.015
schmidt.stability_sd_lag	daily standard deviation of Schmidt stability one week before the sampling day	0.13	--	1
schmidt.stability_mean_diff	difference in mean Schmidt stability between one week before the sampling day and the day of sampling	-0.34	--	0.05
schmidt.stability_median_diff	difference in median Schmidt stability between one week before the sampling day and the day of sampling	-0.36*	--	0.02
schmidt.stability_min_diff	difference in minimum Schmidt stability between one week before the sampling day and the day of sampling	-0.3	--	0.20
schmidt.stability_max_diff	difference in maximum Schmidt stability between one week before the sampling day and the day of sampling	-0.34	--	0.05
schmidt.stability_sd_diff	difference in standard deviation of Schmidt stability between one week before the sampling day and the day of sampling	-0.05	--	1
precip_mm	sum of daily precipitation on day of sampling	-0.3*	--	0.05
precip_mm_1daylag	sum of daily precipitation on day before sampling	-0.23	--	0.73
precip_mm_1weeklag	sum of daily precipitation one week before the sampling day	-0.22	--	0.89
ShortWaveRad_Wperm2_mean	mean shortwave radiation on the day of sampling	0.04	--	1
ShortWaveRad_Wperm2_median	median shortwave radiation on the day of sampling	-0.21	--	1
ShortWaveRad_Wperm2_min	minimum shortwave radiation on the day of sampling	0.27	--	0.16
ShortWaveRad_Wperm2_max	maximum shortwave radiation on the day of sampling	0.07	--	1
ShortWaveRad_Wperm2_sd	standard deviation of shortwave radiation on the day of sampling	0.11	--	1
ShortWaveRad_Wperm2_sum	sum of shortwave radiation on the day of sampling	0.04	--	1
par_mean	mean PAR on the day of sampling	0	--	1
par_median	median PAR on the day of sampling	-0.21	--	1
par_min	minimum PAR on the day of sampling	0.16	--	1

Covariate variable name	Covariate variable description	Spearman's *rho*	Quadratic reg. R^2	p-value
par_max	maximum PAR on the day of sampling	-0.03	--	1
par_sd	standard deviation of PAR on the day of sampling	0.08	--	1
par_sum	sum of PAR on the day of sampling	0	--	1
AveWindSp_ms_mean_in	mean windspeed filtered for wind directions blowing into Site 1 on the day of sampling	0.08	--	1
AveWindSp_ms_median_in	median windspeed filtered for wind directions blowing into Site 1 on the day of sampling	0.09	--	1
AveWindSp_ms_min_in	minimum windspeed filtered for wind directions blowing into Site 1 on the day of sampling	0.16	--	1
AveWindSp_ms_max_in	maximum windspeed filtered for wind directions blowing into Site 1 on the day of sampling	0.03	--	1
AveWindSp_ms_sd_in	standard deviation of windspeed filtered for wind directions blowing into Site 1 on the day of sampling	0.01	--	1
AveWindSp_ms_mean_1daylag_in	mean windspeed filtered for wind directions blowing into Site 1 the day before the sampling day	0.13		1
AveWindSp_ms_median_1daylag_in	median windspeed filtered for wind directions blowing into Site 1 the day before the sampling day	0.15	--	1
AveWindSp_ms_min_1daylag_in	minimum windspeed filtered for wind directions blowing into Site 1 the day before the sampling day	0.14	--	1
AveWindSp_ms_max_1daylag_in	maximum windspeed filtered for wind directions blowing into Site 1 the day before the sampling day	0.13	--	1
AveWindSp_ms_sd_1daylag_in	standard deviation of windspeed filtered for wind directions blowing into Site 1 the day before the sampling day	0.16	--	1
AveWindSp_ms_mean_2daylag_in	mean windspeed filtered for wind directions blowing into Site 1 two days before the sampling day	0.25	--	0.50
AveWindSp_ms_median_2daylag_in	median windspeed filtered for wind directions blowing into Site 1 two days before the sampling day	0.26	--	0.46

Covariate variable name	Covariate variable description	Spearman's *rho*	Quadratic reg. R^2	p-value
AveWindSp_ms_min_2daylag_in	minimum windspeed filtered for wind directions blowing into Site 1 two days before the sampling day	0.29	--	0.14
AveWindSp_ms_max_2daylag_in	maximum windspeed filtered for wind directions blowing into Site 1 two days before the sampling day	0.23	--	0.95
AveWindSp_ms_sd_2daylag_in	standard deviation of windspeed filtered for wind directions blowing into Site 1 two days before the sampling day	0.2	--	1
AveWindSp_ms_mean_3daylag_in	mean windspeed filtered for wind directions blowing into Site 1 three days before the sampling day	0.23	--	0.95
AveWindSp_ms_median_3daylag_in	median windspeed filtered for wind directions blowing into Site 1 three days before the sampling day	0.24	--	0.67
AveWindSp_ms_min_3daylag_in	minimum windspeed filtered for wind directions blowing into Site 1 three days before the sampling day	0.26	--	0.46
AveWindSp_ms_max_3daylag_in	maximum windspeed filtered for wind directions blowing into Site 1 three days before the sampling day	0.19	--	1
AveWindSp_ms_sd_3daylag_in	standard deviation of windspeed filtered for wind directions blowing into Site 1 three days before the sampling day	0.11		1
AveWindSp_ms_mean_1weeklag_in	mean windspeed filtered for wind directions blowing into Site 1 one week before the sampling day	0.08	--	1
AveWindSp_ms_median_1weeklag_in	median windspeed filtered for wind directions blowing into Site 1 one week before the sampling day	0.09	--	1
AveWindSp_ms_min_1weeklag_in	minimum windspeed filtered for wind directions blowing into Site 1 one week before the sampling day	0.13	--	1
AveWindSp_ms_max_1weeklag_in	maximum windspeed filtered for wind directions blowing into Site 1 one week before the sampling day	0.04	--	1
AveWindSp_ms_sd_1weeklag_in	standard deviation of filtered for wind directions blowing into Site 1 one week before the sampling day	0.03	--	1
windsp_cumsum_1day_in	cumulative windspeed into the cove one day prior to sampling	0.09	--	1

Covariate variable name	Covariate variable description	Spearman's *rho*	Quadratic reg. R^2	p-value
windsp_cumsum_2day_in	cumulative windspeed into the cove two days prior to sampling	0.13	--	1
AveWindDir_cove_mean	proportion of daily wind measurements blowing in the direction of Site 1 on the day of sampling	0.2	--	1
AveWindDir_cove_mean_1daylag	proportion of daily wind measurements blowing in the direction of Site 1 one day before sampling	0.19	--	1
AveWindDir_cove_mean_2daylag	proportion of daily wind measurements blowing in the direction of Site 1 two days before sampling	0.37*	--	0.0072
AveWindDir_cove_mean_3daylag	proportion of daily wind measurements blowing in the direction of Site 1 three days before sampling	0.2		1
AveWindDir_cove_mean_1weeklag	proportion of daily wind measurements blowing in the direction of Site 1 on the day one week before sampling	0.11	--	1

Table S3: Estimated mean random year effects for calibrated random walk model with random year effect from 2009-2014. The model parameter τ_{year} was estimated to have a mean of 64.8, corresponding to a standard deviation of 0.12 being fit to the mean random year effects reported in the table.

Year	*2009*	*2010*	*2011*	*2012*	*2013*	*2014*
Mean random year effect	0.069	0.026	0.002	0.026	0.058	0.038

Table S4: Parameter summary for all calibrated Bayesian state-space models: Part I. Model process equations and descriptions of covariates included in each model can be found in Table 1 of the manuscript. Parameter names are provided to match output from R script "4.2_Calibrate_Bayesian_models.R" included as part of the GitHub code repository for this manuscript. tau_proc = precision on the normal distribution representing process error; tau_obs = precision on the normal distribution representing observation error; beta1 = intercept of linear models; beta2 = coefficient of AR term in linear models; S.D. = standard deviation; PSRF = potential scale reduction factor of the Gelman-Rubin statistic, sometimes referred to as R-hat, where a value approaching 1 indicates that the model has converged well on a parameter estimate both within and among chains; SS_{eff} = effective sample size, or the number of independent samples in MCMC output for a parameter once auto-correlation has been accounted for.

Parameters	**tau_proc**				**tau_obs**				**beta1**				**beta2**			
Model name	mean	S.D.	PSRF	SS_{eff}	mean	S.D.	PSRF	SS_{eff}	mean	S.D.	PSRF	SS_{eff}	mean	S.D.	PSRF	SS_{eff}
RW	0.70	0.16	1.00	21851	1.72	0.35	1.00	20044	--	--	--	--	--	--	--	--
AR	0.75	0.17	1.00	18748	1.80	0.37	1.00	18302	-0.26	0.15	1.00	33346	0.76	0.06	1.00	29639
MinWaterTemp	0.93	0.25	1.00	12612	1.72	0.36	1.00	16302	-0.39	0.15	1.00	26303	0.68	0.06	1.00	22165
MinWaterTempLag	0.85	0.21	1.00	16316	1.76	0.37	1.00	16918	-0.47	0.16	1.00	22452	0.63	0.07	1.00	18484
WaterTempMA	0.88	0.23	1.00	14034	1.75	0.37	1.00	17074	-0.39	0.15	1.00	25093	0.66	0.07	1.00	19928
ΔSchmidt	0.74	0.17	1.00	18662	1.89	0.38	1.00	18809	-0.29	0.16	1.00	27059	0.74	0.07	1.00	22980
SchmidtLag	0.89	0.23	1.00	13929	1.73	0.36	1.00	16797	-0.31	0.14	1.00	30254	0.75	0.06	1.00	24900
WindDir	0.84	0.20	1.00	16802	1.76	0.37	1.00	18279	-0.34	0.15	1.00	31447	0.72	0.06	1.00	27858
Precip	0.74	0.17	1.00	18898	1.80	0.37	1.00	18829	-0.27	0.15	1.00	31476	0.76	0.06	1.00	26990
GDD	0.92	0.28	1.00	7849	1.74	0.38	1.00	13033	0.16	0.19	1.00	19188	0.67	0.10	1.00	7888
Schmidt+Temp	0.87	0.21	1.00	15352	1.76	0.38	1.00	16282	-0.45	0.16	1.00	21287	0.62	0.07	1.00	17198
Schmidt+Precip	0.73	0.16	1.00	19113	1.80	0.37	1.00	18498	-0.30	0.16	1.00	26737	0.74	0.07	1.00	22744
Temp+Precip	0.86	0.21	1.00	15752	1.77	0.37	1.00	17294	-0.41	0.15	1.00	25870	0.65	0.07	1.00	20824
Precip+GDD	0.90	0.26	1.00	8985	1.75	0.38	1.00	14309	0.14	0.19	1.00	19120	0.65	0.10	1.00	8296

Table S5: Parameter summary for all calibrated Bayesian state-space models: Part II. Model process equations and descriptions of covariates included in each model can be found in Table 1 of the manuscript. Parameter names are provided to match output from R script "4.2_Calibrate_Bayesian_models.R" included as part of the Github code repository for this manuscript. beta3 = coefficient of covariate in single-covariate models and coefficient on first covariate, which is the first covariate in the model name, in two-covariate models; beta4 = coefficient on quadratic term for growing degree days in GDD model and coefficient on second covariate in two-covariate models; beta5 = coefficient on quadratic term for growing degree days in WindAndGDD model; S.D. = standard deviation; PSRF = potential scale reduction factor of the Gelman-Rubin statistic, sometimes referred to as R-hat, where a value approaching 1 indicates that the model has converged well on a parameter estimate both within and among chains; SS_{eff} = effective sample size, or the number of independent samples in MCMC output for a parameter once auto-correlation has been accounted for.

Parameters	**beta3**				**beta4**				**beta5**			
Model name	mean	S.D.	PSRF	SS_{eff}	mean	S.D.	PSRF	SS_{eff}	mean	S.D.	PSRF	SS_{eff}
RW	--	--	--	--	--	--	--	--	--	--	--	--
AR	--	--	--	--	--	--	--	--	--	--	--	--
MinWaterTemp	0.49	0.13	1.00	38491	--	--	--	--	--	--	--	--
MinWaterTempLag	0.49	0.14	1.00	27828	--	--	--	--	--	--	--	--
WaterTempMA	0.47	0.13	1.00	33718	--	--	--	--	--	--	--	--
ΔSchmidt	-0.09	0.16	1.00	31738	--	--	--	--	--	--	--	--
SchmidtLag	0.36	0.12	1.00	52607	--	--	--	--	--	--	--	--
WindDir	0.42	0.15	1.00	37608	--	--	--	--	--	--	--	--
Precip	-0.08	0.14	1.00	44501	--	--	--	--	--	--	--	--
GDD	0.20	0.19	1.00	8919	-0.58	0.17	1.00	10260	--	--	--	--
Schmidt+Temp	-0.17	0.15	1.00	28500	0.49	0.13	1.00	30182	--	--	--	--
Schmidt+Precip	-0.09	0.16	1.00	31519	-0.07	0.14	1.00	45272	--	--	--	--
Temp+Precip	0.47	0.13	1.00	35021	-0.09	0.13	1.00	43088	--	--	--	--
Precip+GDD	-0.10	0.13	1.00	41062	0.21	0.19	1.00	9751	-0.59	0.17	1.00	11474

Table S6: Uncertainty partitioning results across models for one-week-ahead hindcasts during the 2015-2016 hindcasting period. Mean, minimum (Min.) and maximum (Max.) proportional contributions of initial conditions, parameter, driver, and process uncertainty to hindcasting confidence intervals are reported for each model. Note the RW model does not have parameter or driver uncertainty because the model structure does not include parameters or drivers; similarly, the AR model does not include drivers. *Because contributions of parameter and driver error were so small, the estimated confidence intervals including parameter and/or driver error were occasionally smaller than those without due to numerical approximation error, leading to an estimation of "negative" parameter/driver error; this should be interpreted as no contribution of parameter/driver error, and negative parameter/driver error values were set to zero.

	Initial conditions			**Parameter**			**Driver**			**Process**		
Model name	Mean	Min.	Max.	Mean	Min.	Max.	Mean	Min.	Max.	Mean	Min.	Max.
RW	0.27	0.01	0.58	--	--	--	--	--	--	0.73	0.42	0.99
AR	0.18	0	0.41	0.02	0.01	0.04	--	--	--	0.8	0.56	0.96
MinWaterTemp	0.15	0	0.35	0.03	0.01	0.06	0.05	0	0.15	0.77	0.6	0.87
MinWaterTempLag	0.13	0	0.3	0.03	0.01	0.07	0.04	0	0.14	0.81	0.63	0.94
WaterTempMA	0.14	0	0.34	0.03	0.01	0.07	0.03	0	0.14	0.8	0.6	0.93
ΔSchmidt	0.17	0	0.42	0.03	0.01	0.07	0.01	0	0.03	0.79	0.54	0.96
SchmidtLag	0.19	0	0.43	0.03	0.01	0.06	0.03	0	0.08	0.76	0.54	0.95
WindDir	0.16	0	0.38	0.02	0.01	0.05	0.06	0.01	0.12	0.75	0.54	0.89
Precip	0.17	0	0.41	0.02	0.01	0.04	0.01	0	0.08	0.79	0.55	0.96
GDD	0.16	0	0.37	0.04	0*	0.07	0.01	0	0.04	0.8	0.62	0.94
Schmidt+Temp	0.13	0	0.31	0.04	0.02	0.08	0.04	0	0.12	0.79	0.63	0.92
Schmidt+Precip	0.17	0	0.4	0.03	0.01	0.08	0.02	0	0.08	0.79	0.56	0.95
Temp+Precip	0.14	0	0.33	0.03	0.02	0.07	0.04	0	0.15	0.79	0.62	0.93
Precip+GDD	0.15	0	0.36	0.05	0.02	0.09	0.02	0	0.11	0.78	0.58	0.93
Ensemble	0.18	0.03	0.4	0.03	0.02	0.05	0.03	0*	0.07	0.76	0.57	0.86

Table S7: Uncertainty partitioning results across models for four-week-ahead hindcasts during the 2015-2016 hindcasting period. Mean, minimum (Min.) and maximum (Max.) proportional contributions of initial conditions, parameter, driver, and process uncertainty to hindcasting confidence intervals are reported for each model. Note the RW model does not have parameter or driver uncertainty because the model structure does not include parameters or drivers; similarly, the AR model does not include drivers.

	Initial conditions			**Parameter**			**Driver**			**Process**		
Model name	Mean	Min.	Max.	Mean	Min.	Max.	Mean	Min.	Max.	Mean	Min.	Max.
RW	0.09	0	0.26	--	--	--	--	--	--	0.91	0.74	1
AR	0.02	0	0.06	0.05	0.04	0.08	--	--	--	0.93	0.87	0.95
MinWaterTemp	0.01	0	0.03	0.06	0.03	0.1	0.07	0.01	0.15	0.86	0.79	0.93
MinWaterTempLag	0.01	0	0.02	0.05	0.03	0.09	0.06	0.01	0.12	0.88	0.81	0.94
WaterTempMA	0.01	0	0.02	0.06	0.03	0.1	0.06	0.02	0.1	0.88	0.84	0.93
ΔSchmidt	0.02	0	0.06	0.06	0.04	0.09	0.01	0	0.02	0.91	0.86	0.94
SchmidtLag	0.02	0	0.06	0.06	0.03	0.09	0.09	0.02	0.21	0.83	0.73	0.92
WindDir	0.02	0	0.05	0.05	0.03	0.08	0.06	0.02	0.1	0.88	0.83	0.92
Precip	0.02	0	0.06	0.05	0.04	0.08	0.01	0	0.06	0.92	0.87	0.95
GDD	0.01	0	0.03	0.08	0.06	0.13	0.01	0	0.04	0.89	0.85	0.93
Schmidt+Temp	0.01	0	0.02	0.06	0.04	0.09	0.07	0.02	0.14	0.86	0.79	0.93
Schmidt+Precip	0.02	0	0.05	0.06	0.04	0.09	0.02	0	0.07	0.9	0.86	0.94
Temp+Precip	0.01	0	0.02	0.05	0.04	0.1	0.07	0.03	0.13	0.87	0.8	0.93
Precip+GDD	0.01	0	0.04	0.09	0.06	0.15	0.03	0	0.11	0.87	0.81	0.92
Ensemble	0.06	0.02	0.13	0.06	0.04	0.08	0.04	0.01	0.07	0.85	0.79	0.9

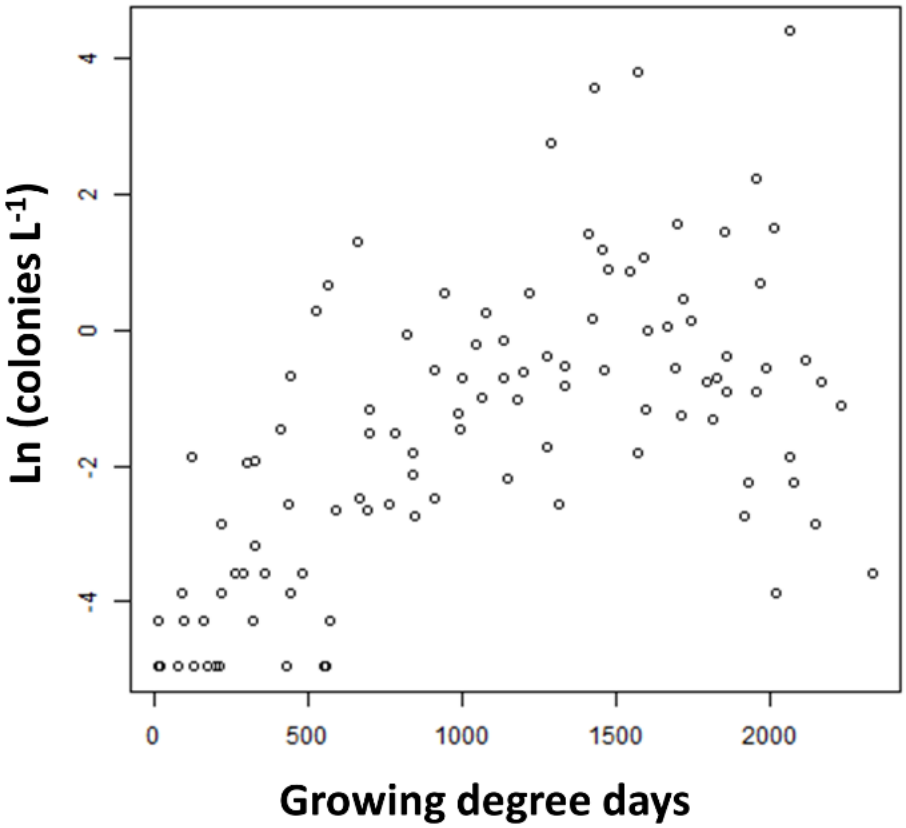

Figure S1: Natural log-transformed *G. echinulata* colonies L^{-1} vs. growing degree days for all sampling days from 2009-2016.

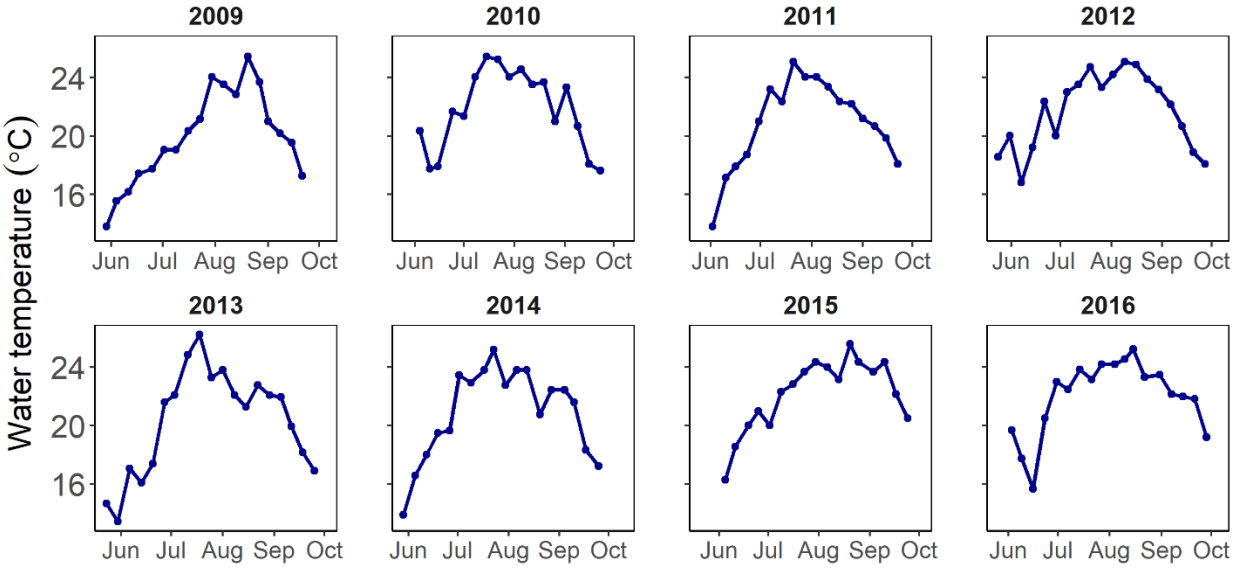

Figure S2: Timeseries of minimum water temperature at Site 1 on the day of sampling from 2009-2016.

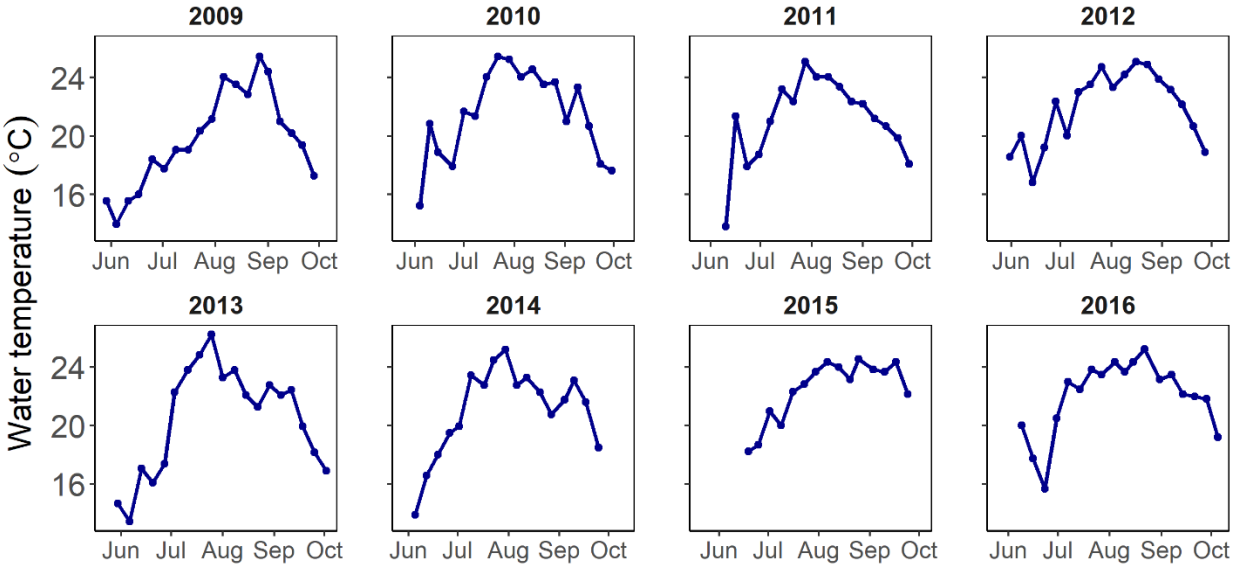

Figure S3: Timeseries of minimum water temperature at Site 1 one week before the sampling day (one week lag) from 2009-2016.

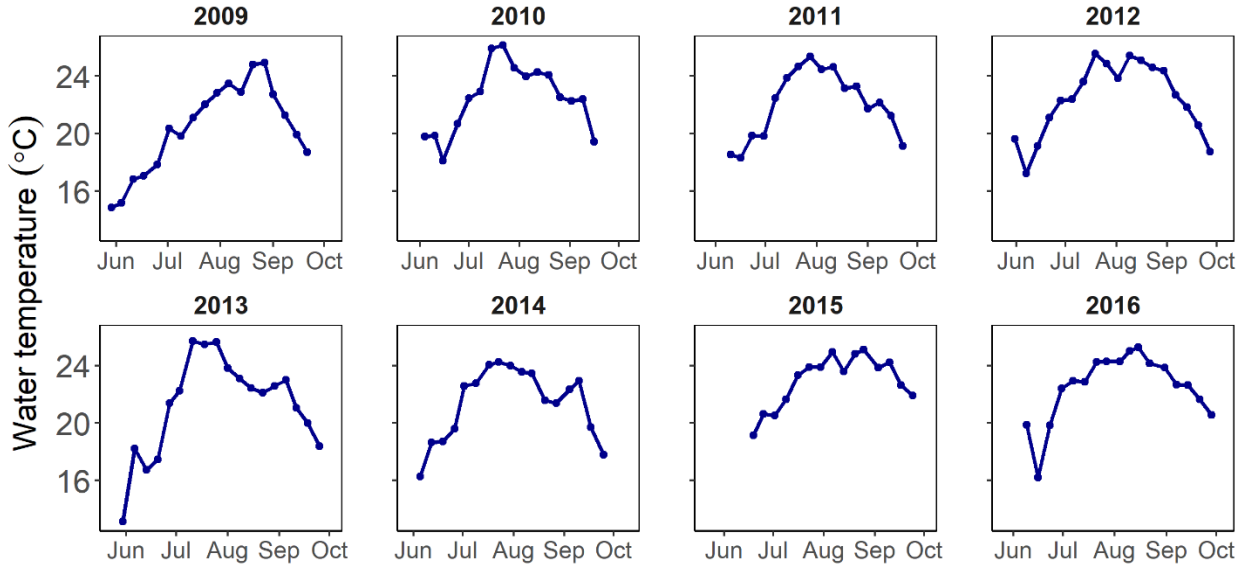

Figure S4: Timeseries of seven-day moving average of water temperature prior to the day of sampling at Site 1 from 2009-2016.

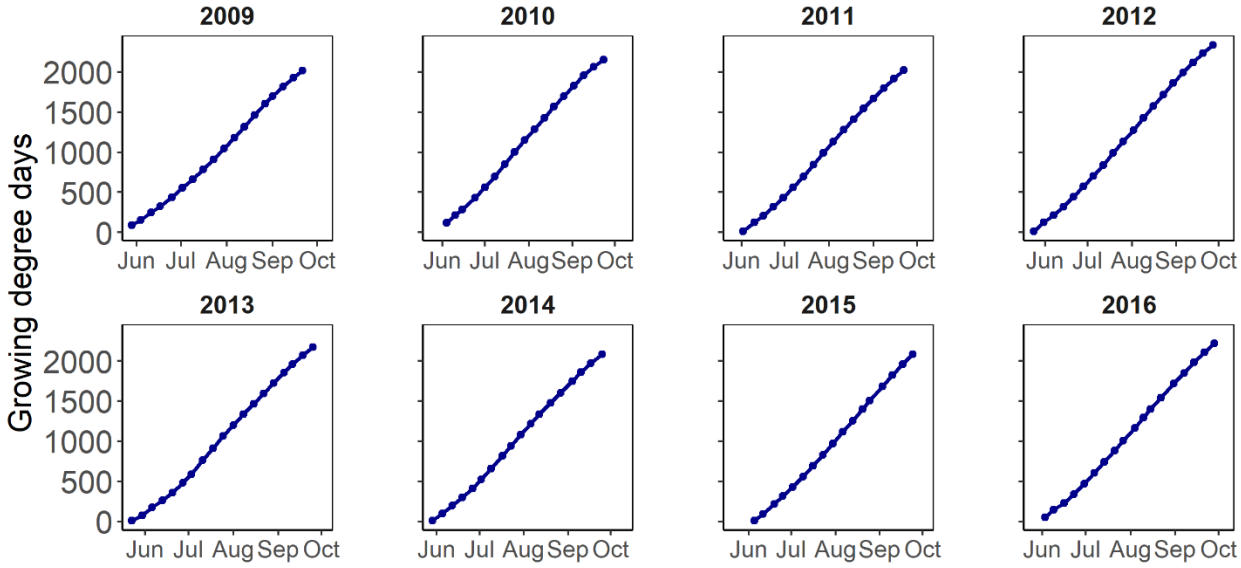

Figure S5: Timeseries of water temperature growing degree days at Site 1 from 2009-2016.

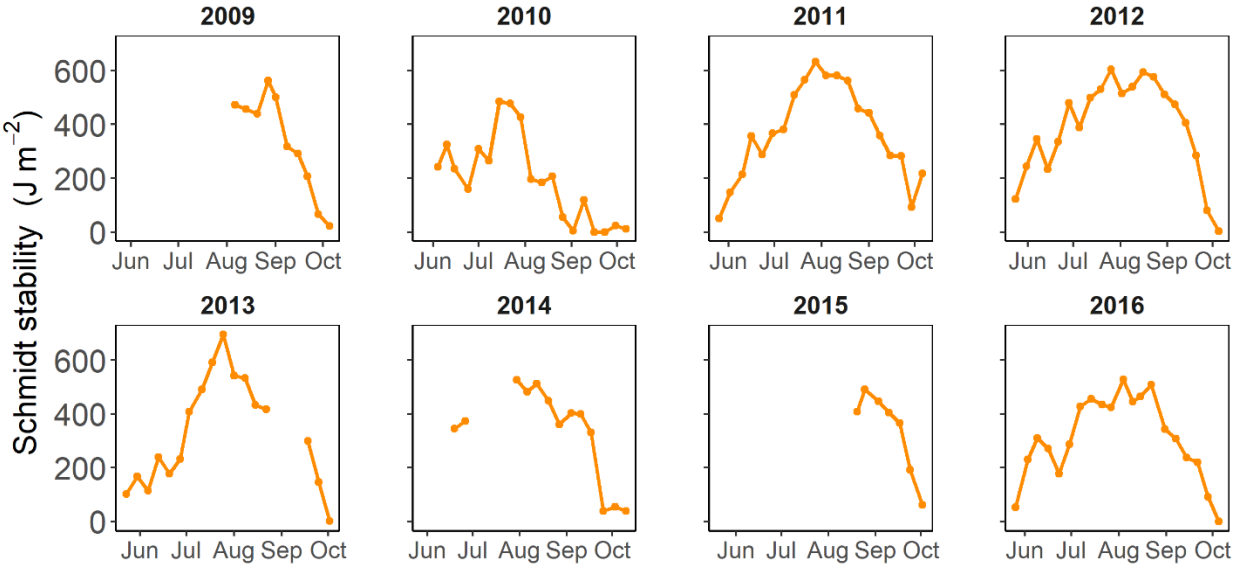

Figure S6: Timeseries of maximum Schmidt stability one week before the sampling day (one week lag) from 2009-2016.

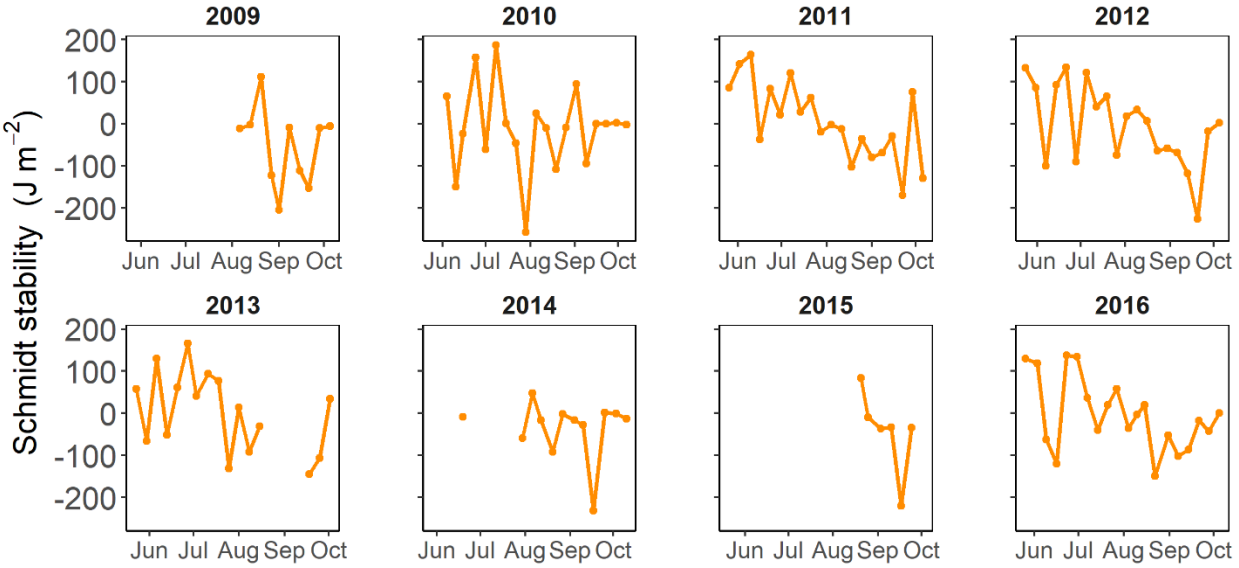

Figure S7: Timeseries of difference in median Schmidt stability between one week before the sampling day and the sampling day from 2009-2016.

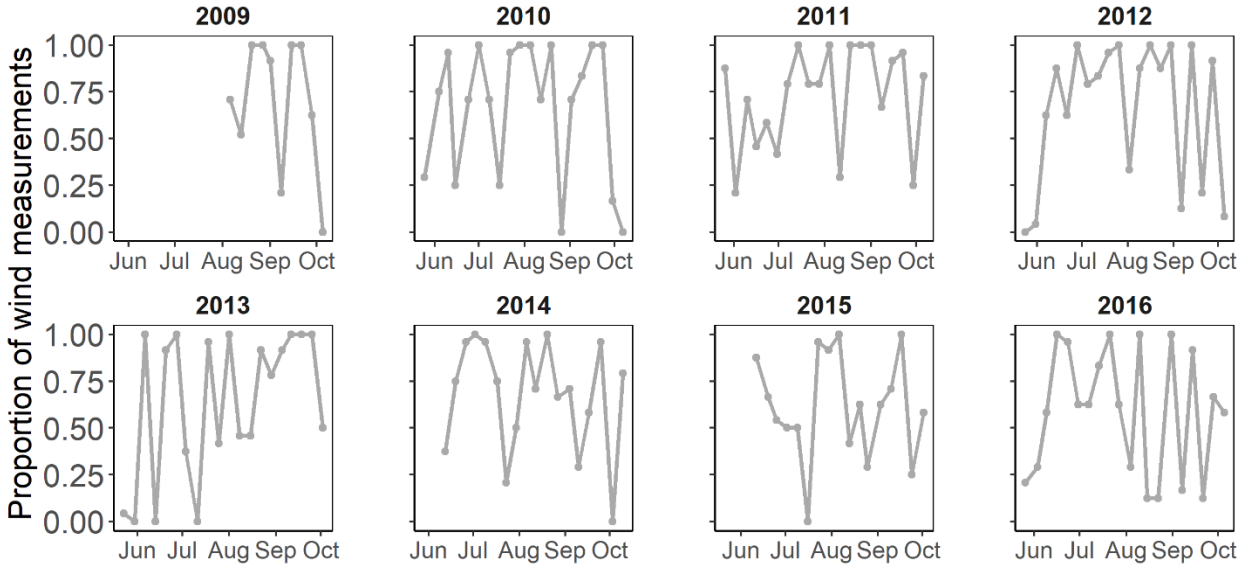

Figure S8: Timeseries of proportion of daily wind measurements blowing in the direction of Site 1 two days before the sampling day from 2009-2016.

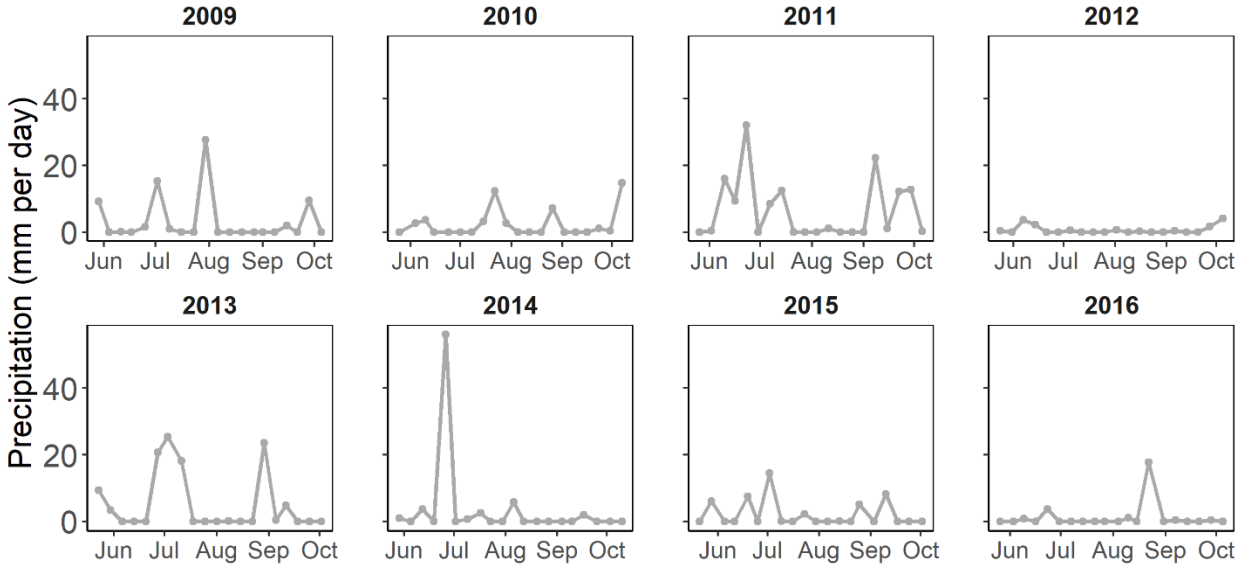

Figure S9: Timeseries of summed daily precipitation on Lake Sunapee from 2009-2016.

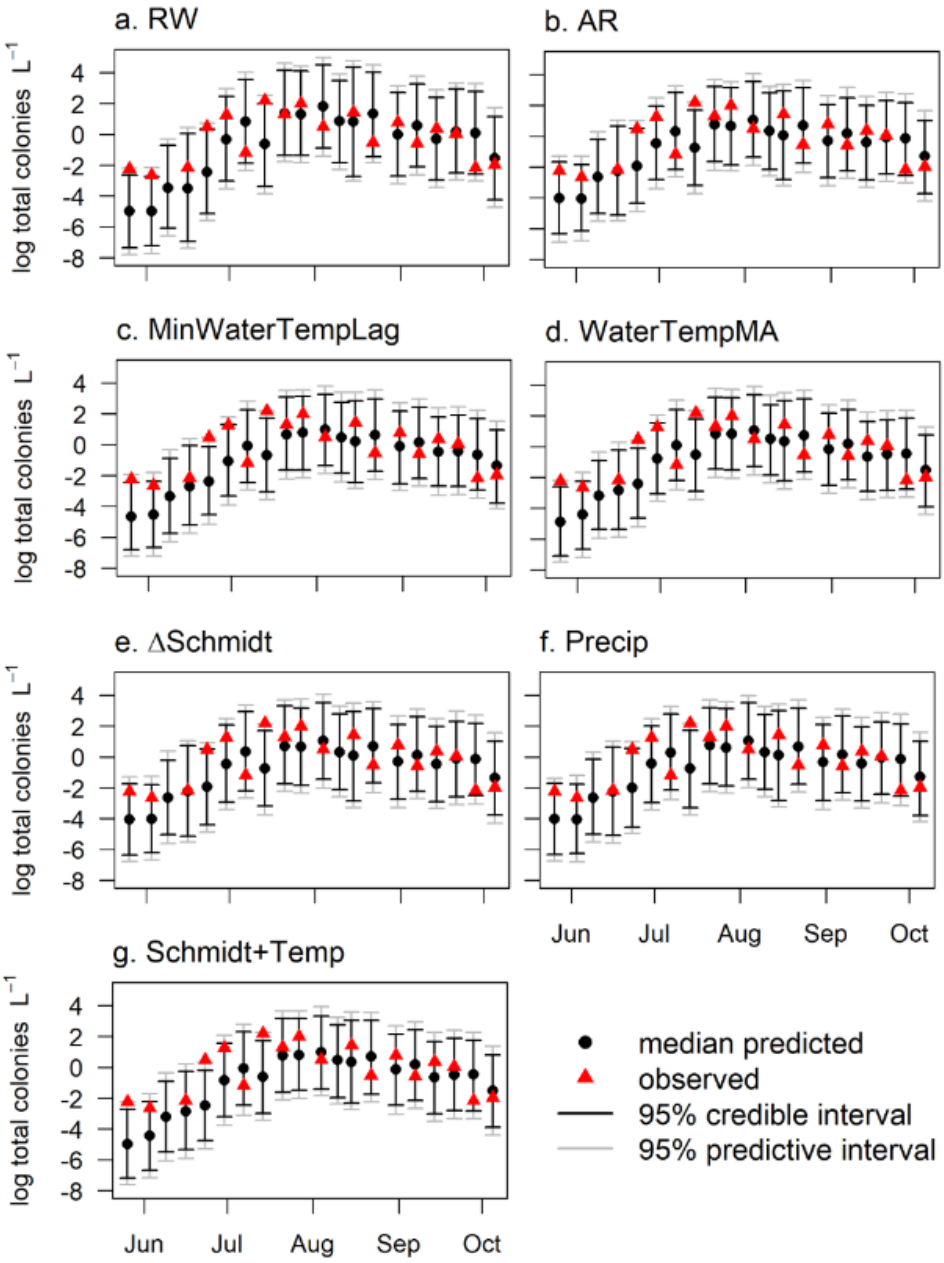

Figure S10: Timeseries of median predicted and observed *G. echinulata* density for one-week-ahead hindcasts in 2016 for the best-performing models (b-g), as well as the RW null model (a).

Figure S11 (next page): Timeseries of median predicted and observed *G. echinulata* density for one-week-ahead hindcasts in 2015 (a, c, e, g, i, k, m, o) and 2016 (b, d, f, h, j, l, n, p) for a subset of developed models. Black points are median predicted values and red triangles and observed values. Black error bars denote the 95% confidence interval, while gray error bars denote the 95% predictive interval. Models shown are MinWaterTemp (a, b), SchmidtLag (c, d), WindDir (e, f), GDD (g, h), Schmidt+Precip (i, j), Temp+Precip (k, l), Precip+GDD (m, n), and the model Ensemble (o, p).

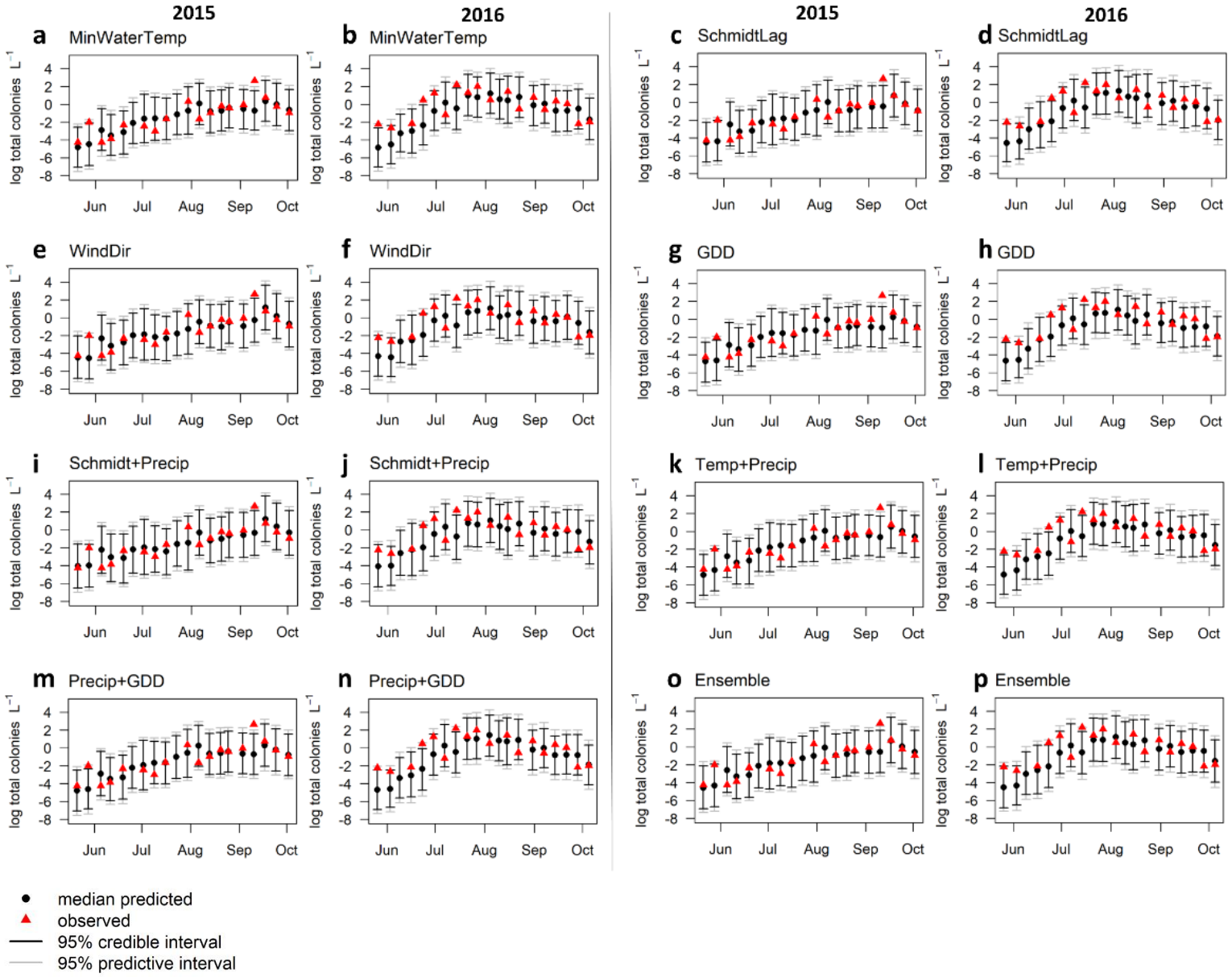
2015
2016
a MinWaterTemp
b MinWaterTemp
c SchmidtLag
d SchmidtLag
e WindDir
f WindDir
g GDD
h GDD
i Schmidt+Precip
j Schmidt+Precip
k Temp+Precip
l Temp+Precip
m Precip+GDD
n Precip+GDD
o Ensemble
p Ensemble
log total colonies L-1
Jun
Jul
Aug
Sep
Oct
median predicted
observed
95% credible interval
95% predictive interval

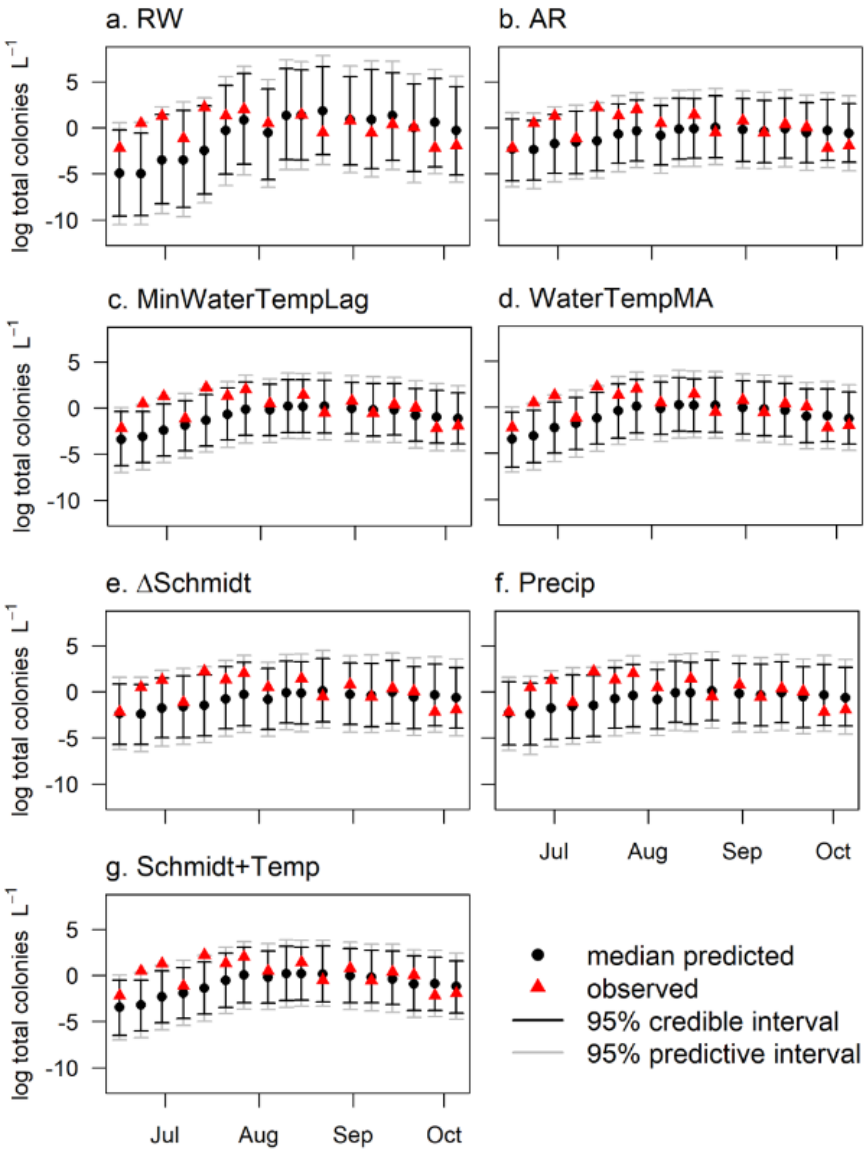

Figure S12: Timeseries of median predicted and observed *G. echinulata* density for four-week-ahead hindcasts in 2016 for the best-performing models (b-g), as well as the RW null model (a). Note the y-axis change from Figure S10 to accommodate larger credible and predictive intervals at the four-week forecast horizon.

Figure S13 (next page): Timeseries of median predicted and observed *G. echinulata* density for four-week-ahead hindcasts in 2015 (a, c, e, g, i, k, m, o) and 2016 (b, d, f, h, j, l, n, p) for a subset of developed models. Black points are median predicted values and red triangles and observed values. Black error bars denote the 95% confidence interval, while gray error bars denote the 95% predictive interval. Models shown are MinWaterTemp (a, b), SchmidtLag (c, d), WindDir (e, f), GDD (g, h), Schmidt+Precip (i, j), Temp+Precip (k, l), Precip+GDD (m, n), and the model Ensemble (o, p). Note the y-axis change from Figure S11.

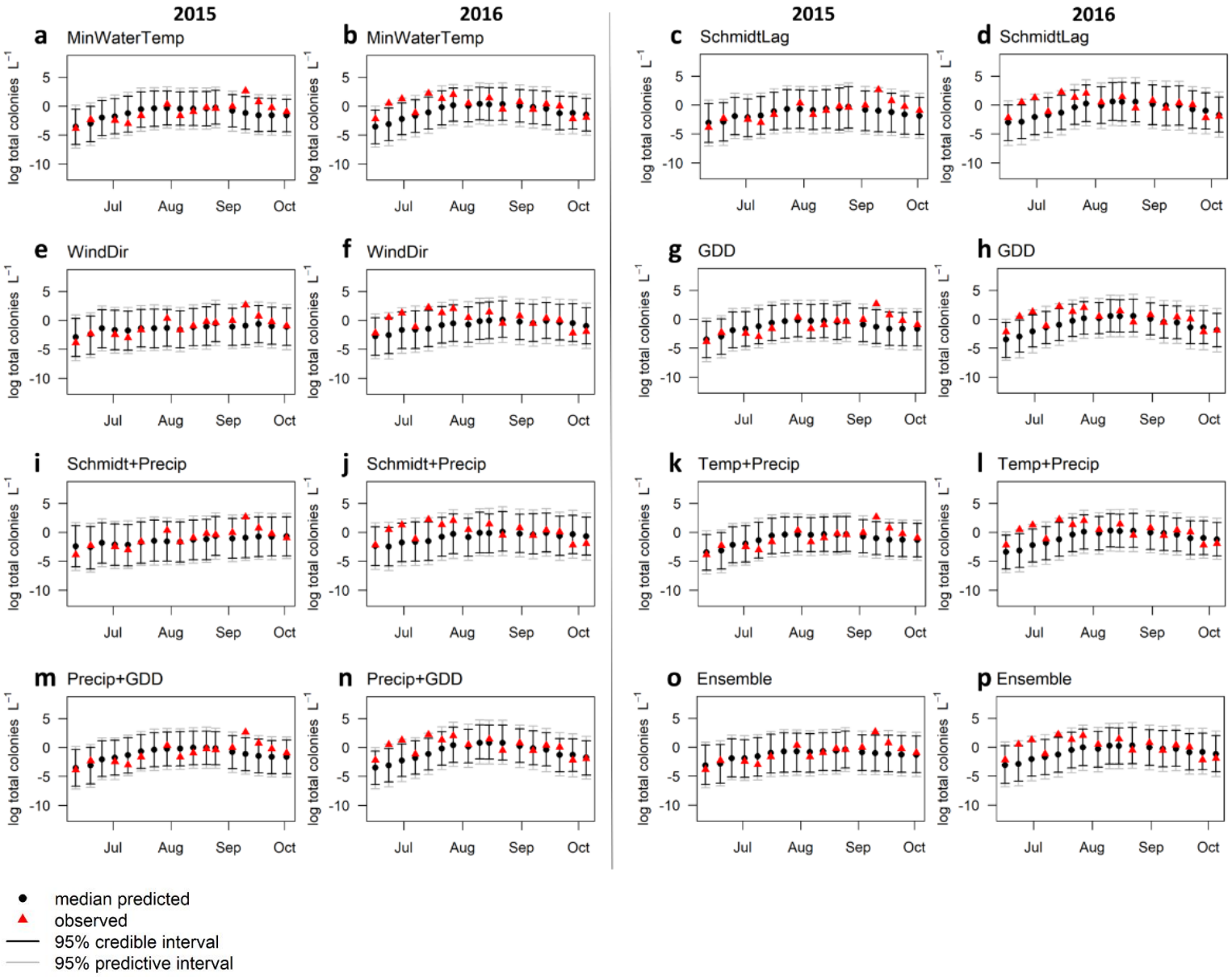
2015
2016
a MinWaterTemp
b MinWaterTemp
c SchmidtLag
d SchmidtLag
e WindDir
f WindDir
g GDD
h GDD
i Schmidt+Precip
j Schmidt+Precip
k Temp+Precip
l Temp+Precip
m Precip+GDD
n Precip+GDD
o Ensemble
p Ensemble
log total colonies L⁻¹
5
0
-5
-10
Jul
Aug
Sep
Oct
median predicted
observed
95% credible interval
95% predictive interval

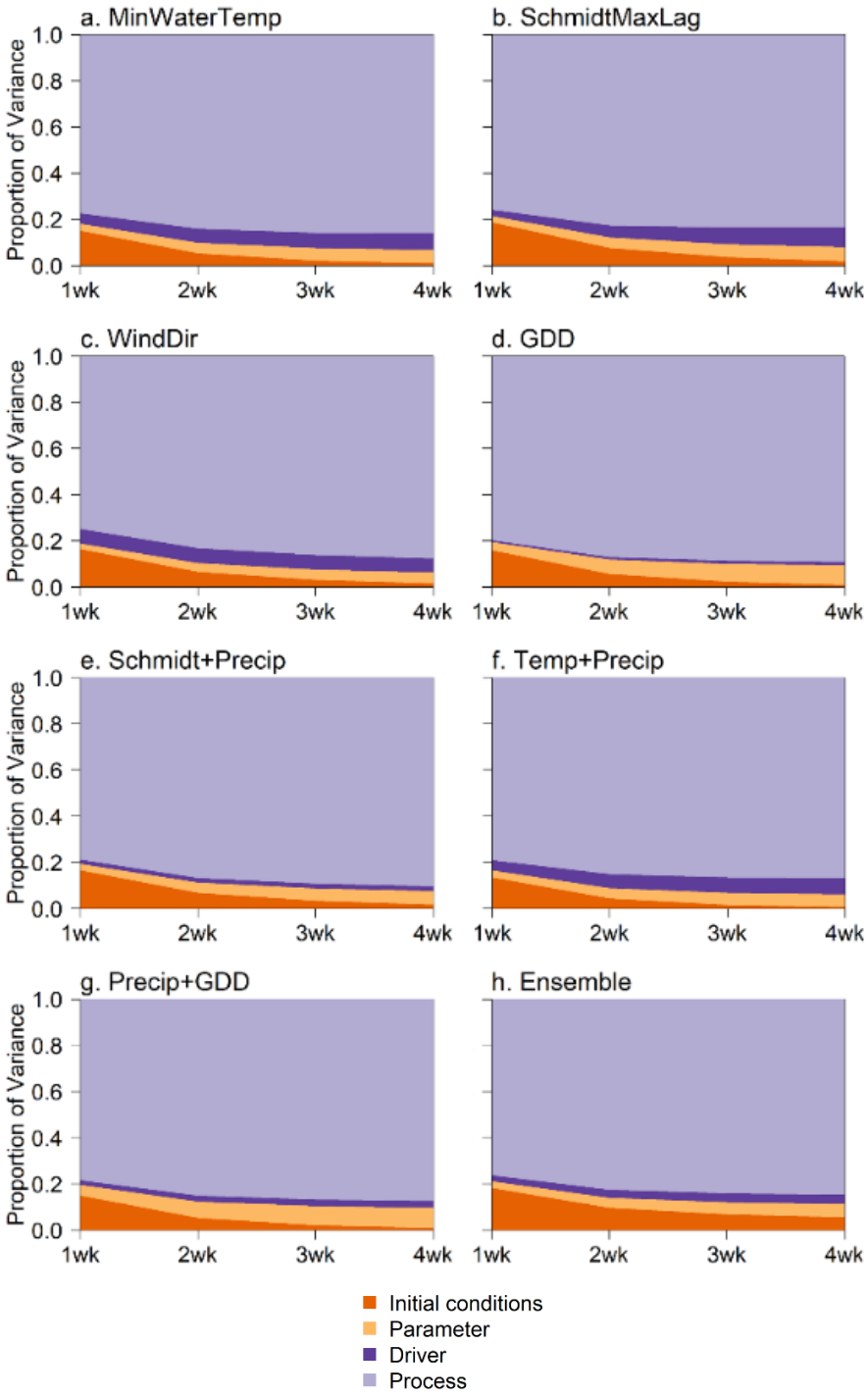

Figure S14: Uncertainty partitioning of the one-week-ahead to four-week-ahead confidence interval for hindcasts averaged across the 2015-2016 hindcasting period for eight models: a) MinWaterTemp, b) SchmidtLag, c) WindDir, d) GDD, e) Schmidt+Precip, f) Temp+Precip, g) Precip+GDD, and h) the model Ensemble.

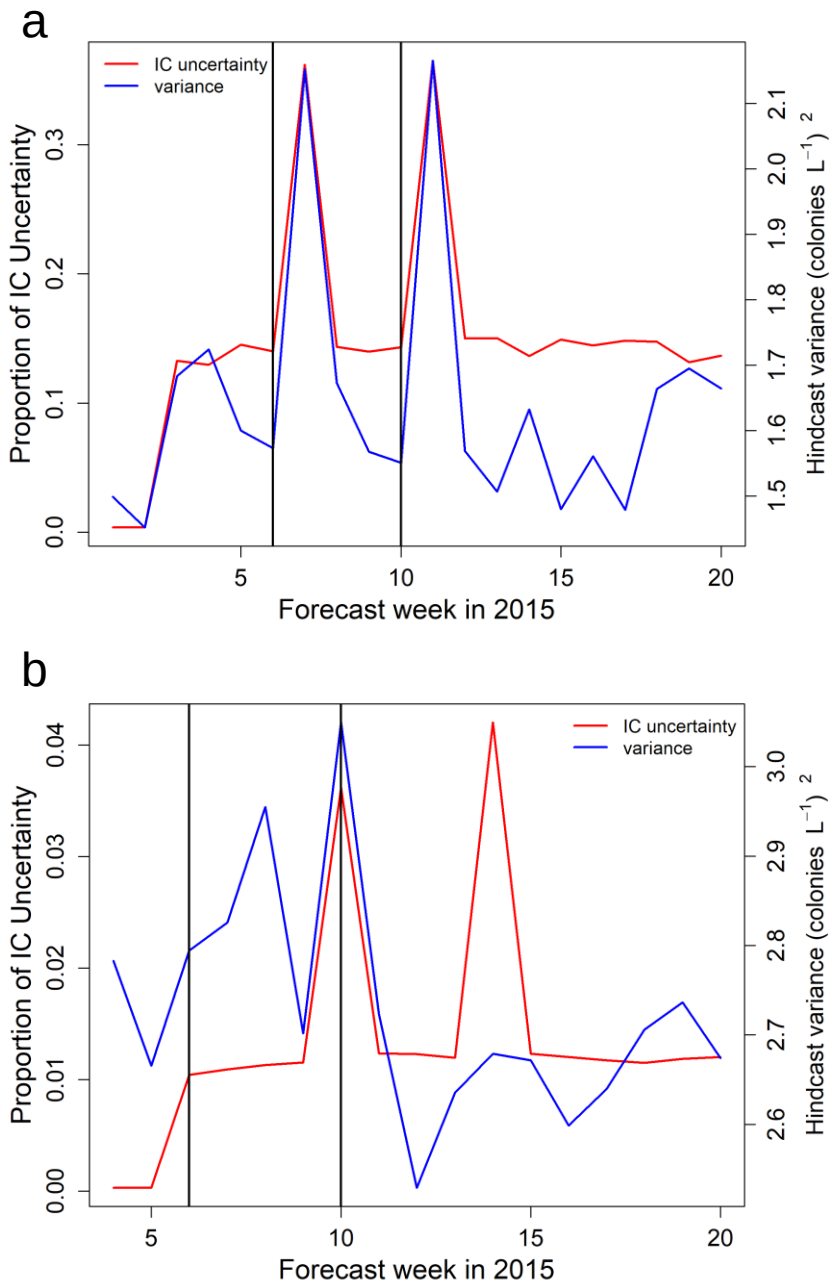

Figure S15: Hindcast variance and proportional contribution of initial contributions uncertainty to the confidence interval of during the 2015 sampling season for an example model (WindDir) for a) one-week-ahead and b) four-week-ahead forecast horizons. Vertical black lines denote times when observational *G. echinulata* data was missing during 2015. Other models exhibit the same pattern.

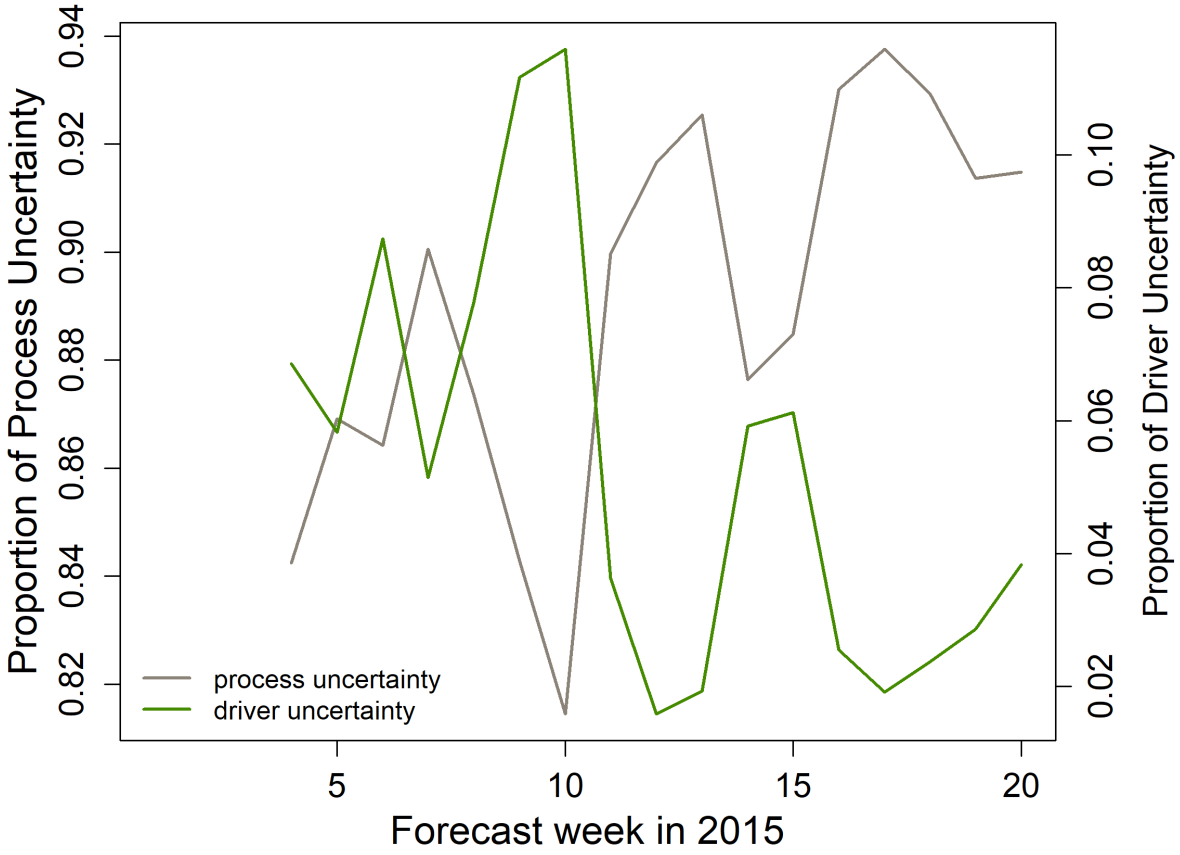

Figure S16: Relative contributions of process and driver uncertainty to total hindcast uncertainty over time for the MinWaterTempLag model in 2015.

References

Barbiero, R. P., and E. B. Welch. 1992. Contribution of benthic blue-green algal recruitment to lake populations and phosphorus translocation. Freshwater Biology 27:249–260.

Bormans, M., P. W. Ford, and L. Fabbro. 2005. Spatial and temporal variability in cyanobacterial populations controlled by physical processes. Journal of Plankton Research 27:61–70.

Carey, C. C., K. L. Cottingham, K. C. Weathers, J. A. Brentrup, N. M. Ruppertsberger, H. Ewing, and N. G. Hairston. 2014. Experimental blooms of the cyanobacterium Gloeotrichia echinulata increase phytoplankton biomass, richness and diversity in an oligotrophic lake. Journal of Plankton Research 36:364–377.

Cottingham, K. L., H. A. Ewing, M. L. Greer, C. C. Carey, and K. C. Weathers. 2015. Cyanobacteria as biological drivers of lake nitrogen and phosphorus cycling. Ecosphere 6:1–19.

Cyr, H. 2017. Winds and the distribution of nearshore phytoplankton in a stratified lake. Water Research 122:114–127.

Dietze, M. C. 2017. Prediction in ecology: A first-principles framework: A. Ecological Applications 27:2048–2060.

Diniz-Filho, A. F., L. M. Bini, T. F. Rangel, R. D. Loyola, C. Hof, D. Nogue, and M. B. Arau. 2009. Partitioning and mapping uncertainties in ensembles of forecasts of species turnover under climate change. Ecography 32:897–906.

Fox, A. M., T. J. Hoar, J. L. Anderson, A. F. Arellano, W. K. Smith, M. E. Litvak, N. MacBean, D. S. Schimel, and D. J. P. Moore. 2018. Evaluation of a Data Assimilation System for Land Surface Models Using CLM4.5. Journal of Advances in Modeling Earth Systems 10:2471–2494.

Gauthier, G., G. Peron, J.-D. Lebreton, P. Grenier, and L. van Oudanhove. 2016. Partitioning prediction uncertainty in climate-dependent population models. Proceedings of the Royal Society B 283:20162353.

Gertner, G., P. Parysow, and B. Guan. 1996. Projection Variance Partitioning of a Conceptual Forest Growth Model with Orthogonal Polynomials. Forest Science 42:474–486.

Huang, J., J. Gao, J. Liu, and Y. Zhang. 2013. State and parameter update of a hydrodynamic-phytoplankton model using ensemble Kalman filter. Ecological Modelling 263:81–91.

Idso, S. B. 1973. On the concept of lake stability. Limnol. Oceanogr. 18:681–683.

Istv́anovics, V., K. Pettersson, M. A. Rodrigo, D. Pierson, J. Padiśk, and W. Colom. 1993. Gloeotrichia echinulata, a colonial cyanobacterium with a unique phosphorus uptake and life strategy. Journal of Plankton Research 15:531–552.

Jiang, J., Y. Huang, S. Ma, M. Stacy, Z. Shi, D. M. Ricciuto, P. J. Hanson, and Y. Luo. 2018. Forecasting Responses of a Northern Peatland Carbon Cycle to Elevated CO2 and a Gradient of Experimental Warming. Journal of Geophysical Research: Biogeosciences 123:1057–1071.

Jiang, Y., Q. Zhuang, S. Schaphoff, S. Sitch, A. Sokolov, D. Kicklighter, and J. Melillo. 2012. Uncertainty analysis of vegetation distribution in the northern high latitudes during the 21st century with a dynamic vegetation model. Ecology and Evolution 2:593–614.

Johansson, M. A., K. M. Apfeldorf, S. Dobson, J. Devita, A. L. Buczak, B. Baugher, L. J. Moniz, T. Bagley, S. M. Babin, E. Guven, T. K. Yamana, J. Shaman, T. Moschou, N. Lothian, A. Lane, G. Osborne, G. Jiang, L. C. Brooks, D. C. Farrow, S. Hyun, R. J. Tibshirani, R. Rosenfeld, J. Lessler, N. G. Reich, D. A. T. Cummings, S. A. Lauer, S. M. Moore, H. E. Clapham, R. Lowe, T. C. Bailey, M. García-Díez, M. S. Carvalho, X. Rodó, T. Sardar, R. Paul, E. L. Ray, K. Sakrejda, A. C. Brown, X. Meng, O. Osoba, R. Vardavas, D. Manheim, M. Moore, D. M. Rao, T. C. Porco, S. Ackley, F. Liu, L. Worden, M. Convertino, Y. Liu, A. Reddy, E. Ortiz, J. Rivero, H. Brito, A. Juarrero, L. R. Johnson, R. B. Gramacy, J. M. Cohen, E. A. Mordecai, C. C. Murdock, J. R. Rohr, S. J. Ryan, A. M. Stewart-Ibarra, D. P. Weikel, A. Jutla, R. Khan, M. Poultney, R. R. Colwell, B. Rivera-García, C. M. Barker, J. E. Bell, M. Biggerstaff, D. Swerdlow, L. Mier-Y-Teran-Romero, B. M. Forshey, J. Trtanj, J. Asher, M. Clay, H. S. Margolis, A. M. Hebbeler, D. George, and J. P. Chretien. 2019. An open challenge to advance probabilistic forecasting for dengue epidemics. Proceedings of the National Academy of Sciences of the United States of America 116:24268–24274.

Karlsson-Elfgren, I., P. Hyenstrand, and E. Riydin. 2005. Pelagic growth and colony division of Gloeotrichia echinulata in Lake Erken. Journal of Plankton Research 27:145–151.

Karlsson-Elfgren, I., K. Rengefors, and S. Gustafsson. 2004. Factors regulating recruitment from the sediment to the water column in the bloom-forming cyanobacterium Gloeotrichia echinulata. Freshwater Biology 49:265–273.

Kim, K., M. Park, J. H. Min, I. Ryu, M. R. Kang, and L. J. Park. 2014. Simulation of algal bloom dynamics in a river with the ensemble Kalman filter. Journal of Hydrology 519:2810–2821.

Madgwick, G., I. D. Jones, S. J. Thackeray, J. A. Elliott, and H. J. Miller. 2006. Phytoplankton communities and antecedent conditions:high resolution sampling in Esthwaite Water. Freshwater Biology 51:1798–1810.

Massoud, E. C., J. Huisman, E. Beninca, M. C. Dietze, W. Bouten, and J. A. Vrugt. 2018. Probing the limits of predictability : data assimilation of chaotic dynamics in complex food webs. Ecology Letters 21:93–103.

Mbogga, M. S., X. Wang, and A. Hamann. 2010. Bioclimate envelope model predictions for natural resource management : dealing with uncertainty. Journal of Applied Ecology 47:731–740.

McMaster, G. S., and W. W. W. Wilhelm. 1997. Growing degree-days: one equation, two interpretations. Agricultural and Forest Meteorology 87:291–300.

Ouellet-Proulx, S., O. Chimi Chiadjeu, M. A. Boucher, and A. St-Hilaire. 2017. Assimilation of water temperature and discharge data for ensemble water temperature forecasting. Journal of Hydrology 554:342–359.

Page, T., P. J. Smith, K. J. Beven, I. D. Jones, J. A. Elliott, S. C. Maberly, E. B. Mackay, M. De Ville, and H. Feuchtmayr. 2017. Constraining uncertainty and process-representation in an algal community lake model using high frequency in-lake observations. Ecological Modelling 357:1–13.

Raiho, A., M. Dietze, A. Dawson, C. Rollinson, J. Tipton, and J. McLachlan. 2020. Determinants of Predictability in Multi-decadal Forest Community and Carbon Dynamics. In prep for Global Change Biology.

Spadavecchia, L., M. Williams, and B. E. Law. 2011. Uncertainty in predictions of forest carbon dynamics: Separating driver error from model error. Ecological Applications 21:1506–1522.

Thomas, R. Q., R. J. Figueiredo, V. Daneshmand, B. J. Bookout, L. K. Puckett, and C. C. Carey. 2020. A near-term iterative forecasting system successfully predicts reservoir hydrodynamics and partitions uncertainty. bioRxiv. https://doi.org/10.1101/2020.01.22.915538.

Thomas, R. Q., A. L. Jersild, E. B. Brooks, V. A. Thomas, and R. H. Wynne. 2018. A mid-century ecological forecast with partitioned uncertainty predicts increases in loblolly pine forest productivity. Ecological Applications 28:1503–1519.

Thuiller, W., M. Guéguen, J. Renaud, D. N. Karger, and N. E. Zimmermann. 2019. Uncertainty in ensembles of global biodiversity scenarios. Nature Communications 10:1–9.

Valle, D., C. L. Staudhammer, W. P. Cropper, and P. R. Van Gardingen. 2009. The importance of multimodel projections to assess uncertainty in projections from simulation models. Ecological Applications 19:1680–1692.

Wang, G., T. Oyana, M. Zhang, S. Adu-prah, S. Zeng, H. Lin, and J. Se. 2009. Forest Ecology and Management Mapping and spatial uncertainty analysis of forest vegetation carbon by combining national forest inventory data and satellite images. Forest Ecology and Management 258:1275–1283.

Watling, J. I., L. A. Brandt, D. N. Bucklin, I. Fujisaki, F. J. Mazzotti, S. S. Roma, and C. Speroterra. 2015. Performance metrics and variance partitioning reveal sources of uncertainty in species distribution models. Ecological Modelling 309–310:48–59.

Winslow, L., J. Read, R. Woolway, J. Brentrup, T. Leach, J. Zwart, S. Albers, and D. Collinge. 2019. rLakeAnalyzer: Lake Physics Tools. https://cran.r-project.org/package=rLakeAnalyzer.

Zhang, Y., Y. Zhao, and L. Feng. 2019. Higher contributions of uncertainty from global climate models than crop models in maize-yield simulations under climate change. Meteorological Applications 26:74–82.